UPTAKE OF SHORT-CHAIN ALCOHOLS BY SULFURIC ACID SOLUTIONS USING RAMAN AND VIBRATIONAL SUM FREQUENCY SPECTROSCOPIES, AND ATMOSPHERIC IMPLICATIONS

DISSERTATION

Presented in Partial Fulfillment of the Requirements for
the Degree Doctor of Philosophy in the Graduate
School of The Ohio State University

By
Lisa Lauralene Van Loon, M. Sc.

*****

The Ohio State University
2007

Dissertation Committee:

Approved by

Professor Heather Allen, Advisor

Professor Christopher Hadad

Professor Barbara Wyslouzil

_____
Advisor
Graduate Program in Chemistry

ABSTRACT

The uptake and reaction of methanol at the air-liquid interface of 0 to 96.5 wt% sulfuric acid (SA) solutions has been observed directly using vibrational sum frequency generation spectroscopy (VSFG) and Raman spectroscopy. Evidence for the formation of methyl hydrogen sulfate (MHS) was obtained by the presence of a new peak in the 800 cm^{-1} region, not present in either the neat methanol or concentrated sulfuric acid spectra. This peak is attributed to the singly bonded OSO symmetric stretch of MHS. The maximum yield of MHS with a large SA excess (7 SA : 1 methanol) is shown to be (95 ± 5) % at –(15 ± 2) ºC. No evidence was found to suggest formation of dimethyl sulfate.

As the concentration of SA increases from 0 – 96.5 wt%, the SFG spectra shift from that of methanol to that of methyl hydrogen sulfate. The surface is saturated with a mixture of the three methyl compounds after 15 minutes, although the relative amounts of MeOH, $MeOH_2^+$, and MHS vary with SA concentration. The uptake of MeOH, $MeOH_2^+$, and MHS into the solutions was also observed, although this occurred on a much longer timescale. This suggests that uptake of methanol by sulfuric acid solutions is diffusion-limited.

The diffusion coefficients for methanol into 0 – 96.5 wt% sulfuric acid solutions were measured by passing MeOH vapor in N_2 over the SA solutions and monitoring the uptake using Raman spectroscopy. The value obtained for methanol into water, D = (0.7 ± 0.2) x 10^{-5} cm^2/s, is in agreement with values found in the literature. The values of D in 39.2 to 96.5 wt% SA range from (1 – 2.7) x 10^{-6} cm^2/s with the maximum value of D occurring for the 59.5 wt% SA solution. This may be due to the speciation of MeOH in the SA solutions or to speciation of the SA solutions.

The organization of two longer but still slightly miscible alcohols, 1-butanol and 1-hexanol, at the air-liquid interface of aqueous, aqueous ammonium bisulfate, and sulfuric acid solutions was investigated using vibrational broad bandwidth sum frequency generation spectroscopy. There is spectroscopic evidence supporting the formation of centrosymmetric structures at the surface of pure butanol and pure hexanol. At aqueous, ammonium bisulfate, and at most sulfuric acid solution surfaces, butanol molecules organize in all-trans conformations. This suggests that butanol self-aggregates. The 0.052 M butanol in 59.5 wt% sulfuric acid solution is different from the other butanol solution spectra; that is, the surface butanol molecules possess a significant number of gauche defects. Relative to surface butanol, surface hexanol chains are significantly more disordered at the surface of their respective solutions. The surface spectra for butanol and hexanol also show evidence for salting out from the ammonium bisulfate solutions.

ACKNOWLEDGMENTS

I wish to thank my advisor, Dr. Heather Allen, for her guidance and mentorship during the past six years.

I thank Dr. Gang Ma for all his invaluable help. I also thank him for creating the SFG fitting routine, and the Mathcad files used in Chapter 6.

I thank Dr. Laura Voss for taking the time to automate our data processing.

I thank Dr. Sandhya Gopalakrishnan for assistance with the ab initio calculations presented in Chapter 3.

Finally I must thank all members of the Allen group, past and present, for putting up with me during the years!

VITA

October 10, 1975	Born – Keynsham, England
June 1999	B. Sc. Chemistry (Honours) University of Ottawa
June 2001	M. Sc. Chemistry (Chemical and Environmental Toxicology) University of Ottawa Advisor: Dr. Susannah Scott
2001 – 2006	Graduate Teaching Associate The Ohio State University.
2001 – 2007	Graduate Research Associate The Ohio State University.

PUBLICATIONS

1. Lisa Van Loon, Elizabeth Mader, and Susannah L. Scott, **2000**, *Reduction of the Aqueous Mercuric Ion by Sulfite: UV Spectrum of $HgSO_3$ and its Intramolecular Redox Reaction*, **J. Phys. Chem. A** 104, 1621-1626.

2. Lisa L. Van Loon, Elizabeth A. Mader, and S. L. Scott, **2001**, *Sulfite Stabilization and Reduction of the Aqueous Mercuric Ion: Kinetic Determination of Sequential Formation Constants*, **J. Phys. Chem. A** 105, 3190-3195.

3. Lisa L. Van Loon, Heather C. Allen, **2004**, *Methanol Reaction with Sulfuric Acid: A Vibrational Spectroscopic Study*, **J. Phys. Chem. B** 108, 17666-17674.

FIELDS OF STUDY

Major Field: Chemistry

TABLE OF CONTENTS

LIST OF TABLES

LIST OF FIGURES

CHAPTER 1

BACKGROUND

The work presented in this thesis was motivated by a desire to understand the role of uptake of volatile short-chain alcohols by acidic sulfate aerosols in aerosol growth. For growth to occur, the volatile alcohol from the vapor phase must be transformed into a compound of lower volatility. In this work, the interactions between methanol (MeOH), 1-butanol (BuOH), and 1-hexanol (HexOH) and sulfuric acid (SA) solutions were investigated as model systems for the interactions between volatile gas-phase alcohols and acidic sulfate aerosols. The formation of less volatile sulfate esters may be the mechanism for aerosol growth.

The reaction between MeOH and 96.6 wt% SA solution is the focus of chapter 3. Chapters 4 and 5 discuss the uptake and diffusion of methanol in 40 - 80 wt% SA solutions. Chapter 6 investigates the interfacial structure of BuOH and HexOH at the air-solution interface of water, 59.5 wt% SA, and aqueous NH_4HSO_4. Experimental details can be found in Chapter 2 and in subsequent chapters.

As mentioned above, the uptake of volatile organics by tropospheric aerosols is postulated as a possible mechanism for aerosol growth.[1] Recent field measurements show that aerosols and cloud droplets can contain organic compounds from 20 % to 70 % by mass.[2-4] And recent field campaigns have detected a large number of short-chained oxygenated compounds present in tropospheric aerosols.[5] A decrease in surface tension relative to that of pure water has been observed in wet aerosol and cloud/fog samples[2] suggesting that organic compounds are present at the surfaces of aerosols. This is important since the presence of organic compounds at the surface may change the

uptake capabilities and hygroscopicity of aerosols, affecting aerosol growth and ultimately cloud albedo.[6,3,7]

Only recently has the role of semi-volatile organic compounds (SVOC) been considered in the formation of cloud condensation nuclei.[8-12] Highly water-soluble organics are shown experimentally to be important in CCN formation.[10] More recently, reactions of SVOC in the aerosol aqueous phase were considered as possible initiators of CCN growth. Such formation requires that the atmospheric lifetime of the organic compounds be longer than the timescale required to diffuse into the aqueous phase and react, and that the products be non-volatile to contribute to particle growth.[12] In spite of the critical nature of these atmospheric processes, more experimental data is needed to determine the importance of the heterogeneous pathway to aerosol growth.[9]

One possible important group of compounds is esters, formed from volatile compounds condensing on acidic aerosols.[1] Sulfate esters have recently been measured in field samples.[13,14] In laboratory experiments, their formation has been detected for both unoxygenated[14,15] and oxygenated[16-18] starting products. An increase in sulfate ester formation is observed with increasing sulfate acidity, suggesting that sulfate ester formation may be a contributor to secondary organic aerosol formation in acidic aerosols.

Oxygenated compounds are the dominant organic species in the upper troposphere, with methanol making up half of all emissions.[19,20] Methanol concentrations up to 1100 ppt have been measured in the remote Pacific troposphere[5,21,22] and in Asian plumes,[23] while tropospheric concentrations in urban regions are much higher (>20,000 pptv).[21] Due to its much longer lifetime than other compounds such as isoprene, methanol is transported from the boundary layer (lifetime = 1 week) to the upper troposphere (lifetime = few weeks) and lower stratosphere.[20,24] Plants are the largest single source of methanol emissions to the atmosphere (37-212 Tg/yr)[19,25] with 67% of emissions from plant growth.[19] Recent continental measurements have shown a diurnal cycle for methanol emissions.[26,27] Rural measurements[28] also show a correlation of methanol emissions with temperature, with the lowest emissions recorded during the coldest period of the year. Together, these measurements strongly suggest that biogenic emissions are very important.

Tropical regions are found to be a major contributor to global annual biogenic emissions.[29] Biomass burning plumes are estimated to emit 29-35 Tg CH_3OH/year.[30] In plumes over the Mediterranean, methanol attributed to combustion[23] and methanol found in aged plumes may suggest that oxidation of methane is an important atmospheric source of methanol.[31] However, methanol emissions from biomass burning plumes can be highly variable, suggesting that factors other than hydroxyl reaction with methane may determine the methanol concentrations in these plumes.[32] Measurements of methanol in North Atlantic marine air[31] indicate that oxidation of volatile organic compounds (VOCs) is likely to contribute to the observed methanol concentrations several days from the point of emission.

The main tropospheric reaction sink for methanol is its reaction with hydroxyl radical.[21] The ocean is also found to be a slight net sink since the marine boundary layer has slightly lower methanol concentrations than the rest of the troposphere.[22,33] However there are still large discrepancies between the sources and sinks of methanol.[34]

Sulfate is the dominant inorganic species in atmospheric particulate matter throughout the troposphere and the lower stratosphere.[35] In the troposphere over tropical regions, measurements suggest that sulfuric acid and water nucleate to form aerosols,[36] indicating that higher sulfuric acid concentrations are related to smaller particle sizes.[37] Although atmospheric sulfur is primarily from anthropogenic sources, sulfate aerosols are distributed throughout both polluted and remote areas. Sulfuric acid is formed as an oxidation product of sulfur dioxide, a fossil fuel combustion product. Global SO_2 emissions are estimated at $(130\text{-}180)\times10^{12}$ g of S/yr,[38] and sulfur emissions are much greater in the Northern Hemisphere, where 90% of emissions are from anthropogenic sources. Marine sea spray and volcanic emissions account for 87% of all natural emissions.[35]

CHAPTER 2

EXPERIMENTAL DETAILS

This chapter presents an overview of the theory of vibrational sum frequency generation (VSFG) spectroscopy, followed by the instrumental and experimental details for both VSFG and Raman spectroscopies. The spectral fitting methodology is presented in the last section. Experimental details relevant to each experiment are provided in particular chapters.

Vibrational Sum Frequency Generation Spectroscopy

VSFG is a surface selective technique. It is a second-order nonlinear optical technique sensitive to environments lacking inversion symmetry. It has been used to study, among others, solid and liquid surfaces with atmospheric relevance.[39-43] It is sensitive to both the number density and the molecular orientation of the molecules at the interface. Thorough treatments of VSFG theory can be found in the literature,[44-47] and a brief introduction is given here.

The intensity of the SFG signal, I_{SFG}, is proportional to the absolute square of the macroscopic nonlinear susceptibility, $\chi^{(2)}$, and to the intensity of the infrared and 800 nm incident beams, equation 2.1.

$$I_{SFG} \propto | \chi^{(2)} |^2 \, I(\omega_{IR}) I(\omega_{800}) \qquad (2.1)$$

The macroscopic nonlinear susceptibility, $\chi^{(2)}$, is described by a nonresonant term, $\chi^{(2)}_{NR}$, and the sum of the resonant terms, $\chi^{(2)}_{\nu}$, equation 2.2.

$$|\chi^{(2)}|^2 = |\chi^{(2)}_{NR} + \sum_{\nu}\chi^{(2)}_{\nu}|^2 \quad (2.2)$$

When the frequency of the incident infrared beam is resonant with a vibrational mode, ν, then the resonant term dominates the nonlinear susceptibility. The resonant susceptibility term, $\chi^{(2)}_{\nu}$, is related to the number density of the surface species and to the molecular hyperpolarizability, β_{ν}, through the orientationally averaged Euler angle transformation, $\langle \mu_{IJK:lmn} \rangle$, between the laboratory coordinates (IJK) and the molecular coordinates (*lmn*), equation 2.3.

$$\chi^{(2)}_{\nu} = N\sum_{lmn}\langle \mu_{IJK:lmn} \rangle \beta^{lmn}_{\nu} \quad (2.3)$$

The molecular hyperpolarizability is proportional to the infrared transition moment, μ, and the Raman polarizability tensor, α, showing that SFG active modes must be both Raman- and IR-active, equation 2.4.

$$\beta^{lmn}_{\nu} = \frac{-\mu^{n}_{\nu 0}(\alpha^{lm}_{\nu 0})}{2\hbar(\omega_{\nu} - \omega_{IR} - i\Gamma_{\nu})} \quad (2.4)$$

From equation 2.4, the resonant macroscopic nonlinear susceptibility is shown in equation 2.5.

$$\chi^{(2)}_{\nu} \propto \frac{A_{\nu}}{\omega_{IR} - \omega_{\nu} + i\Gamma_{\nu}} \quad (2.5)$$

In the above equation A_{ν} is the strength of the transition moment and ω_{ν} is the frequency of the transition.

From equations 2.4 and 2.5, it becomes clear that only non-centrosymmetric systems, such as the air-liquid interface, will be SFG-active. When the frequency of a vibrational mode, ω_{ν}, is resonant with the infrared frequency, ω_{IR}, the denominator in equation 2.5 becomes small and β_{ν} and therefore $\chi^{(2)}_{\nu}$, will be enhanced. A VSFG spectrum results from the nonlinear response over the frequency range probed.

BBSFG Instrumentation and Experimental Details

Details of the Allen lab broad bandwidth SFG (BBSFG) system can be found in previous publications.[48,49] Two 1-kHz repetition rate regenerative amplifiers (Spectra Physics Spitfire, femtosecond and picosecond versions) are utilized. The picosecond amplifier produces a narrow bandwidth (17 cm^{-1}), 2 ps pulse at a wavelength of ~ 800 nm. (Air-liquid spectra were also obtained with an ~5 cm^{-1} bandwidth;[49] no improvement of resolution was observed, indicating that the linewidth is limited by the chemical system.) The femtosecond amplifier is used to pump an optical parametric amplifier (Spectra-Physics OPA 800F) to produce a broad bandwidth, ~ 100 fs, infrared pulse. The spectral window of the IR pulse varied from 330-600 cm^{-1} in the C-H stretching region, depending on the experiment.. The energy of the 800 nm beam used and the IR energy in the C-H stretching region are noted in the individual chapters. The BBSFG experiment is performed in reflection geometry.

The SFG beam is dispersed spectrally in a monochromator (Acton Research, SpectraPro 500i) using a 1200 g/mm diffraction grating blazed at 750 nm. The beam waist of the focused SFG beam limits the monochromator resolution. The SFG signal is collected with a CCD detection system (Roper Scientific, LN400EB, 1340 x 400 pixel array, back-illuminated CCD). Spectral resolution was determined to be 8 cm^{-1}.[50] Calibration of the CCD camera was completed using the 435.833 nm line from a fluorescent lamp.

Three polarization combinations were used in this study: ssp (s-SFG, s-800 nm, p-infrared), ppp (p-SFG, p-800 nm, p-infrared), and sps (s-SFG, p-800 nm, s-infrared). The polarization of the 800 nm beam is determined by rotation of a zero-order waveplate. By rotation of a MgF_2 Berek's compensator, the desired IR beam polarization is determined. A glan polarizer in the SFG detection line selects the SFG polarization. The ssp polarization combination probes the isotropic Raman response and the IR-active dipole moment that is perpendicular to the surface, the ppp polarization combination probes the anisotropic Raman response and the IR active dipole moment that is perpendicular to the surface, and the sps polarization condition probes the anisotropic Raman response and the IR transition moment in the plane of the interface. S and P polarized light denotes light

that is polarized perpendicular and parallel to the plane of incidence, respectively. ssp or sps by convention is listed in the order of: SFG, incident visible and incident IR light.

The final spectra shown in this thesis are the average of the three spectra with the average of three background spectra subtracted, unless otherwise stated. The VSFG spectrum is normalized against a smoothed nonresonant VSFG spectrum from a GaAs crystal to remove any structure present in the IR pulse profile. The dips in a polystyrene-GaAs spectrum are used to calibrate the wavenumber position for each set of experiments.

Raman Instrumentation

Raman spectra were obtained using 120 - 225 mW depending on the experiment from a 785 nm continuous wave laser (Raman Systems Inc). The backscattered light was collected by a fiber optic probe (Inphotonics) coupled to the entrance slit of a 500-nm monochromator (Acton Research, SpectraPro 500i) using a 600 groove/mm grating blazed at 1 μm. The slit width was set to 20 or 50 μm, depending on the experiment, and the bandpass for both, limited by the CCD pixel effective slit width, was measured to be 3 cm^{-1}. The spectra were collected in 60 sec exposures to a liquid nitrogen cooled CCD camera (Roper Scientific, LN400EB, 1340 x 400 pixel array, back-illuminated and deep depletion CCD). CCD calibration was completed using the 435.833 nm line from a fluorescent lamp. Calibration of the wavenumber position was completed for each set of experiments by taking a spectrum of crystalline naphthalene and comparing peak positions with the literature values.[51]

Spectral Fitting

Spectra are fit using the software package IgorPro 4.05 (WaveMetrics, Inc.). The VSFG spectra are fit with Lorentzian line shapes according to equations (2.1) and (2.5) using IgorPro with user-added fitting functions. The Igor procedure, written by Dr. Gang Ma, is found at the end of this section. The fitting procedure requires user input for the following parameters: two non-resonant terms, the peak amplitudes and phases, peak positions, and peak widths for each component peak. The parameters can be held

constant or allowed to vary with the fit. Unless otherwise noted in this thesis, the parameters were allowed to vary and the peak positions reported are the best fits found with the software. The number of peaks fit corresponds to the number of vibrational modes expected to be SFG-active.

Raman spectra were fit using the multipeak fitting function with Voigt line shapes, with the background subtraction option enabled. Care was taken to ensure that the best-fit Voigt line shapes remained consistent between spectra, in order to properly compare any changes.

SFG fitting procedure:

```
#pragma rtGlobals=1                    // Use modern global access method.
function sfg_lor(w,x) : fitfunc
        wave w   //coefficient wave for the lorentzian fit
                        // term 0, 1 are the non resonant
                        // 2, 5, 8, ... amplitude
                        // 3, 6, 9, ... peak position
                        // 4, 7,10,... lorentzian width
        variable x  //Infrared frequency
        variable j = 2, np = (numpnts(w)-2)/3          //np is the number of peaks to be fit
        variable/c val    // val is a holding variable for the fitting equation
        variable/c i = sqrt(-1)  // defining the imaginary i
        val = w[0] + i*w[1]              // the nonresonant wave
        do                                      // Loop which collects the peaks into the holding variable val
                val += w[j]/(x-w[j+1]-i*w[j+2])
                j += 3
        while (j < np*3+1)
        return magsqr(val)               // Returns the calculated fit back to Igor
End
```

CHAPTER 3

METHANOL REACTION WITH SULFURIC ACID[1]

Introduction

This chapter was motivated by an interest in understanding atmospheric aerosol chemistry. The reaction between sulfuric acid aerosols and tropospheric methanol is not well understood at the molecular level. Therefore, this reaction, under simplified experimental conditions, is the focus of this chapter.

The uptake of methanol by sulfuric acid solutions has recently been studied,[52,53] and the 'esterification' of methanol by sulfuric acid has been known since the 1950's.[54] Yet, direct measurement of the reaction products has remained elusive. We present spectroscopic evidence of the formation of methyl hydrogen sulfate (CH_3OSO_3H) using Raman spectroscopy to investigate the bulk solution. Surface studies are also presented. Surface tension measurements provide a macroscopic understanding of the surface, and broad bandwidth sum frequency generation (BBSFG) spectra present a molecular view of the surface.

---

[1] Much of this chapter is published as

Lisa L. Van Loon, Heather C. Allen, **2004**, *Methanol Reaction with Sulfuric Acid: A Vibrational Spectroscopic Study*, **J. Phys. Chem. B** 108, 17666-17674.

Chemical abbreviations used in this chapter are:

MeOH (methanol); SA (sulfuric acid); MHS (methyl hydrogen sulfate); $DMSO_4$ (dimethyl sulfate)

Experimental section

Methanol (HPLC grade, Fisher Scientific), sodium methyl sulfate (99 %, Aldrich), dimethyl sulfate (99+ %, Aldrich), sulfuric acid (redistilled, 96.6 wt%, GFS) and hydrochloric acid (Fisher Scientific, 36.5 wt%) were used as received. Nanopure water (17.8-18.3 MΩ·cm) was used. The only water present in the methanol-sulfuric acid reaction system was brought in with the addition of the 96.6 wt% sulfuric acid. To completely dissolve CH_3OSO_3Na in SA, solution vials were placed in a warm water bath.

In the low temperature study, a vial containing 96.6 wt% sulfuric acid was placed in a freezer at -(15 ± 2) ºC to temperature-equilibrate and was stirred. 1.00 mL of MeOH was delivered to the vial (1.37 molal) and Raman spectra were acquired every minute for a minimum of twelve hours. The room temperature study was conducted at (23 ± 1) ºC beginning with cold sulfuric acid and methanol since mixing is exothermic. The high temperature study was conducted by mixing cold sulfuric acid and methanol in a water bath and Raman spectra were obtained before mixing with a stir-bar began; the solutions were stirred and then heated in an oven to (82 ± 2) ºC for several days. In the high temperature study, spectra were obtained until peak intensities did not change, revealing that reactions had come to completion.

Surface Tension Measurements

Surface tension measurements were made using the Kibron Inc μ-trough system (Kibron DeltaPi, Kibron, Inc.), based on the Wilhelmy Plate Technique, with DeltaGraph v 2.15 software (Kibron, Inc.). 1.00 mL of solution was delivered into a PTFE tray for each measurement. The temperature varied between 26.0 and 28.7 ºC.

Ab initio calculations

Calculations were performed using Gaussian 03 for Windows;[55] the 6-31+G** basis set was chosen for all ab initio calculations.[56]

Raman Instrumentation

Raman spectra were obtained using 120 - 225 mW depending on the experiment. The slit width was set to 20 μm and the bandpass was limited by the CCD pixel resolution to 3 cm^{-1}. The spectra were collected in 60 sec exposures.

SFG Instrumentation

The infrared pulse energy used in the SFG experiments in this chapter is 10 μJ and the visible pulse energy is 115 μJ. Spectra were obtained by integration of the SFG signal for 1- 5 minutes depending on the experiment. ssp polarization conditions were used for the BBSFG spectra shown here. However, sps polarization conditions were used for additional analysis.

Scanning SFG

A Nd:YAG laser with a 20-Hz repetition rate (EKSPLA PL2143) is used to generate one beam at 532 nm (30 ps). The remaining fundamental 1064 nm beam is converted into the second and third harmonics (532 nm and 355 nm respectively) in the Harmonics Unit (Ekspla). The PG/401/DFG (Ekspla) uses these two beams to create tunable IR from 4000-1000 cm^{-1} with a $AgGaS_2$ crystal. The IR energy at 1070 cm^{-1} is ~ 100 μJ. The 532 nm energy used is ~ 500 μJ. The bandwidth of the IR beam in the 2800-4000 cm^{-1} region is 4-8 cm^{-1}. The SFG experiment is set up in reflectance geometry. The 532 nm and IR beams are directed to the sample in co-propagating geometry with input angles of 56.8º (IR) and 66.3º (532 nm) to the surface normal. The resulting SFG beam (~ 65.3º) is detected by a monochromator (SOLAR TII, Ltd, M2001i) CCD/PMT setup. Either the CCD (Andor Technology, DV412BV) or the PMT (Hamamatsu Corporation, R5929) detector is selected by rotating a mirror inside the monochromator to the appropriate exit slit. The appropriate polarizations (s or p) are chosen by rotating half wave plates in the 532 nm and SFG detection lines. The IR polarization is determined by the rotation of two gold mirrors. The SFG spectrum is normalized against the IR and 532 nm intensities to remove fluctuations in the spectrum due to the energy profile. The

calibration of the spectral wavenumber is done by obtaining an IR spectrum of polystyrene and comparing it with the known literature peak positions.

Results and Discussion

Before studying the reaction of MeOH with SA, it was important to understand the spectroscopic signatures of neat MeOH and SA. Therefore the liquid Raman spectra of neat methanol and sulfuric acid were obtained and these spectra are shown in Figure 3.1a. Their peak assignments are found in Table 3.1. Of particular interest to this study in the methanol spectrum is the peak at 1034 cm^{-1} assigned as the symmetric O-C stretch, the peak at 2835 cm^{-1} attributed to the CH_3 symmetric stretch, the 2920 cm^{-1} shoulder and the peak at 2944 cm^{-1} are assigned to two Fermi resonances. The high-energy side of the 2944 cm^{-1} peak has a shoulder at 2977 cm^{-1} attributed to the CH_3 asymmetric stretching modes.

The 96.6 wt% SA solution contains both H_2SO_4 and HSO_4^- molecules with the bisulfate ion solvated by multiple H_2SO_4 molecules.[57] Three SA peaks shown in Figure 3.1a are of particular interest to this study. The peak at 912 cm^{-1} is attributed to the in-phase symmetric stretching of $S(OH)_2$ from H_2SO_4. The 1044 cm^{-1} peak is assigned to the SO_3 symmetric stretch of HSO_4^- in the $(HSO_4^-)(H_2SO_4)$ complex. The peak at 1153 cm^{-1} is assigned to the O=S=O symmetric stretch.

The reacted mixture of methanol with sulfuric acid (7 SA : 1 MeOH: 1 H_2O) is shown in Figure 3.1b. Due to the high concentration of SA, it is difficult to distinguish between O-S vibrations due to any reaction product and SA in the region between 400 and 1500 cm^{-1} since the peaks appear at approximately the same frequency. However, in Figure3.1b, a peak at 808 cm^{-1} is observed; this peak is not present in either the neat MeOH or the 96.6 wt% SA spectra (Figure 3.1a) and is attributed to the singly bonded OSO symmetric stretch of a new species, methyl hydrogen sulfate (CH_3OSO_3H; MHS). The spectrum of a MHS standard solution is shown in Figure 3.3. In addition to the 808 cm^{-1} peak in Figure 3.1b, the shoulder on the low energy side of the SO_3 symmetric stretch peak of SA observed at 995 cm^{-1} is of interest to this study and is assigned to the O-C symmetric stretch of MHS. This peak is shifted to lower energy as compared to the

methanol O-C symmetric stretch (1034 cm^{-1}).

The CH_3 stretching region in the MeOH + SA spectrum of Figure 3.1b is different from that of neat MeOH. The entire methyl stretching region of Figure 3.1b is shifted to higher energy relative to the neat MeOH spectrum of Figure 3.1a. Like for methanol, the 2859 and 2975 cm^{-1} peaks are assigned to the CH_3 symmetric stretch and a Fermi resonance with the smallest peak at 3047 cm^{-1} assigned to the CH_3 asymmetric stretching modes. All peak assignments for spectra of Figure 3.1 are shown in Table 3.1.

The relative peak intensities in the CH_3 stretching region are also different in the reacted mixture of MeOH + SA compared to the neat methanol spectrum as shown in Figure 3.2. In addition, the relative intensities of the methanol CH_3 symmetric stretch (2835 cm^{-1}) to the Fermi resonance (2944 cm^{-1}) is 2:1 in the methanol spectrum while the relative intensity of the reacted mixture 2859 to 2975 cm^{-1} peaks is 1:2.

To investigate the possibility that the reacted MeOH + SA spectrum in Figure 3.1b is the spectrum of protonated MeOH, $CH_3OH_2^+$, the spectrum of methanol in HCl was obtained and is shown in Figure 3.2 (a and b). The peak assignments are found in Table 3.1. Methanol is only weakly basic (for $CH_3OH_2^+$; $pK_{BH^+} = -4.86 \pm 0.37$),[58] and under concentrated acid conditions (4 HCl : 1MeOH : 13 H_2O; 12M HCl added), 35% of the methanol is protonated.[58] In the Raman spectrum, protonation is observed as a red-shifting of the O-C symmetric stretch from 1034 cm^{-1} for neat methanol to 1003 cm^{-1} for protonated MeOH in HCl[58] and 995 cm^{-1} (small peak) for the MeOH + SA solution as shown in Figure 3.2a. This shift to lower energy suggests that the O-C bond lengthens as a result of protonation.[59] The decrease in O-C peak intensity for $MeOH_2^+$ of MeOH in HCl and the MHS product of MeOH + SA as compared to the intensity in neat MeOH is mainly due to dilution. (Normalization of the data to equalize the number density produced O-C peaks of comparable intensity.) The reacted MeOH + SA solution spectrum, Figure 3.2a, has a peak at 808 cm^{-1} not present in the spectrum of MeOH in HCl so it cannot be attributed to protonated methanol.

The CH_3 stretching regions of neat methanol, methanol reacted with sulfuric acid, and methanol in hydrochloric acid are compared in Figure 3.2b. The CH_3 stretching region of methanol in HCl is blue-shifted relative to that of neat methanol but less than that of the

reacted mixture. This shift to higher energy for MeOH in HCl indicates that the CH bonds of MeOH are strengthened in HCl. The relative intensity of the symmetric stretch to the higher energy peak has changed from 2:1 to 1:1 for the HCl mixture, and 1:2 for the reacted mixture. The observed decrease in intensity of the CH_3 stretching region relative to the MeOH spectrum in Figure 3.2b is again mainly due to dilution for the MeOH in HCl solution. However, the MeOH + SA solution CH_3 region is less intense even after normalization to equalize number density effects (Figure 3.11b) consistent with the shifting of the CH_3 asymmetric stretch to higher wavenumber.

The formation of MHS from the reaction of MeOH with SA has been investigated since the 1950's. The reactions, as postulated by Deno and Newman, are shown in reactions (A)-(C).[54]

$$ROH_2^+ + H_2SO_4 \leftrightarrows ROSO_3H + H_3O^+ \quad (A)$$

$$ROH + H_3SO_4^+ \leftrightarrows ROSO_3H + H_3O^+ \quad (B)$$

$$ROH + H_2SO_4 \leftrightarrows ROSO_3H + H_2O \quad (C)$$

More recently, the reaction sequence has been expressed by Torn and Nathanson[60] and is shown below in reactions (a) – (f).

$$H_2SO_4 + H_2O \leftrightarrows HSO_4^- + H_3O^+ \quad (a)$$

$$HSO_4^- + H_2O \leftrightarrows SO_4^{2-} + H_3O^+ \quad (b)$$

$$ROH + H_3O^+ \leftrightarrows ROH_2^+ + H_2O \quad (c)$$

$$HSO_4^- + ROH + H_3O^+ \leftrightarrows ROSO_3H + 2H_2O \quad (d)$$

$$ROSO_3H + H_2O \leftrightarrows ROSO_3^- + H_3O^+ \quad (e)$$

$$ROSO_3H + ROH \leftrightarrows (RO)_2SO_2 + H_2O \quad (f)$$

MHS may further react with methanol to form $DMSO_4$ based upon a drop in the desorbing methanol fraction in flow-tube experiments as suggested by reaction (f).[53] To confirm the product of the reaction between methanol and sulfuric acid in this study, the Raman spectra of MHS in SA (11 SA : 1 MHS : 1 H_2O) and $DMSO_4$ in SA (12 SA : 1 $DMSO_4$: 2 H_2O) were obtained as shown in Figure 3.3. Both compounds have a peak in

the 800 cm^{-1} region attributed to their singly bonded OSO symmetric stretch, but the positions differ: 769 cm^{-1} for $DMSO_4$ in H_2SO_4 and 807 cm^{-1} for MHS in SA. Shown in the inset of Figure 3.3, the 2860 cm^{-1} of MHS and the 2976 cm^{-1} peaks of both MHS and $DMSO_4$ are assigned to CH_3 symmetric stretching and Fermi resonance modes, respectively. The 2859 cm^{-1} peak of $DMSO_4$ is assigned to a CH_3 symmetric stretch, although it has been previously assigned as a combination band or a Fermi resonance of the CH_3 bending mode with the CH_3 symmetric stretch.[61] The 3043 cm^{-1} peak of MHS and the 3050 cm^{-1} peak of $DMSO_4$ are assigned to CH_3 asymmetric stretches. The CH_3 stretching regions of MHS and $DMSO_4$ are shifted to higher wavenumber relative to that of methanol. The relative intensity of the peaks in the methyl symmetric stretching regions is 1:2, unlike that for neat methanol, but the same as that of the reacted mixture of MeOH + SA. Additional peak assignments are found in Table 3.1.

The Raman spectra of a series of reacted MeOH + SA mixtures are shown in Figure 3.4a. The MeOH + SA singly bonded OSO peak at ~800 cm^{-1} shifts with changing SA concentration as shown in Figure 3.4a. Figure 3.4b shows the shift of the singly bonded OSO symmetric stretch of $DMSO_4$, MHS, and reacted MeOH with increasing sulfuric acid concentration to higher wavenumber. Shown in Figure 3.4a, the in-phase $S(OH)_2$ stretch of H_2SO_4 shifts from 912 cm^{-1} at high SA concentrations to 895 cm^{-1} in low SA concentration, the position of the S(OH) stretch of HSO_4^-.[57] The peak at 1043 cm^{-1} is attributed to the $\nu_s(SO_3)$ of H_2SO_4 in the largest SA concentration. As the SA concentration decreases, the peak shifts to 1055 cm^{-1}, the peak position attributed to ν_s (SO_3) of HSO_4^-.[57]

Unlike the 1043 and 912 cm^{-1} bands, the O=S=O stretch at 1153 cm^{-1} does not shift significantly (< 5 cm^{-1}) with changing composition (ref. 62 and unpublished data from our lab) indicating that the O=S=O stretch is less dependent on the hydrogen bonding. The SA peak shifts indicate that the major sulfuric acid species present in the solution changes from H_2SO_4 at high SA to HSO_4^- in lower SA regimes due to protonation of the methanol. In the 0.5 SA : MeOH reaction mixture there is only enough SA to protonate half of the methanol, giving $MeOH_2^+$ + MeOH.

The peak position for the O-C symmetric stretch is $\leq$ 1003 cm^{-1} in Figure 3.4a,

indicating the methanol molecules are either protonated or reacted, and partially or fully solvated by sulfuric acid. In ^{1}H NMR studies of CD_3OH in SA, methanol is completely protonated in a 1:1 mixture and the H-H distance in $CD_3OH_2^+$ is larger than predicted due to hydrogen bonding.[63] Sulfuric acid has two S-(OH) available for H-bonding and perhaps forms a network involving all of the methanol molecules even under the lowest SA concentrations. The O-C symmetric stretch at 1003 cm^{-1} in the 0.5 SA per MeOH reaction system shifts to lower energy with increasing SA concentration due to O-C bond lengthening as it is solvated more fully by SA. The lengthening of the bond decreases the bond polarizability and the peak intensity decreases with increasing SA as well.

AM1 calculations suggest that $CH_3OSO_3^-$ is solvated by 8-9 H_2O molecules.[56] Spectroscopically, this is observed by a change in the position of the vibrational mode affected by the solvation. The solvation of MHS by H_2O was investigated here (data not shown) by monitoring the position of the singly bonded OSO stretching peak with increasing H_2O excess. The position shifts from 765 cm^{-1} for the crystalline compound to 785 cm^{-1} in a solution of 4 or more H_2O molecules per MHS, signifying that one MHS molecule is solvated by four water molecules. The peak position shift is more dramatic in sulfuric acid ($\Delta \sim 40$ cm^{-1}), Figure 3.4b, indicating that SA with MHS form a stronger H-bond network than H_2O with MHS. A smaller shift of 5 cm^{-1} is observed for $DMSO_4$ in SA.

Ab initio 6-31+G** calculations were performed to aid in understanding the differences between the MHS and $DMSO_4$ solvation shifts. The sulfate moiety of $CH_3OSO_3^-$ consists of two doubly bonded oxygens with bond lengths of 1.47-1.48 Å, and a singly bonded oxygen with a bond length of 1.62 Å, in agreement with previous calculations.[56] The HOMO is distributed amongst these three oxygens, rendering the sulfate moiety available to participate in hydrogen bonding with sulfuric acid. In MHS, CH_3OSO_3H, the HOMO is predominately on the two doubly bonded O=S moieties and to a lesser extent on the oxygen bonded to the methyl group as shown in Figure 3.5. The LUMO is on the oxygen of SOH; however, the hydrogen of the SOH may be available for hydrogen bonding to the solvent SA. Again the sulfate moiety is available for hydrogen bonding. Upon solvation, electron density may be transferred from the O=S

bonds of MHS to O—H hydrogen bonds (the MHS oxygen with a SA hydrogen), reducing the electron density around the sulfur atom. The sulfur atom then pulls electron density from the two singly bonded O-S bonds, shortening their length. Spectroscopically, this is observed as a shift to higher energy for the singly bonded OSO ν_s vibration.

These calculations also revealed that the HOMO of $DMSO_4$ is also located on the oxygens of the O=S bonds. However, solvation of $DMSO_4$ by SA is sterically hindered by the presence of two CH_3 moieties, reducing the ability of H_2SO_4 to fully solvate the molecule. This translates as a smaller energy shift for the singly bonded OSO symmetric stretch of $DMSO_4$.

MHS Reaction

Temperature studies were conducted to determine the effect that temperature might have on the extent of reaction, the formation of MHS versus $DMSO_4$, and the effect, if any, on frequency of the product peak. The reaction between MeOH and SA was investigated at –15º C, 23 ºC and 82 ºC.

In the low temperature regime, most relevant to middle and upper tropospheric temperatures, the reaction was followed for a 7 SA : 1 MeOH ratio. The Raman spectra were obtained at several times after the initial mixing and representative spectra are shown in Figure 3.6. Clearly the ~800 cm^{-1} MHS product peak is increasing with time as is the peak at 1044 cm^{-1} due to HSO_4^- in the SA/HSO_4^- complex. The peaks at ~912 cm^{-1} due to the in-phase $S(OH)_2$ stretch and the 1153 cm^{-1} peak due to the ν_s O=S=O decrease with time. These observations are consistent with the formation of MHS and related solvent changes from the MeOH + SA reaction. The singly bonded OSO symmetric stretch peak is observed at a higher frequency than the characteristic $DMSO_4$ peak position (Figure 3.4b), indicating that no $DMSO_4$ is formed. (Detection limits for this instrument are in the micromolar range.)

To determine the extent of reaction between methanol and sulfuric acid for the low temperature study, the area of the singly bonded OSO symmetric stretch peak of known concentrations of MHS in SA was plotted as a function of concentration as a calibration

curve and is shown in Figure 3.7. According to the reaction sequence, water is also produced as a product and is therefore included stoichiometrically in the calibration curve concentrations. The extent of the MHS calibration curve is limited by the solubility of MHS in SA. The concentration of MHS in the reaction mixture is derived by this method. The data shown in Figure 3.8a was obtained at (-15 ± 2) ºC for initial conditions of 7 SA : 1 MeOH. From Figure 3.8a, the MHS yield is determined to be (95 ± 2) % for this low temperature study.

From the low temperature experiment, a rate constant was determined from the data plotted in Figure 3.8a. The rate law used to fit the data has been previously determined[54] and is shown in equation 3.1.

$$\frac{d[ROSO_3H]}{dt} = k[ROH][H_2SO_4][H^+ activity] \qquad (3.1)$$

$$\frac{[MHS]_t}{[MeOH]_t[H_2SO_4]_t} = [H^+ activity]kt \qquad (3.2)$$

Plotting equation 3.2 as a function of time gives a straight line with a slope corresponding to [H^+ activity] multiplied by k. The slope of the line is determined to be 0.0149t + 0.1164. (Forcing the intercept through zero gave a slope of 0.0152t.) The value of [H^+ activity]k is then determined to be 2.48 x 10^{-4} s^{-1}. (Due to the high concentration of the sulfuric acid used in the kinetics studies, the Hammett acidity function cannot be used to determine the activity).[64] Using an activity for H^+ of 7.42[64] produces a rate constant k of 3.4 x 10^{-5} s^{-1}.

This rate constant value is slightly different than other experiments that produced values of 69 x 10^{-7} s^{-1}(mole per 1000g solution)$^{-1}$ in 70.4 wt% SA at 25 ºC[54] and 1.9 x 10^4 s^{-1} using D_2SO_4 at an equivalent of 70.62 wt% SA at 25 ºC.[65] Increasing the equivalent wt% SA to 77.05 wt% increased the rate constant by a factor of five to 9.15 x 10^{-4} s^{-1}.[65] More recently, Knudsen cell studies measured the uptake constants for methanol by SA solutions.[52,53] Kane and Leu[53] measured rate constants of 0.1 – 10 s^{-1} for methanol uptake

at 213 K in 65 – 80 wt% SA solutions. From uptake measurements, Iraci *et al.*[52] determined a maximum rate constant, $k \leq 3 \times 10^{-5}$ s^{-1} for the reaction between methanol and SA at 72.2 wt% SA for temperatures of 197 – 223 K. Differences in surface uptake versus bulk reaction, temperature, experimental technique and/or sulfuric acid concentration may explain the differences in rate constants. Studies using additional low temperature ranges need to be conducted to completely understand this system and thus the impact on middle and upper tropospheric aerosol growth.

The low temperature studies did not reveal evidence for the formation of $DMSO_4$. Room temperature and the high temperature studies were completed as well to further explore the possibility of $DMSO_4$ production. MHS formation was noted by the presence of the singly bonded OSO symmetric stretch peak at ~809 cm^{-1}.

For $DMSO_4$ production, neither the room temperature studies nor the high temperature studies provide evidence for $DMSO_4$ formation (our detection limit was determined to be 683 SA : 1 DMSO4 : 105 H_2O for $DMSO_4$). However, $DMSO_4$ formation is not necessarily expected without the aid of a catalyst. A search of the literature[66,67] gives several patents for the formation of $DMSO_4$, suggesting high temperatures and the addition of dimethyl ether are required.

Surface Studies

To further understand the impact of the reaction of methanol and sulfuric acid as it relates to atmospheric aerosol growth, a surface study with surface tension measurements and sum frequency generation was undertaken. Surface tension data for MeOH + SA, MHS in SA and $DMSO_4$ in SA at varying SA to solute ratios are presented in Figure 3.9. As the SA concentration increases the surface tension measurements tend toward the surface tension of 96.6 wt% SA, suggesting that the alkyl sulfate species are not preferentially segregating to the air-liquid interface particularly at SA : solute ratios greater than 5:1, and that the surface forces resemble that of highly concentrated sulfuric acid. Surface tension measurements of butanol in sulfuric acid-water solutions found similar results and concluded that addition of SA to water suppresses surface segregation of butanol by protonation and conversion to butyl-sulfate species.[60] Also, an ultra-high

vacuum surface study of SA monolayers suggested that propanol segregates into the bulk before undergoing reaction.[68]

Surface vibrational spectroscopy was used to provide insight into the equilibrium surface structures and surface number density. The BBSFG spectrum of the CH region was obtained from the air-liquid interface of neat methanol, MeOH in HCl, $DMSO_4$ and MHS in SA, and the MeOH + SA reaction mixture. The BBSFG spectrum of neat MeOH is consistent with previously obtained spectra.[49] Peaks observed at 2832 cm^{-1} (fit to 2835 cm^{-1}), 2910 cm^{-1} (fit to 2898 cm^{-1}), and 2944 cm^{-1} (fit to 2847 cm^{-1}) are assigned as the CH_3 symmetric stretch, and the two Fermi resonances. Additionally, a small peak at 2980 cm^{-1} is assigned to the CH_3 asymmetric stretch. Methanol at its air – neat methanol interface is somewhat ordered with its methyl groups pointing toward the air phase.[49]

Three peaks are observed for MeOH in HCl at 2840 cm^{-1} (fit to 2843 cm^{-1}), 2920 cm^{-1}, and 2947 cm^{-1} (fit to 2957 cm^{-1}) and are given the same assignments as those for neat MeOH although a fourth peak, the methyl asymmetric stretch, is further shifted to higher energy. Overall, there is a shift to higher energy for MeOH in HCl versus neat MeOH in the BBSFG spectrum shown in Figure 3.10, which is also observed in the Raman spectrum of Figure 3.2b. The blue shift is due to shortening of the CH bonds from protonation of the OH group.

The frequencies for the CH region of MHS, $DMSO_4$, and the MeOH + SA reaction mixture of Figure 3.10 are shifted to higher energy relative to neat MeOH. The spectra of MHS and $DMSO_4$ in SA are similar and the reacted mixture MeOH + SA spectrum is comparable to both, with two observed peaks at 2850 cm^{-1} (fit to 2856 cm^{-1}) and 2968 cm^{-1} (fit to 2970 cm^{-1}). Peaks assignments are consistent with the Raman assignments. The CH_3 asymmetric stretch modes have shifted to higher frequencies relative to neat MeOH and MeOH in HCl.

Polarization BBSFG studies were also conducted to elucidate orientation effects; however, poor signal to noise due to small SFG transition moment strengths for the CH_3 stretching region only allowed an estimate that the CH_3 symmetric stretch transition moment which bisects the CH_3 group is somewhat perpendicular to the surface plane. This is based on the intensity ratio of the ssp to the sps (spectrum not shown here) VSFG

CH_3 symmetric stretching peaks.

There is a decrease in signal intensity of the CH_3 symmetric stretch relative to the higher energy Fermi resonance peak for the MeOH in HCl (1:1), the MeOH + SA (1:2), and the MHS (1:2) and $DMSO_4$ (1:2) relative to neat MeOH (2:1). Normalization of the BBSFG spectra in Figure 3.10 to equalize number density of bulk concentrations reveals interesting changes in the intensity as shown in Figure 3.11a. These observed intensity changes are dissimilar from the Raman spectra in which the intensities were also normalized to number density of the solute. The equalized number density Raman spectrum is shown in Figure 3.11b. In Figure 3.11a, the MeOH in HCl surface spectrum has the highest intensity, which is consistent with increased ordering of protonated surface methanol in addition to charge effects. The reacted mixture of MeOH + SA normalized surface spectrum ((95 ± 5) % conversion to MHS) intensity relative to the neat MeOH normalized surface spectrum is however consistent with the intensity changes observed in the Raman spectrum. The results for the reacted mixture reveal that although the surface tension data suggests that the surface is sulfuric acid-like, the BBSFG data indicates a similar concentration of the MHS from the reaction mixture in the air-liquid interfacial region relative to the bulk.

Recently the charged sulfate headgroup of SDS has been observed using SFG spectroscopy.[39,69] Here, the air-liquid interfacial structure of reaction mixtures of 1 SA: 1 MeOH was investigated in the fingerprint region, Figure 3.12. The ssp spectra reveal the ν_{CO} stretch centered at 1021 cm^{-1}, the ν_{SO_3} at 1082 cm^{-1}, and other peaks between 1100 and 1300 cm^{-1} attributed to sulfate modes. The presence of the CO stretch in the ssp spectrum confirms the finding from the CH stretching region SFG spectra that the O-CH_3 moiety is perpendicular to the air-liquid interface.

Conclusions

Clearly, the reaction of methanol with concentrated sulfuric acid produces MHS with almost complete conversion of available methanol. The MHS product has different physical properties relative to methanol, both in the bulk liquid and at the surface of a

solution mixture. In the 7 SA : 1 MeOH : 1 H_2O system studied extensively here, it is clear that MHS is the end product, while protonated methanol is likely an intermediate species

Peak (cm^{-1}) MeOH[70]	Peak (cm^{-1}) MeOH in HCl	Assignment	Peak (cm^{-1}) 96.6 wt% SA	Assignment
	1003	ν_s O-C of $CH_3OH_2^+$ [58]	417	torsion[71,72]
1034		ν_s O-C	564	S=O_2 rock and bend[71,73,72]
1111	1100	γ CH_3	912	in-phase stretching S-$(OH)_2$ of H_2SO_4[57]
1451		δ_s CH_3	969	ν_{as} S-$(OH)_2$[74]
1470	1461	δ_{as} CH_3	1044	ν_s SO_3 of HSO_4^- in (HSO_4^-)(H_2SO_4) [57]
1544		ν O-C + δ O-H…O	1153	ν_s O=S=O[74]
2835	2851	ν_s CH_3	1369	ν_{as} O=S=O[74]
2920	2912	FR (ν_s CH_3 + 2 δ CH_3)[49]		
2944	2958	FR (ν_s CH_3 + 2 δ CH_3)[49]		
2977		ν_{as} CH_3		
	3009	ν_{as} CH_3		

Peak (cm^{-1}) MHS in SA[75]	Peak (cm^{-1}) $DMSO_4$ in SA[61]	Assignment	Peak (cm^{-1}) 7 SA:1 MeOH	Assignment
414	419	torsion (SA)	419	torsion (SA)
	503	δwag O=S=O ($DMSO_4$)		
565	565	S=O_2 rock and bend (SA)	569	S=O_2 rock and bend (SA)
807	769	ν_s O-S-O ($DMSO_4$, MHS) [75,76]	808	ν_s O-S-O (MHS)
909	910	in-phase S-$(OH)_2$ (SA)	912	in-phase S-$(OH)_2$ (SA)
			995	ν_s O-C (MHS)*
1044	1046	ν_s SO_3 (SA)	1046	ν_s SO_3 (SA)
1164	1158	ν_s O=S=O (SA)	1164	ν_s O=S=O
	1197	ν_s O=S=O ($DMSO_4$)		
1371	1367	ν_{as} O=S=O (SA, MHS* and $DMSO_4$)	1369	ν_{as} O=S=O
			1445	δ_s CH_3 (MHS)
1457	1457	δ CH_3	1459	δ_{as} CH_3 (MHS)
2860	2859	ν_s CH_3	2859	ν_s CH_3 (MHS)
2976	2976	FR (ν_s CH_3 + 2 δ CH_3)*	2975	FR (ν_s CH_3 + 2 δ CH_3)*
3043	3050	ν_{as} CH_3	3047	ν_{as} CH_3 (MHS)

Table 3.1. Raman spectra peak assignments for neat methanol, 96.6 wt% sulfuric acid, methyl hydrogen sulfate in SA, dimethyl sulfate in SA, and the reacted MeOH-SA solution. Symbols used in the table are FR = Fermi resonance, ν = stretch, γ= torsion, and δ= deformation modes. The resolution of the peaks is ± 2 cm^{-1}. * denotes assignment by the authors.

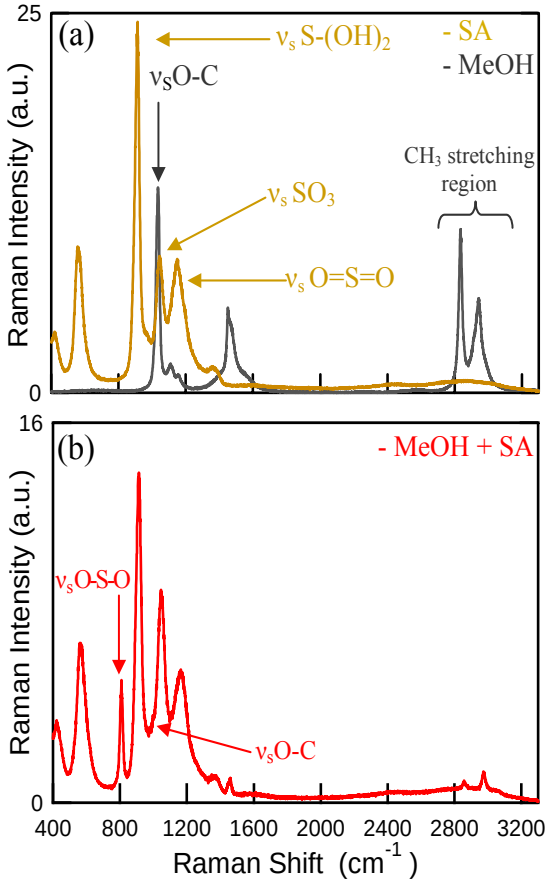

Figure 3.1. Raman spectra of (a) methanol (grey) and sulfuric acid (gold), and (b) the reaction mixture of methanol + sulfuric acid (red).

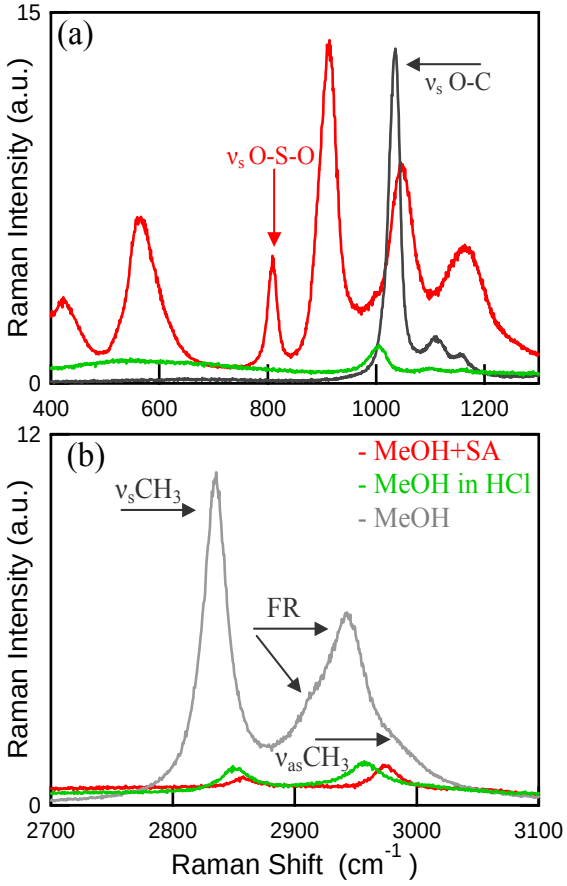

Figure 3.2. Raman spectra of methanol (grey), methanol in HCl (green), and the reacted mixture of methanol + sulfuric acid (red) (a) from 400-1300 cm^{-1} and (b) in the CH_3 stretching region (the methanol spectrum in this region has been reduced by a factor of five).

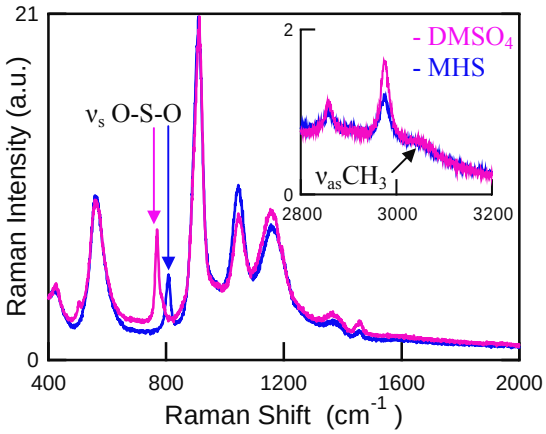

Figure 3.3. Raman spectra of dimethyl sulfate in sulfuric acid (pink), and methyl hydrogen sulfate in sulfuric acid (blue) from 400-2000 cm^{-1} and in the CH_3 stretching region (inset).

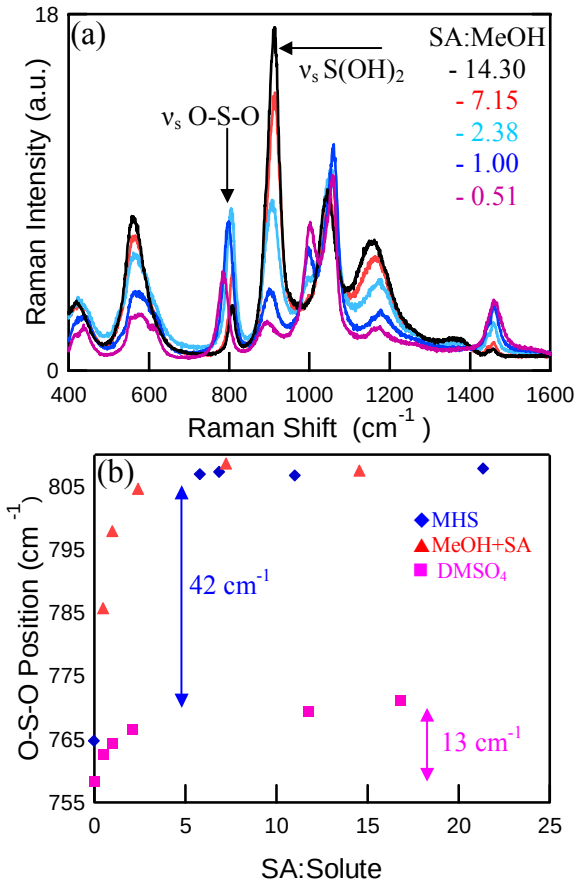

Figure 3.4. Raman spectra of (a) methanol + sulfuric acid reaction mixtures for various concentrations and (b) the position of the singly bonded OSO symmetric stretch as a function of the ratio of sulfuric acid molecules to solute molecules.

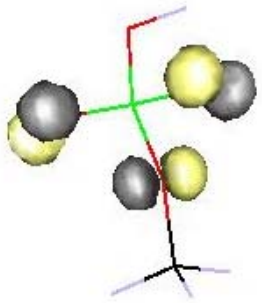

Figure 3.5. Ab Initio 6-31+G** calculation schematic of the HOMO of methyl hydrogen sulfate.

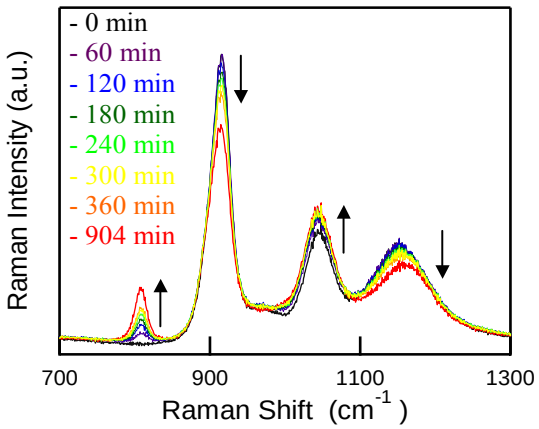

Figure 3.6. Raman spectra of methanol + sulfuric acid over time (7 SA : 1 MeOH: 1 H_2O at -15 ºC).

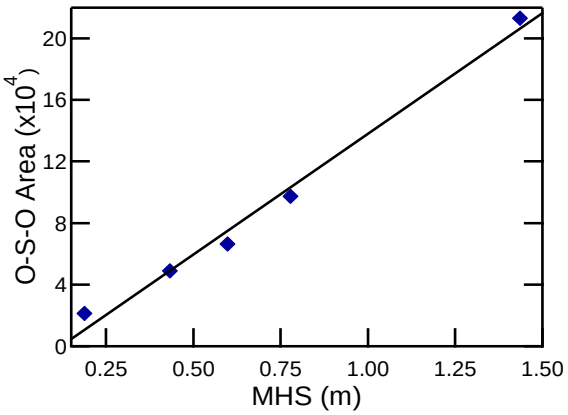

Figure 3.7. Methyl hydrogen sulfate in sulfuric acid (calculated in molality), the singly bonded OSO symmetric stretch (at ~800 cm^{-1}) peak area as a function of concentration (blue diamonds).

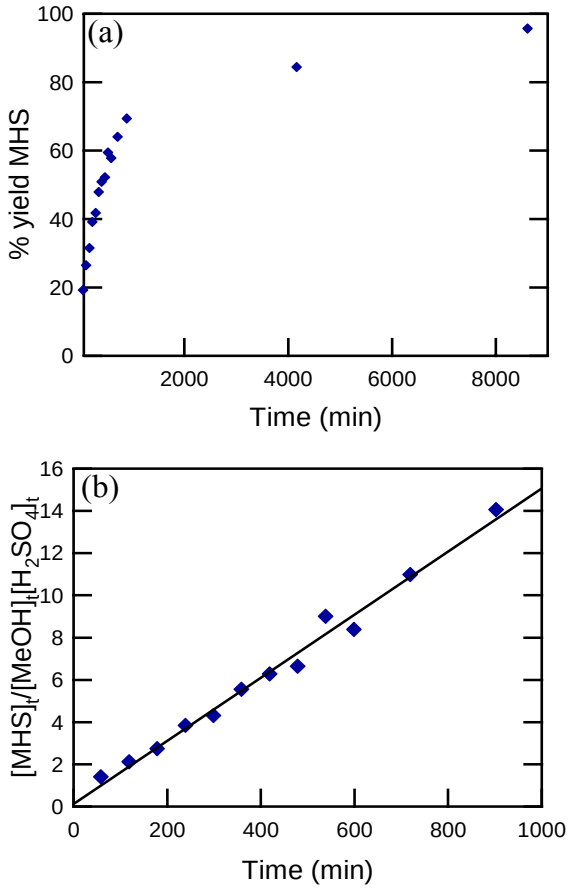

Figure 3.8. a) Plot of the % yield of methyl hydrogen sulfate as a function of time. The data begins at t = 60 min. b) Plot of $[MHS]_t/[MeOH]_t[H_2SO_4]_t$ versus time (min). The slope of the line corresponds to $[H^+$ activity] k.

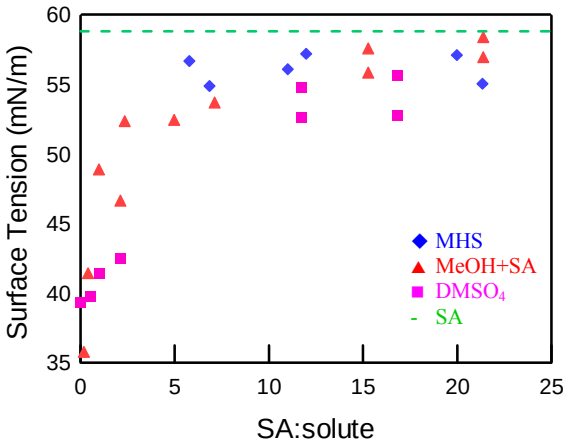

Figure 3.9. Surface tension measurements of methyl hydrogen sulfate in sulfuric acid (blue diamonds), dimethyl sulfate in sulfuric acid (pink squares), and reaction mixture of methanol + sulfuric acid (red triangles). The surface tension of 96.6 wt% sulfuric acid is shown as a green dotted line.

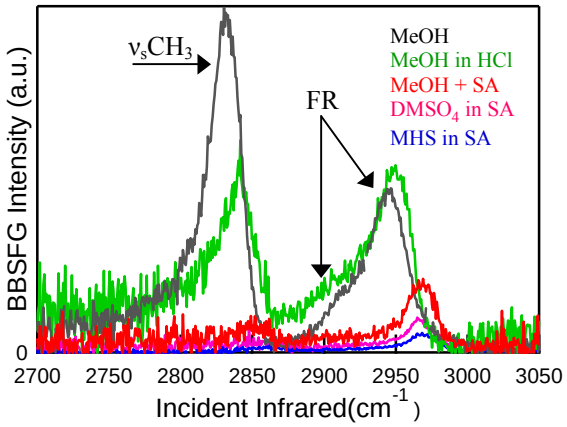

Figure 3.10. BBSFG spectra of methanol reduced by a factor of three (grey), methanol in HCl (green), the reacted mixture of methanol + sulfuric acid (red), methyl hydrogen sulfate in sulfuric acid (blue), and dimethyl sulfate in sulfuric acid (pink) in the CH_3 stretching region.

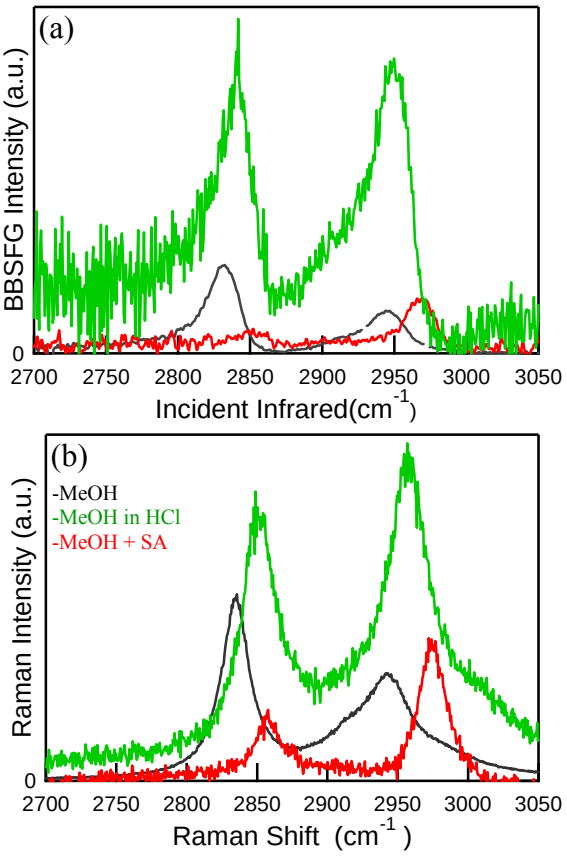

Figure 3.11. Spectra normalized to equalize the number of solute molecules in order to compare spectral intensities, a) BBSFG surface spectra, b) Raman spectra from the bulk solution.

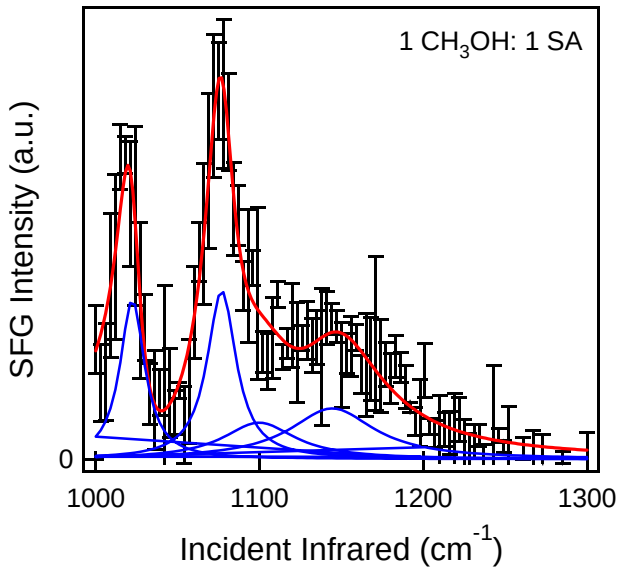

Figure 3.12. SFG ssp polarization spectra of MeOH + SA in the fingerprint region of a 1 SA: 1 MeOH mixture. The original spectrum is shown as black data points with error bars, the overall fit is shown in red, and the component peaks are shown in blue.

CHAPTER 4

UPTAKE AND SURFACE REACTION OF METHANOL BY SULFURIC ACID SOLUTIONS INVESTIGATED BY VIBRATIONAL SUM FREQUENCY GENERATION AND RAMAN SPECTROSCOPIES

Introduction

The uptake of small oxidized organics such as methanol by sulfate aerosols may be a mechanism for aerosol growth[1] and may affect the properties of atmospheric aerosols.[7] In this chapter the uptake of methanol by sulfuric acid (SA) solutions ranging from 0 to 96.5 wt% is investigated. First the uptake at the air-liquid interface of SA solutions was investigated using vibrational sum frequency generation spectroscopy (VSFG). The diffusion of methanol into sulfuric acid solutions was monitored using Raman spectroscopy. Finally, the detection limit of methyl hydrogen sulfate (MHS) in SA solutions was determined.

Chemical abbreviations used in this chapter are MeOH (methanol), MHS (methyl hydrogen sulfate), and SA (sulfuric acid). MHS is used to refer to both protonated (CH_3OSO_3H) and unprotonated ($CH_3OSO_3^-$) methyl sulfate. In addition, vibrational sum frequency generation (VSFG), broad bandwidth SFG (BBSFG), symmetric stretch (ss), asymmetric stretch (as), and Fermi resonance (FR) are used.

Experimental

BBSFG Instrumentation and Experimental Details

The spectral window of the IR pulse was ~ 330 cm^{-1} in the C-H stretching region for these experiments. The energy of the 800 nm beam used was 400 μJ, and the IR energy in the C-H stretching region was 1.0 μJ at the sample.

The polarization combination used in this chapter is ssp. The ssp-polarized spectra were obtained continuously with a one-minute acquisition time. Thirty spectra were collected for each uptake experiment. A background spectrum was obtained by changing the temporal overlap of the 800 nm and IR beams. The VSFG spectra are normalized against a smoothed (Savitzky-Golay, 2^{nd} order, 11 points) nonresonant VSFG spectrum from a GaAs crystal to remove any structure present in the IR pulse profile.

Raman Spectroscopy

Raman spectra were obtained using 150 mW from a 785 nm continuous wave laser (Raman Systems Inc.). In the uptake experiments, spectra were collected as the average of three thirty-second exposures every ten minutes for several hours with a liquid nitrogen-cooled CCD camera (Roper Scientific, LN400EB, 1340 x 400 pixel array, back-illuminated and deep depletion CCD). The laser shutter is controlled electronically (Princeton Instruments, ST-133 Controller) to only open during collection to prevent sample heating during the experiment. For the protonation experiments the laser shutter was opened manually and spectra were collected as the average of three one-minute exposures.

FTIR Spectroscopy

A Thermo Nicolet FTIR spectrometer (Avatar 370, Thermo Electron Corporation) was employed to determine the concentration of methanol in the flow experiments. The N_2/MeOH mixture flowed at 25 standard cubic centimeters per minute (SCCM) into an open-ended cell placed in the FTIR sample compartment. Spectra were collected with a spectral resolution of 4 cm^{-1} and 200 scans. A background spectrum was taken and subtracted from each sample spectrum. The concentration of methanol was determined by

FTIR using the absorbance of the ν_{CO}-ss at 1052 cm^{-1} with equation 4.1.[77]

$$T=\exp[-kc_m l] \quad (4.1)$$

T is the infrared transmission. The molar naperian absorption coefficient, k (cm^2/mole), is calculated according to equation 4.2. The concentration of methanol is c_m. The pathlength, l, was determined to be 22.86 cm.

$$k = \frac{SN_A}{\Delta \nu} \quad (4.2)$$

The absorption line intensity, S, for methanol is 3.77 x 10^{-20} cm^{-1}/(molecule cm^{-2}) at 1052.16845 cm^{-1}.[78] N_A is 6.022 x 10^{23} $mole^{-1}$ and $\Delta\nu$ is assumed to be 0.1 cm^{-1}.[77] The concentration of methanol, c_m, with a N_2 flow rate of 25 SCCM was determined to be (2.2 ± 0.2) x 10^{-7} mol/cm^3 or (1.3 ± 0.1) x 10^{17} molecules/cm^3.

Chemicals

Methanol (HPLC Grade, Fisher Scientific), sulfuric acid (redistilled, 96.5wt%, GFS), ammonium hydrogensulfate (98%, Aldrich), and nitrogen gas (N.F.) were used as received. Deionized water was obtained from a Millipore Nanopure system (18.1-18.2 MΩ•cm).

The sulfuric acid solutions were prepared by diluting 96.5 wt% sulfuric acid with deionized water. The concentrations used in the Raman uptake experiments were (79.3 ± 0.3) wt%, (61.6 ± 0.1) wt%, and (39.2 ± 0.1) wt%. For the SFG uptake experiments the SA solution concentrations were (80.5 ± 0.1) wt%, (57.24 ± 0.02) wt%, and (42.2 ± 0.5) wt%. The difference in SA concentrations used in the VSFG versus the Raman experiments is due to variations in subsequent solution preparations. The concentrations were determined to ± 0.1 wt% by titration with a standardized sodium hydroxide solution. To prepare the ammonium bisulfate solution the salt was dissolved in deionized water and filtered twice through a carbon filter (Carbon-Cap 75, Whatman). The concentration (0.78 ± 0.1 M) was determined spectroscopically using the sulfate vibrational mode at 985 cm^{-1}.

Uptake experiments

In the SFG uptake experiments nitrogen is bubbled into methanol at a flow rate of 25 SCCM (Mass Flow Controller 1479A51CS1BM, powered by PRF4000-F2VIN, MKS Instruments). A three-way valve connects the N_2/MeOH mixture flow to the experimental cell (made of Teflon) and to an exhaust line. Prior to the start of an experiment, the mixture flows to the exhaust line. The mixture is allowed to flow into the cell for the duration of the experiments. Between SFG uptake experiments, the N_2 line is connected directly to the cell for 10 minutes to flush the cell of any gaseous species. In the Raman uptake experiments, the three-way valve is not used, and instead, the N_2/MeOH mixture (MeOH concentration of $(1.3 \pm 0.1) \times 10^{17}$ molecules/cm^3) is connected directly to the cell. The Raman probe is placed 3.5 mm below the solution surface. Spectra were reproduced several times over a period of 18 months. All experiments were conducted at room temperature (23±2 °C).

Results and Discussion

A previous study by the authors investigated the reaction between methanol and 96.6 wt% sulfuric acid (SA) to form methyl hydrogen sulfate (MHS).[42] The experiments were performed by mixing the two reactants together and taking the SFG or Raman spectrum of the mixture. Here the formation of MHS or protonated methanol is investigated in lower wt% SA solutions in real time. Previous investigations by others[52,53] of the uptake of methanol by sulfuric acid solutions were performed using mass spectrometry to monitor changes in the gas-phase methanol concentration. Using VSFG we are able to monitor spectral changes at the air-liquid interface of the sulfuric acid solutions to determine the methanol species (MeOH, $MeOH_2^+$, or MHS) present at different SA concentrations.

VSFG experiments

The ssp polarization VSFG spectra of the uptake of methanol at the surface of SA solutions are shown in Figure 4.1 (a-d). One-minute spectra were acquired continuously during the surface uptake experiments. Figure 4.1e shows the SFG spectra obtained after

the N_2/MeOH flow was stopped and the cell lid was removed. Also shown in Figure 4.1e are the VSFG spectra with water and 0.78 M ammonium bisulfate since methanol was observed at the surface after the uptake experiment, although no peaks were observed during the flow experiment. In Figure 4.1 (a-d) it is observed that peaks attributable to MeOH or MHS were first detectable after 4 to 6 minutes. No further increase in VSFG signal intensity was observed after 14 to 16 minutes, suggesting that the surface is fully saturated with MeOH or MHS molecules.

There are three vibrational modes observed in the CH region of the aqueous methanol VSFG spectrum in Figure 4.1e, the ν_{CH_3}-ss at 2843 cm^{-1}, and two Fermi resonances (FR) at 2925 cm^{-1} and 2953 cm^{-1}, in agreement with previous VSFG studies.[49,79,80] The observed peak positions change with changing SA concentration due to speciation (MeOH, $MeOH_2^+$, MHS). The peak positions in each SA solution are found in Table 4.1. For each of the four sulfuric acid concentrations investigated (Figure 4.1a-d), no shifts from the initial peak positions are observed during the flow experiments. However, there are differences in peak positions between SA solutions, as is seen in Figure 4.1 (a-e). The peak positions shift to higher wavenumber with increasing SA concentration. Again, in aqueous solution the methanol ν_{CH_3}-ss and FR are found at 2843 and 2954 cm^{-1}, respectively. These two peaks are centered at the same positions in 0.78 M NH_4HSO_4. This lack of shift in alcohol peak position from water to ammonium bisulfate has also been observed for butanol and hexanol.[81] In the four SA solutions investigated, the two peaks blueshift from the positions in water by 9 and 18 cm^{-1}. These shifts indicate that new methyl species must be present in more concentrated SA. In our previous investigation, the VSFG spectrum of protonated methanol, $CH_3OH_2^+$, showed a shift in the ν_{CH_3}-ss to 2851 cm^{-1},[42] consistent with the shift observed here from 0 wt% (water) to 42.2 wt% SA. In the more concentrated SA solutions, methanol and sulfuric acid are also reacting to form methyl sulfate. This is observed as an increase in intensity of the peak observed at 2972 cm^{-1}, attributed to the ν_{CH_3}-ss of MHS.[75] The spectrum in 96.5 wt% SA is in agreement with our previous investigation of the formation of methyl sulfate in concentrated SA.[42]

Because the peak positions in Figure 4.1(a-d) are not changing during each flow experiment, the reaction between methanol and sulfuric acid is occurring under the spectral acquisition time of 60 seconds at the air-liquid interface. The first detectable signal occurs in the 4-minute spectrum (3-4 minute spectrum, 60 second signal accumulation), and using an estimated diffusion coefficient of 1 x 10^{-6} cm^2/s (see Chapter 3) for methanol, MeOH can travel a total of 200 nm into the bulk solution. During this time, it may be possible for a reaction to occur in the bulk (up to 100 nm depth), and the reacted species to return to the surface. However, if the reaction was occurring on a similar time scale as our signal collection, we would observe broadening and blue shifting of the peaks relative to those of methanol. This is not observed. Therefore, the reaction of MeOH is occurring at the SA solution surface.

The relative peak intensities in Figure 4.1(a-d) also change with increasing SA concentration. The relative peak intensities are noticeably different for the water, NH_4HSO_4, and 42.2 wt% SA solutions from the more concentrated SA solutions. In the water, NH_4HSO_4, and 42.2 wt% SA solution spectra in Figure 4.1e, the peaks at 2843 and 2955 cm^{-1} have similar intensities, consistent with the VSFG spectra of methanol in water[49,79,80] and in HCl.[42] In the more concentrated solutions, the peak present at 2970 cm^{-1} is more intense than the one at 2854 cm^{-1} again confirming that the surface methyl species is changed from MeOH to $MeOH_2^+$ and MHS. This reversal in relative intensities was previously noted for methyl sulfate in 96.5 wt% SA.[42,44]

Raman experiments

The complementary flow experiments monitoring the uptake of methanol or methyl sulfate into the SA solutions were performed using Raman spectroscopy. The Raman spectra were collected as one-minute acquisitions every ten minutes during the uptake experiments. The spectra showing the uptake of methanol into the SA solutions are shown in Figure 4.2 (a-e). The uptake of methanol into water was monitored by the appearance of the ν_{CO} at 1020 cm^{-1}, Figure 4.2b. The appearance of the ν_{OSO}-ss at 790 cm^{-1} was monitored for the appearance of MHS in 96.5 wt% SA, Figure 4.2a. Because of the overlap of SA peaks with the MeOH C-O stretch, the uptake of MeOH into 39.2,

61.1, and 79.7 wt% SA was monitored in the CH stretching region (2700-3100 cm^{-1}) where no SA peaks are observed, Figure 4.2 (c-e). It is important to note that the peaks appear at much later times in the Raman spectra than in the SFG experiments. The SFG experiments were conducted on a time scale of minutes while the Raman experiments were done over several hours. Unlike for the surface-uptake experiments, the peak intensities in the bulk solutions continued to increase.

As in the surface uptake experiments, the peak positions in each solvent do not shift with time, Figure 4.2, suggesting that the methyl species present in each solvent do not appear to change during the course of the experiments. From the SFG experiments, it appears that the reaction is occurring at the interface and then the surfaces species must diffuse into the bulk. (Details of methanol diffusion experiments are found in Chapter 5). The peak shifts and changes in relative intensities are the same as those observed in the SFG experiments. This indicates that the species present in each solution are the same at the air-liquid interface and in bulk solution.

Protonation versus Reaction

The degree of protonation and esterification of methanol in 47.1 to 68.3 wt% SA were calculated using a pK_{BH^+} of -2.05.[82] (After the work presented in Chapter 1 was published, it came to our attention that a pKa of -4.86 is much lower than the typical values expected for alcohols. The experiments presented in reference 82, with pKa's of ~2 are more accepted in the organic chemistry community. However, the value of -4.86 for $MeOH_2^+$ is still found in the literature.) To calculate the extent of MHS formation in 47.1 to 68.3 wt% SA solutions at equilibrium, values for K_{eq} were determined by plotting the known values of K_{eq}[54] as a function of wt% SA. In the Raman spectra of equilibrium mixtures of methanol in 47.1 to 68.3 wt% SA presented in Figure 4.3a, the formation of methyl sulfate is detected by the appearance of the ν_{OSO}-ss at 790 cm^{-1}. Figure 4.3b shows the ν_{OSO}-ss region expanded to better determine the first appearance of ν_{OSO}-ss. Mass balance calculations indicate that in 47.1 wt% SA there is 11 % methyl sulfate, Table 4.2. In 51.4 wt% SA, 13.6 % of the methyl species is MHS. Since the ν_{OSO}-ss is not easily visible in the 47.1 wt% SA solution, the detection limit of MHS using Raman

spectroscopy is determined to be 11-14.2%.

It is also of interest to examine any changes in the CH stretching region that occur with increasing wt% SA and methyl sulfate formation, Figure 4.3c. With increasing wt % SA (and increasing methyl sulfate formation), the MeOH ν_{CH_3}-ss at 2850 cm^{-1} decreases in intensity. The decrease in intensity (23%) of the 2850 cm^{-1} peak from the 47.1 wt% solution to the 68.3 wt% SA solution is consistent with the observed decrease in MeOH fraction. With increasing MHS formation, the peaks in the CH stretching region shift to higher wavenumber, Figure 4.2 (c-e). The increase in intensity in the peaks observed at 2970 and 3015 cm^{-1} is due to the appearance of the MHS ν_{CH_3}-ss attributed to the increase in MHS concentration, with a MHS ν_{CH_3}-ss centered at 2970 cm^{-1}. These findings suggest that in atmospheric aerosols containing 60+ wt% SA, 20% of the methanol that adsorbs to the surface will be transformed into the much less volatile species, MHS. Only fresh, highly acidic aerosols will be expected to experience aerosol growth from the uptake of methanol.

Conclusions

In this study, the uptake of methanol both at the surface of and into water and sulfuric acid solutions was observed directly using VSFG and Raman spectroscopies. The surface spectra remain unchanged on the timescale of the uptake experiments. Contributions from MeOH, $MeOH_2^+$, and MHS are observed at the intermediate SA concentrations at the surface and in the bulk. Uptake of methanol by SA solutions is limited by diffusion of the methyl species into the solutions. Surface saturation occurs, and for high SA concentrations, the reaction between methanol and sulfuric acid takes place at the air-liquid interface.

SFG			Raman		
	MeOH ν_{CH_3}-ss and MHS FR (cm^{-1})	MeOH FR and MHS ν_{CH_3}-ss (cm^{-1})		MeOH ν_{CH_3}-ss and MHS FR (cm^{-1})	MeOH FR and MHS ν_{CH_3}-ss (cm^{-1})
96.5 wt%	2858	2972			
80.5 wt%	2854	2967	79.7 wt%	2855	2969
57.2 wt%	2851	2960	61.6 wt%	2856	2961
42.2 wt%	2846	2957	39.2 wt%	2851	2959
0 wt% (Water)	2843	2954			
0.78 M NH_4HSO_4	2843	2954			

Table 4.1. Observed peak positions for two peaks in the SFG ssp spectra and Raman spectra.

wt % SA	% MeOH	% $MeOH_2^+$	% $MeOSO_3$-/$MeOSO_3H$
47.1	76.2	12.4	11.4
51.4	70.8	14.9	14.2
54.5	66.9	17.1	16.0
58.4	62.0	20.3	17.8
61.5	58.1	23.0	19.0
64.7	54.1	26.1	19.8
68.3	49.6	29.9	20.4

Table 4.2. The calculated equilibrium distribution of methyl species in 47.1 – 68.3 wt% SA solutions.

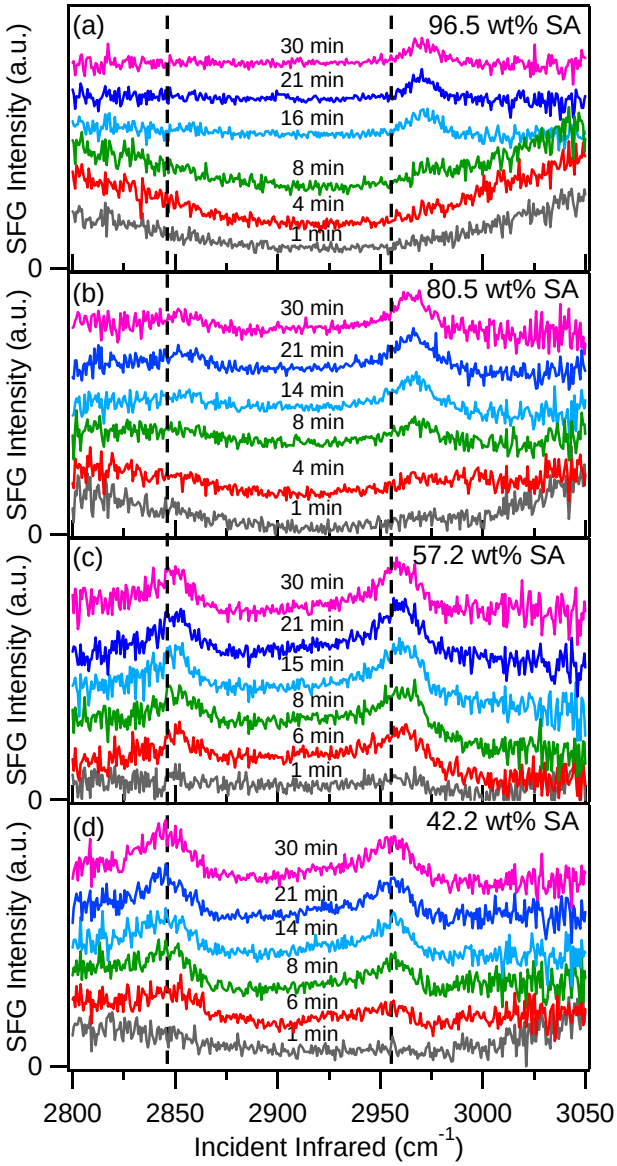

Figure 4.1. VSFG spectra of the uptake of methanol at the surface of 42.2 to 96.5 wt% SA solutions. (a) – (d) Changes in the air-liquid interface spectra with time. (e) The spectra of the solution air-liquid interfaces after the experiment with the cell lid removed. The spectra are offset for easier viewing.

Figure 4.1. Continued

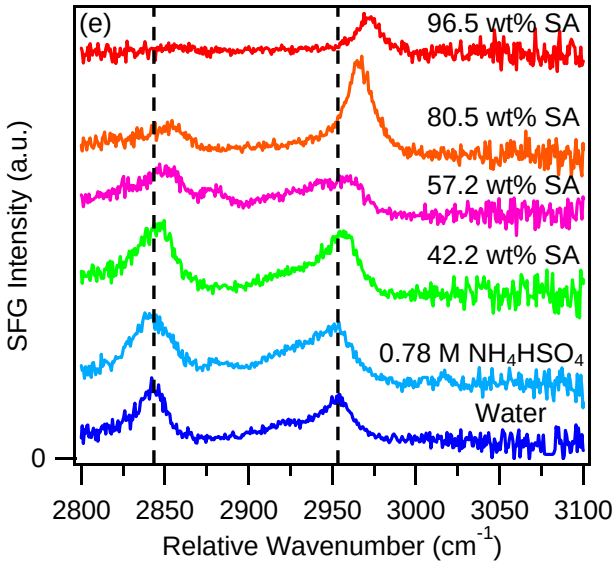

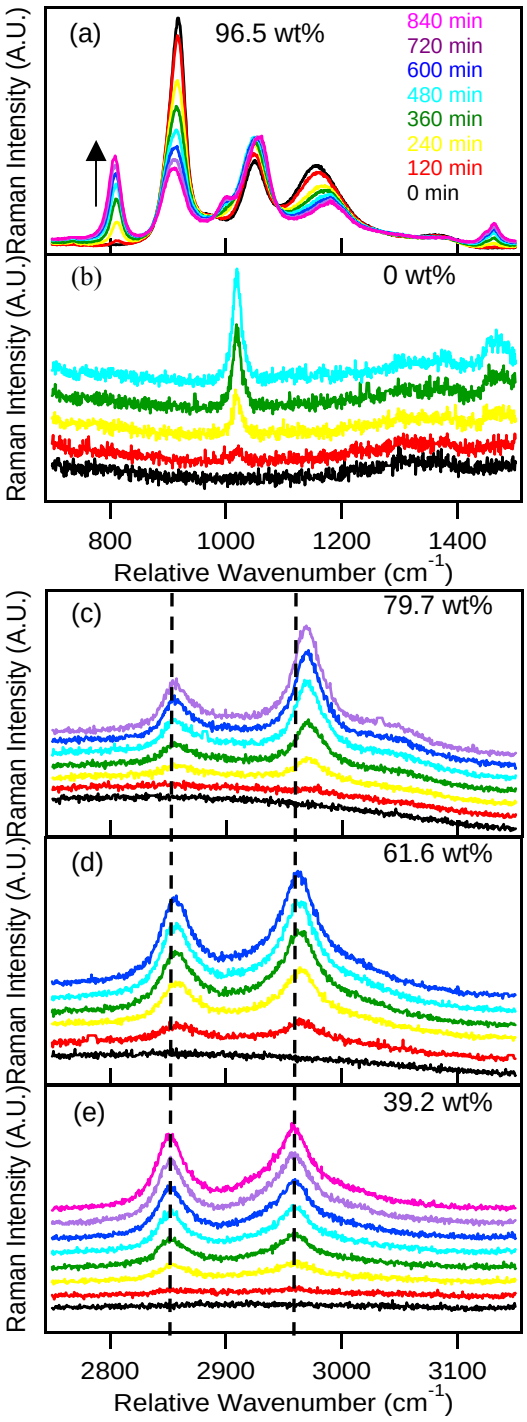

Figure 4.2. Raman spectra of the uptake of methanol into sulfuric acid solutions. The uptake is observed by (a) the appearance of the ν_{OSO}-ss of MHS at 790 cm^{-1}, (b) the appearance of the ν_{CO} of MeOH at 1020 cm^{-1}, and (c-e) the appearance of peaks in the CH_3 stretching region. Figures (b-e) are offset for easier viewing.

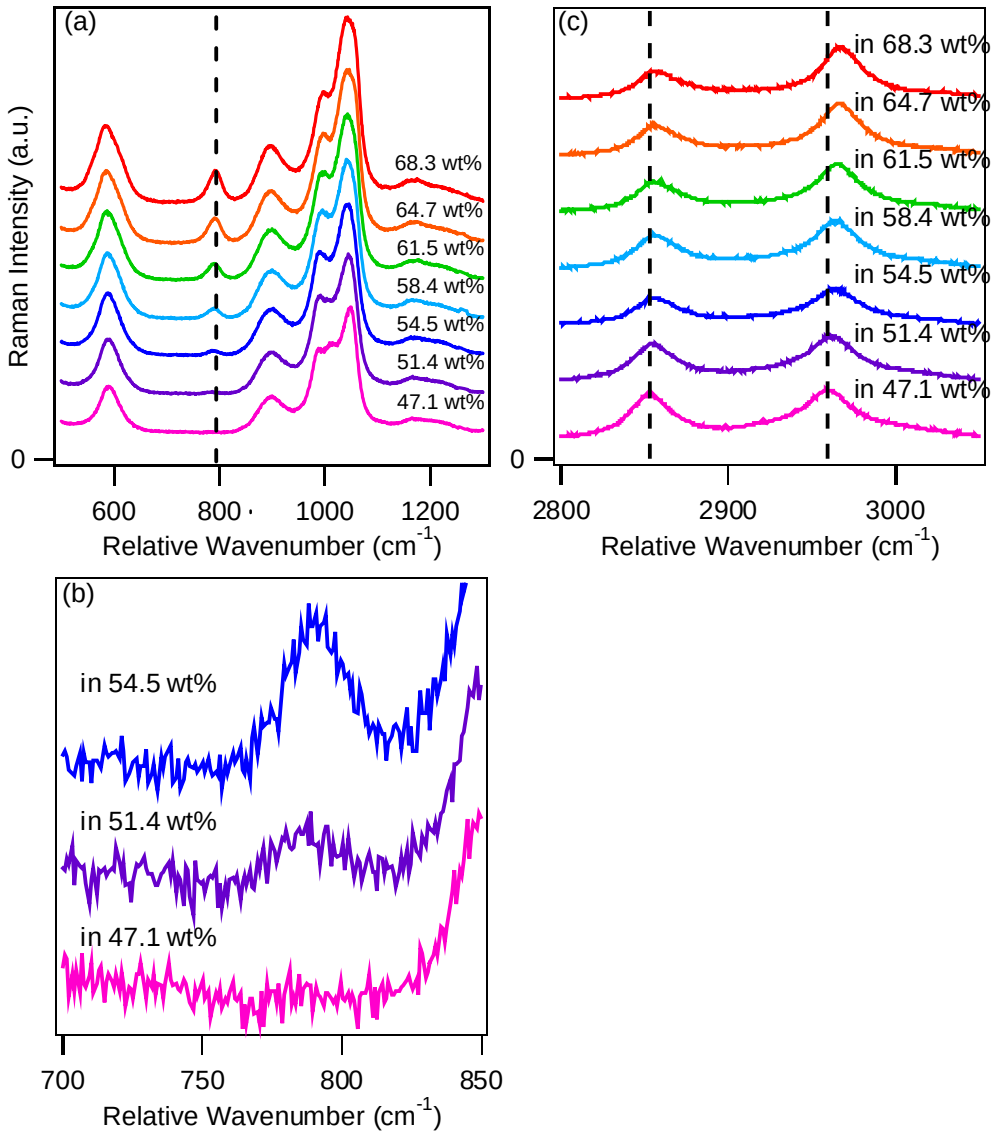

Figure 4.3. Raman spectra of methanol-SA mixtures at equilibrium in (a) the 400-1400 cm^{-1} region. In (b) the 700 – 850 cm^{-1} region is enlarged to highlight the appearance of $\nu_{O\text{-}S\text{-}O}$-ss. In (c) the CH stretching region (2800-3050 cm^{-1}) is shown.

CHAPTER 5

DIFFUSION COEFFICIENTS OF METHANOL INTO SULFURIC ACID SOLUTIONS MEASURED BY RAMAN SPECTROSCOPY

Introduction

The diffusion of volatile species into atmospheric aerosols containing sulfuric acid (SA) is an important part of chemical processing that occurs in the atmosphere. The rate of uptake and solubility of gaseous species are parameters that require consideration in aerosol chemistry.[83] Slower diffusion will limit the uptake of reactants from the aerosol surface to the bulk, reducing the scavenging ability of the aerosol.[84]

Currently, there are few measured diffusion coefficients for species of atmospheric importance into sulfuric acid solutions.[84-86] In this chapter we present diffusion coefficients for methanol in 0 – 96.5 wt% sulfuric acid solutions obtained using Raman spectroscopy. The measurements were done by continually flowing methanol vapor in $N_{2(g)}$ over the solution, keeping the surface concentration constant. The viability of the method was confirmed by measuring the diffusion coefficient of methanol into water and comparing the result with values found in the literature. While the experiments presented here are performed at 295 K, the experimental design will lend itself to colder temperatures, allowing diffusion coefficients to be determined at tropospheric and stratospheric temperatures.

Experimental Section

Chemicals

Methanol (HPLC Grade, Fisher Scientific), sulfuric acid (redistilled, 96.5wt%, GFS), and nitrogen gas (N.F. standard) were used as received. Deionized water was obtained from a Millipore Nanopure system (18.1-18.2 MΩ•cm).

The SA solutions were prepared by diluting 96.5 wt% SA with deionized water. The concentrations were determined by titration with a standardized sodium hydroxide solution to ± 0.1 wt%. The concentrations used in the Raman uptake experiments were (79.3 ± 0.3) wt%, (61.6 ± 0.1) wt%, and (39.2 ± 0.1) wt%.

A Thermo Nicolet FTIR spectrometer (Avatar 370, Thermo Electron Corporation) was employed to determine the concentration of methanol in the flow experiments. The N_2/MeOH mixture flowed at 25 standard cubic centimeters per minute (SCCM) into an open-ended cell placed in the FTIR sample compartment. Spectra were collected with a spectral resolution of 4 cm^{-1} and 200 scans. A background spectrum was taken and subtracted from each sample spectrum. The concentration of methanol was determined by FTIR using the absorbance of the ν_{CO}-ss at 1052 cm^{-1}.[87] The concentration, c, with a N_2 flow rate of 25 SCCM was determined to be to be (1.3 ± 0.1) x 10^{17} molecules/cm^3.

Experimental setup

The experimental setup used is shown in Figure 5-1. The cell contains a space for a petri dish filled with the appropriate solution. The dish has a surface area of 19.63 cm^2. Nitrogen is bubbled into methanol at a flow rate of 25 SCCM (Mass Flow Controller 1479A51CS1BM, powered by PRF4000-F2VIN, MKS Instruments).The N_2/MeOH flows into the cell above the solution surface. An exit valve is located across the cell from the inlet. The flow is constant for the duration of the experiment.

The Raman probe is inserted in the side of the cell and rests against the dish wall. By rotating the probe in its holder, the probe depth is varied. In these experiments, the probe depths varied between 1.5 mm and 8.5 mm below the surface. The majority of the experiments were conducted at a probe depth of 3.5 mm.

Raman spectra were obtained using 150 mW from a 785 nm continuous wave laser (Raman Systems Inc.) The backscattered light was collected by a fiber optic probe

(InPhotonics) coupled to the entrance slit of a 500 mm monochromator (Acton Research, SpectraPro 500i), using a 600 groove/mm grating blazed at 1 μm. The slit width was set at 50 μm and the bandpass was 4 cm^{-1} for the SA solution experiments. The slit width was set at 100 μm and the bandpass was 5.5 cm^{-1} for the water experiments. Spectra were acquired every ten minutes as the average of three thirty-second spectra.

Recently, methods developed with Raman spectroscopy have been used to determine diffusion coefficients.[88] By using a vibrational mode that is unique to the diffusing species, its concentration can be followed as a function of time and the diffusion coefficient can be obtained. Peaks that had minimal overlap with sulfate vibrational modes were used. The uptake of MeOH into water was monitored using the C-O symmetric stretch present at 1020 cm^{-1}. The uptake of MeOH into 96.5 wt% SA was monitored using the O-S-O symmetric stretch present at 800 cm^{-1}. Due to overlapping of sulfate modes with the CO stretch of MeOH, the CH_3 stretching region (2800 and 3200 cm^{-1}) was used to monitor the uptake of MeOH into 39.2 to 79.3 wt% SA solutions.

Methanol vapor is passed over the solution in a carrier gas, N_2. Previously, we investigated the uptake of methanol at the surface of SA solutions by sum frequency generation spectroscopy.[87] Saturation of the surface spectra was observed after fifteen minutes of methanol flow. By flowing methanol into the cell during the entire experiment, the surface concentration remains constant, ensuring that gas-phase diffusion is not a limiting factor. Tests were done using different N_2 flow rates (25 – 100 SCCM) to confirm that the liquid-phase diffusion was independent of the gas flow rate.

In the uptake experiments, spectra were collected as the average of three 30-second exposures every ten minutes for several hours with a liquid nitrogen-cooled CCD camera (Roper Scientific, LN400EB, 1340 x 400 pixel array, back-illuminated and deep depletion CCD). The laser shutter is controlled electronically (Princeton Instruments, ST-133 Controller) to only open during collection to prevent sample heating during the experiment. Calibration of the CCD camera was completed using the 435.833 nm line from a fluorescent lamp. Acquiring a spectrum of crystalline naphthalene and comparing the experimental peak positions with the accepted literature values completed calibration of the wavenumber position for each set of experiments.[51] The diffusion into water

experiments were conducted at (24 ± 1 °C) and the SA experiments were conducted at room temperature (23 ± 2 °C).

Spectra are fit using the software package IgorPro 4.05. To determine the peak areas, the spectra are fit with Voigt line shapes using the IgorPro multipeak fitting function with the baseline subtraction enabled. Care was taken to keep the Voigt shape similar in each fitting routine.

Results and Discussion

To date, only a few reports of measured diffusion coefficients for atmospherically relevant species in sulfuric acid solutions are found in the literature.[84-86] These values are necessary for understanding the processing of atmospherically relevant chemical species by aerosols. By choosing the correct solution to Fick's second law for the experimental setup the diffusion coefficient can be extracted by fitting concentration versus time data. Fick's second law, equation 5.1, relates the change in concentration, c, as a function of time, t to the changing concentration gradient, $\partial c/\partial z$. They are related through D, the diffusion coefficient (cm^2/s).

$$\frac{\partial c}{\partial t} = D\frac{\partial^2 c}{\partial z^2} \tag{5.1}$$

For the experimental setup used in these experiments (diffusion into a finite slab) the boundary conditions are:

2. c=0 for 0<z<L
3. $c=c_0$ for z=0
4. $\partial c/\partial z=0$ at z=L
5. z=L for t>0

With these boundary conditions, the solution to equation 5.1 for the experiments presented in this chapter is that for one-dimensional diffusion into a finite slab with one open boundary, equation 5.2.[89,90]

$$c = c_0\{1 - \frac{4}{\pi}\sum_{\nu=0}^{\nu=\infty}\frac{1}{2\nu+1}\sin\frac{(2\nu+1)\pi x}{2L}\exp[-(\frac{(2\nu+1)}{2L}\pi)^2 Dt]\} \tag{5.2}$$

In equation 5.2, c is the concentration, c_0 is the surface concentration, ν is an integer, L is the solution thickness (cm), and x is the probe position beneath the surface (cm), and t is time (seconds). D is assumed to be independent of concentration. It was determined that six terms were required to fit the data properly (ν=6). (The peak area versus time data was also fit with ten terms with no improvement in the fit.)

Raman spectroscopy is a quantitative method so the solute concentration is proportional to the measured peak area. Therefore, peak area was used to avoid additional error being introduced by the conversion to concentration. The peak area versus time data was fit with equation 5.3, where A is the peak area and A_0 is the surface peak area, and six terms were used.

$$A = A_0 \{1 - \frac{4}{\pi} \sum_{\nu=0}^{\nu=6} \frac{1}{2\nu+1} \sin \frac{(2\nu+1)\pi x}{2L} \exp[-(\frac{(2\nu+1)}{2L}\pi)^2 Dt]\} \qquad (5.3)$$

The derivation of equation 5.2 is found in Appendix B. The user-defined fitting function used to extract the diffusion coefficients from the area versus time data is also found in Appendix B. In the fitting, the function requires user input for the following parameters: the diffusion coefficient, D, the surface peak area, the probe depth (held constant), and the solution thickness (held constant). Ideally, the peak used in the analysis would not have interference from solvent peaks. To minimize the error in the measured peak area, the most intense peak for MeOH or MHS was used. The methyl species present in the solution have several Raman-active vibrational modes and so it was necessary to confirm that for a given experiment, using different peaks did not result in different values for the diffusion coefficient. In all experiments, the most intense peak available was used.

Different probe depths were tested for both the diffusion of MeOH into water and into 96.5 wt% SA. Figure 5.2 shows the fitted diffusion curves of MeOH into water for two different probe positions x=0.35 and x=0.63 cm. The diffusion curves with fits are also shown for both the nCO-ss and nCH_3-as peaks monitored at a probe depth of 0.35 cm in Figure 5-2. The values of D obtained with the two different peaks agree with each other. (D_{CO} = (6±1) x 10^{-6} cm^2/s and D_{CH_3} = (5.1±0.8) x 10^{-6} cm^2/s) The value for D with a deeper probe depth (x=0.63 cm) is larger (D = (10±2) x 10^{-6} cm^2/s) than at a probe depth

of x = 0.35 cm, although the reason for this is not clear.

The three variables, L, x, and t were tested to determine the limits on the measured value for D. Varying the value of the solution thickness, L, by ± 3 mm changed the value of D by less than 2.5%. However, changing the probe depth, x, by ± 1 mm resulted in a difference in D of 45–80%. If the probe depth is incorrect by ± 0.5mm then the introduced error is 27-34%. Changing the start time of the experiment by ± 10 min changed the value of D by 11-15%. However, because the acquisition times were controlled electronically, this is an unlikely problem. The measurement of the position of the probe is the most likely determinate error in these experiments.

Before measuring the diffusion coefficients of methanol in sulfuric acid solutions it was necessary to test the validity of the method. The diffusion of methanol into water has previously been studied so it was chosen as a comparison system. The plot of increasing peak area with time is shown in Figure 5.2. The diffusion coefficient of MeOH in water measured using the Taylor dispersion technique[91,92] at 30 °C is 1.83 x 10-5 cm^2/s [92] to (1.62 ± 0.02) x 10^{-5} cm^2/s.[91] Using ultrasound and capillary-cell techniques,[93] the experimentally determined value at 288 K is 1.26 x 10^{-5} cm^2/s. In this study, at 295 K we obtain a value for D of (0.7 ± 0.2) x 10^{-5} cm^2/s at 24 °C, Table 5.1. The value measured in this study agrees with the known literature values, suggesting that this method can be used to obtain reliable diffusion coefficients. The values obtained for D for methyl species into 39.2 to 96.5 wt% SA solutions are found in Table 5.1 and the uptake plots are shown in Figure 5.3 a-d. The coefficients range from (1 to 2.7) x 10^{-6} cm^2/s with a maximum value for the diffusion into 61.6 wt% SA solution. The values obtained for the diffusion coefficient into SA solutions are a factor of ten smaller than the diffusion of MeOH into H_2O.

As was previously mentioned, there are very few measured diffusion coefficients with sulfuric acid as the solvent. Instead, D is often estimated using a method such as the Wilke-Chang estimation method,[93] equation 5.4.

$$D = \frac{CT}{\eta} \qquad (5.4)$$

In the above equation C is a constant, T is the temperature (K) and η is the viscosity of the solvent. The values calculated from equation 5.4 for viscosity of the SA solutions are found in Table 5.1. The constant C is related to the molecular weight of the solvent, M_B, the molar volume of the solute, V_A, and an association factor, ϕ, equation 5.5.

$$C = \frac{(7.4\times10^{-8})(\phi M_B)^{\frac{1}{2}}}{V_A^{0.6}} \qquad (5.5)$$

The diffusion coefficients measured in this study do not appear to decrease with increasing SA wt%, as would be expected according to equation 5.4. Indeed, the largest value for D among the SA solutions is for 61.6 wt% SA and not for 39.2 wt% SA as would be predicted with equation 5.4. Deviations from the Wilke-Chang method have also been observed by others for viscous solvents.[93] For example, the diffusion coefficients for CO_2 into various solvents remained nearly constant for a range of viscosities (1-27 cP). All the SA solutions used here fall within this range of viscosities and so perhaps this result is to be expected. There is very little data in the literature to compare with, but a study by Kleno *et al*[84] using a pulsed gradient spin-echo NMR technique did find that the diffusion coefficients of dimethyl sulfoxide and dimethyl sulfone decreased with increasing SA concentration as predicted by equation 5.4.

Methanol is both protonated by SA to form $MeOH_2^+$ and can react with SA to form MHS in the SA solutions investigated here.[42,52-54] The speciation of methanol in these different SA solutions may be affecting the observed diffusion coefficients. In water, the methanol is present as MeOH. In concentrated acid, the conversion to MHS is (95±5) %,[42] so the experiment is in fact measuring the diffusion coefficient of *MHS* into 96.5 wt% SA, and not MeOH into 96.5 wt% SA. In 39.2 wt% to 79.3 wt% SA, three species, MeOH, $MeOH_2^+$, and MHS are present in the solutions, Table 5.2. To determine the speciation in 39.2 wt% to 79.3 wt%, a pK_{BH^+} of –2.05[82] was used with the acidity functions measured for alcohols, H_{ROH}.[94] The equilibrium constants used are based on those found in the literature.[54] Previous work[87] studying the uptake of MeOH at the surface of and into SA solutions showed a blueshift in peak positions with increasing wt% SA indicating that the methyl species change with SA concentration. The different

species may diffuse in at different rates, resulting in no apparent dependence of the diffusion coefficient, D, on the viscosity.

The speciation of sulfuric acid in the different solutions may be affecting the observed diffusion of the methanol species. In SA solutions greater than 80 wt%, ionization is suppressed due to insufficient water concentration[62] and the dominant species is H_2SO_4. Therefore, the 96.5 wt% SA solution is uncharged (or only very weakly charged) and molecular interactions will be weak (van der Waals interactions).[62] Below 80 wt% SA, SA is fully dissociated into $(H_3O^+)(HSO_4^-)$[95] and ionic interactions become important.[62] Based on the second dissociation constants for the three different SA solutions[95,96] HSO_4^- will be further dissociated to $(H_3O^+)(SO_4^{2-})$. In 39.2 wt% SA, 40% of the sulfate species are SO_4^{2-} while in 79.3 wt% SA, ~ 9% of the sulfate species are present as SO_4^{2-}. (These values are higher than would be expected simply using the dissociation constant of 10^{-2} since the activities for HSO_4^-, SO_4^{2-}, and H_2O must be considered).[95] The different sulfate species may interact differently with the different methyl species diffusing into the solutions. Referring to Table 5.2, methanol is present as uncharged (MeOH, MHS) and charged ($MeOH_2^+$ and possibly MHS^-) species. The interactions between the charged species and the SA solutions may be different from that between the neutral species and the SA solutions. The different interactions between solute and solvent species could be affecting the observed diffusion coefficients. Clearly, more work needs to be done to understand these systems. From these results, it appears that estimations of D based solely on the viscosity of the solvent may not be accurate for compounds such as alcohols that can undergo protonation or reaction in very acidic solutions.

Conclusions

Raman spectroscopy offers a straightforward method for obtaining diffusion coefficients. These are necessary for understanding the chemical processing of volatile organic compounds by atmospheric aerosols in the upper troposphere and lower stratosphere. A value of $(0.7 \pm 0.2) \times 10^{-5}$ cm^2/s at 23 °C was obtained for methanol into water, in agreement with values found in the literature. However, the function is not fitting the curve properly. Further work will correct this problem. Values for D were also

measured for 39.2 to 96.5 wt% SA solutions. The values do not appear to depend on the viscosity of the SA solutions, indicating that speciation of both methanol and sulfuric acid may be important. This result has important consequences for uptake studies of organics into acidic solutions that rely on empirically calculated diffusion coefficients.

Solution	H_2O:SA	Viscosity (η, cP)	Estimate of D (cm^2/s) ($x\ 10^{-6}$)	Measured D (cm^2/s) ($x\ 10^{-6}$)
0 wt% (Water)		0.890 (298 K)[97]		7 ± 2
39.2 wt%	8.4	2.4 (295 K)[98]	4.5	1.2 ± 0.2
61.6 wt%	3.4	6.0(295 K) [98]	1.8	2.8 ± 0.5
79.3 wt%	1.4	18.6(295 K)[98]	0.58	1.0 ± 0.1
96.5 wt%	0.2	22-23[99]	0.49	1.0 ± 0.8

Table 5.1. Measured diffusion coefficients for MeOH into SA solutions and the viscosities of the different SA solutions used in this study. The error on the measured values of D is the larger of either the propagated error or the standard deviation.

Wt% SA	MeOH	$MeOH_2^+$	MHS
0	100		
39.2	85.5	8.5	6.0
61.6	57.7	22.9	19.3
79.3	36.2	43.0	20.8
96.5			~ 100

Table 5.2. Distribution of methyl species (fraction of MeOH, $MeOH_2^+$, and MHS) in the SA solutions.

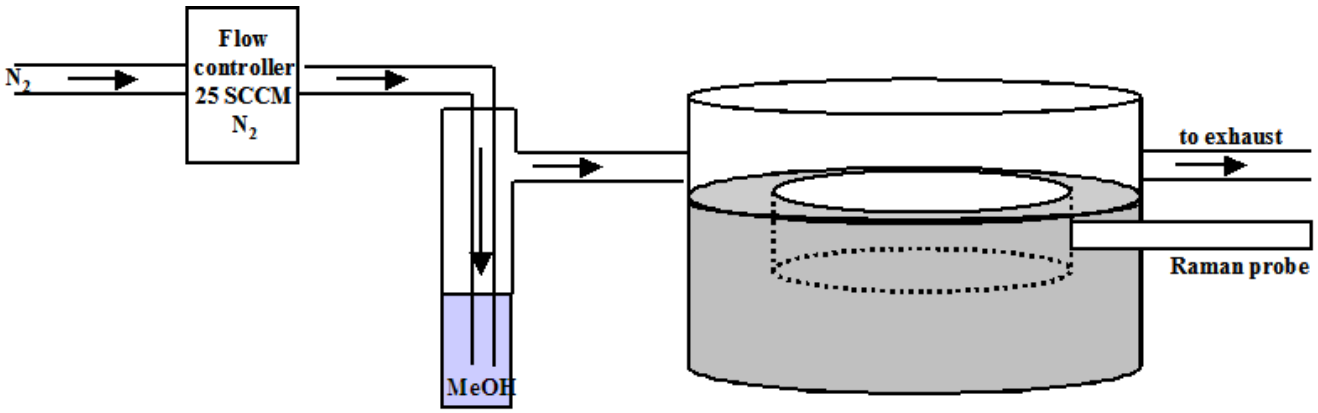

Figure 5.1. Setup used for the diffusion experiments.

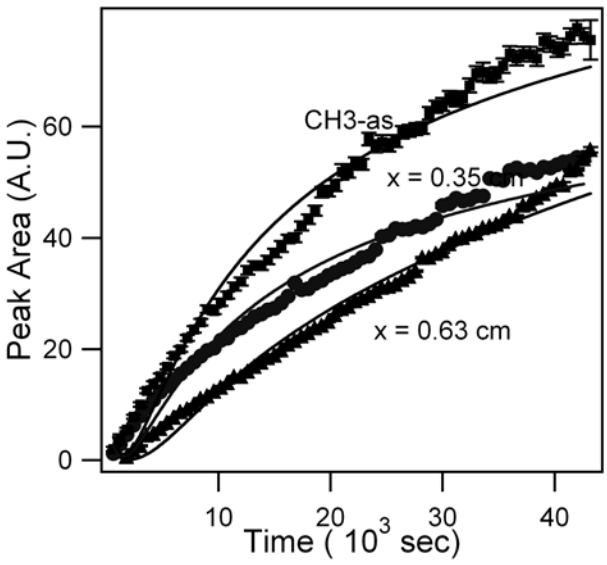

Figure 5.2. Peak area (A.U.) versus time (seconds) for methanol diffusion into water. The squares (■)are the fit using the ν_{CH_3}-as centered at 2970 cm^{-1} with a probe depth was 0.35 cm; the circles (●) are fit using the ν_{CO}-ss at 1020 cm^{-1} with a probe depth of 0.35 cm; and the triangles (▲) are fit using the ν_{CO}-ss at 1020 cm^{-1} with a probe depth of 0.63 cm.

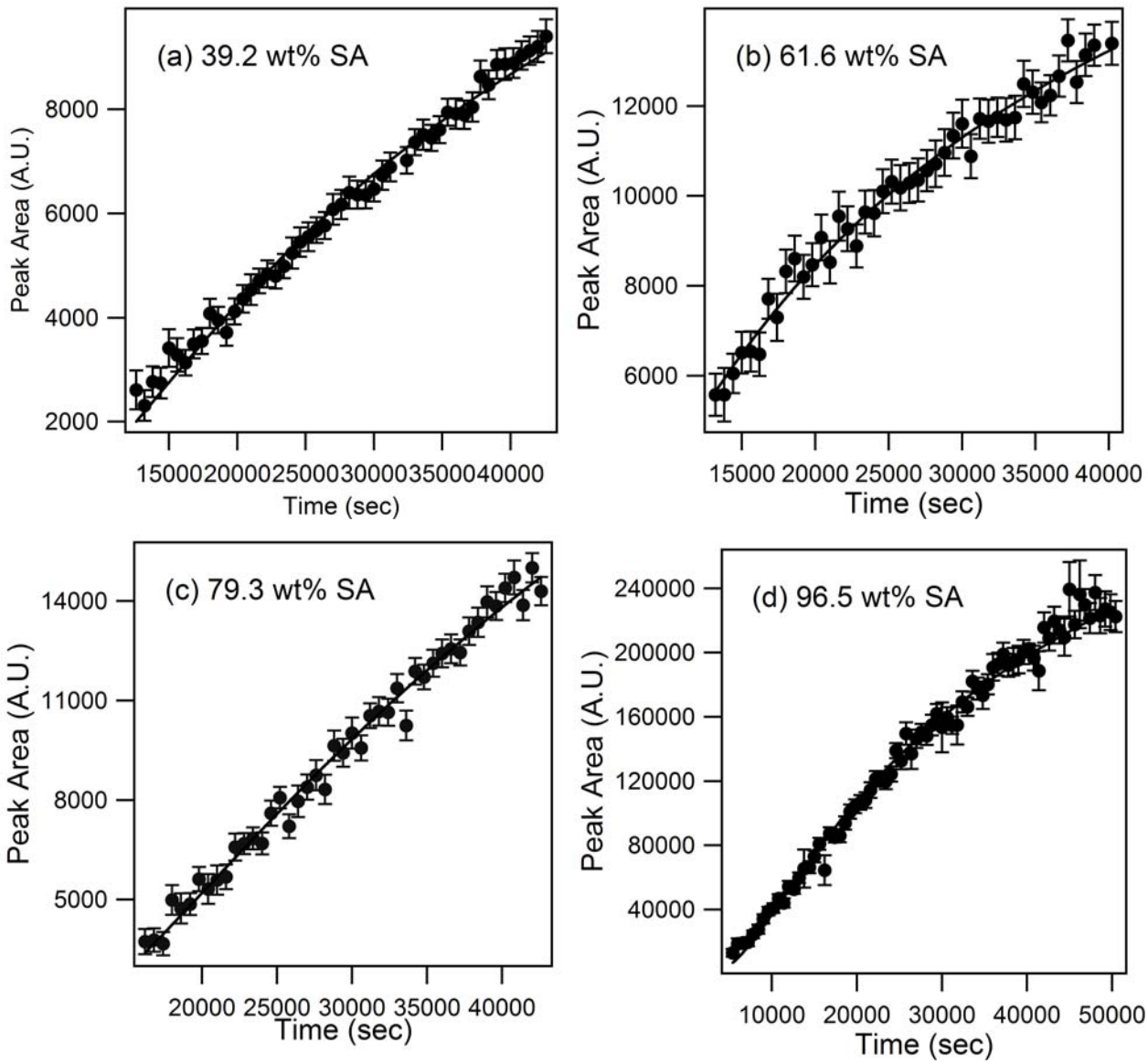

Figure 5.3. Peak area versus time (seconds) for the diffusion of MeOH into SA (a) 39.2 wt%, (b) 61.6 wt%, (c) 79.3 wt%, and (d) 96.5 wt% SA solutions

CHAPTER 6

STRUCTURE OF BUTANOL AND HEXANOL AT AQUEOUS, AMMONIUM BISULFATE, AND SULFURIC ACID SOLUTION SURFACES

Introduction

It has long been known that long-chain surfactants are able to form monolayers at the surface of water.[100,101] However, the ordering of shorter, more soluble alcohols such as butanol and hexanol at the surface of aqueous-alcohol mixtures is not yet well understood.[80,102] Inorganic species such as sulfuric acid and ammonium sulfate salts have also long been known to be the predominant fraction of tropospheric aerosols.[35] At the surface of acidic solutions, the orientation of short-chained organics is even more poorly characterized.[60,102] The structure of the short-chain surfactant layer is likely to be important in the ability of the underlying aqueous solvent to absorb gas phase compounds. Monte Carlo simulations found that the hexanol hydroxyl groups hydrogen bond with water molecules at the 1-hexanol-water interface.[103] Packing of the hexanol molecules allowed for minimal water penetration into the alkyl chain region suggesting that hexanol impedes the evaporation of water from the bulk. A configurational bias Monte Carlo simulation of 1-butanol on water showed that the butanol monolayer has an excess of surface hydrogen bond acceptor sites in the subsurface layer.[104]

Recent molecular beam experiments showed that the presence of butanol films does not impede the evaporation of water from sulfuric acid solutions.[105] The uptake of HCl and HBr gases is enhanced with the butanol hydroxyl groups providing basic sites available for protonation by the acids.[106] However, the evaporation of H_2O from 56 wt% to 60 wt% D_2SO_4 is impeded by the presence of a hexanol film. The hexanol film also raises

the entry probability of HCl and HBr into 60 wt% D_2SO_4.[102] In another study, the presence of millimolar hexanoic acid concentrations reduced the uptake of N_2O_5 by artificial seawater by a factor of 3 to 4.[107] These results suggest that there are differences in the surface structure of butanol and hexanol solutions.

In this chapter, the organization of butanol and hexanol molecules at the air-liquid interface of aqueous, aqueous ammonium bisulfate, and sulfuric acid solutions was investigated using vibrational sum frequency generation (VSFG) spectroscopy. After providing a brief overview of VSFG theory, experimental details including fitting procedures are presented, and then in the Results section, VSFG spectral assignments are provided. (Spectral fits are shown in Appendix A.) The Discussion section presents the interpretation of the spectra in terms of organization at the surface beginning with neat alcohol comparisons.

Chemical abbreviations used in this chapter are BuOH (butanol), HexOH (hexanol), and SA (sulfuric acid). In addition, vibrational sum frequency generation (VSFG), broad bandwidth sum frequency generation (BBSFG), symmetric stretch (ss), and asymmetric stretch (as) are used.

Experimental

BBSFG Instrumentation and Experimental Details

The spectral window of the IR pulse is ~ 450 cm^{-1} in the C-H stretching region for these experiments. The energy of the 800 nm beam used was 160-165 μJ, and the IR energy in the C-H stretching region was 5.2-5.6 μJ at the sample. Three polarization combinations were used in this chapter: ssp (s-SFG, s-800 nm, p-infrared), ppp (p-SFG, p-800 nm, p-infrared), and sps (s-SFG, p-800 nm, s-infrared). The polarization of the 800 nm beam is determined by rotation of a zero-order waveplate. By rotation of a MgF_2 Berek's compensator, the desired IR beam polarization is determined. A glan polarizer in the SFG detection line selects the SFG polarization.

The ssp-polarized spectra were obtained with a 2-minute acquisition time. The ppp and sps spectra used 5-minute acquisition times. For comparison of the different polarization spectra, the ssp spectra were multiplied by a factor of 5/2. For each solution and

polarization combination, three spectra were obtained. Three background spectra were also obtained by changing the timing of the 800 nm beam. The final spectra shown in this thesis are the average of the three spectra with the average of three background spectra subtracted. The VSFG spectrum is normalized against a smoothed nonresonant VSFG spectrum from a GaAs crystal to remove any structure present in the IR pulse profile.

Spectral Fitting

The number of peaks fit corresponds to the number of vibrational modes expected to be SFG-active. The inclusion of a component peak due to the presence of water in the interfacial region was tested in the spectral fitting of the water and NH_4HSO_4 solutions and included if it improved the overall fit. Attempts were also made for the butanol in water solutions to include contributions from the asymmetric CH_2 and CH_3 modes to the ssp spectra. Further details and examples of the spectral fits are found in Appendix A.

The average orientation of the terminal methyl group for butanol, θ_{CH_3}, and the average chain tilt, α, of the surface butanol molecules when assuming an all-trans conformation were calculated. θ_{CH_3} is calculated from the ratio of the square roots of the intensity of the CH_3-ss in the ssp and ppp polarization spectra.[44,108] The obtained ratio is related to the orientation angle, θ_{CH_3}, as shown in equation 6.1.

$$\sqrt{\frac{I_{CH_3-ss,ssp}}{I_{CH_3-ss,ppp}}} = \frac{d^2_{ss-ssp}R(\theta)}{d^2_{ss-ppp}R(\theta)} \tag{6.1}$$

where

$$R(\theta) = \left|\langle\cos\theta\rangle - c\langle\cos^3\theta\rangle\right|^2 \tag{6.2}$$

The parameters d and c are defined using the Fresnel coefficients, the hyperpolarizability ratio, the molecular hyperpolarizability and the related Euler angle transformations[109,110] as derived in Wang et al.[108,111,112]

The variable input parameters used in this study (SF, IR, visible beam angles,

depolarization ratio, indices of refraction) and an example calculated plot of $\frac{d_{ss-ssp}^2 R(\theta)}{d_{ss-ppp}^2 R(\theta)}$ versus θ are available in Appendix A. The calculated average orientation angles for neat butanol and the butanol solutions are also found in the Appendix A. It is assumed that the CH_3 group has C_{3v} symmetry, that the surface is isotropic, and that the orientation angle distribution is a δ function.[109,110] The average orientation angle of the methyl group in neat butanol is the largest at θ_{CH_3} = 57°. The various butanol solutions have methyl orientation angles ranging from 39.5° to 48.5°. Using the orientation angle of the methyl group, and an angle of 109° between the CH_2 carbons in the chain, the average tilt angle of the butanol chains is calculated[110,113] to be 4° to 13° from the surface normal using equation 6.3.

$$\alpha = \left|35.5 - \theta_{CH_3}\right| \qquad (6.3)$$

Chemicals

1-Butanol (HPLC grade, Fisher Scientific), hexyl alcohol (98%, Acros Organics), sulfuric acid (redistilled, 95.6wt%, GFS), and ammonium hydrogensulfate (98%, Aldrich) were used as received. Deionized water was obtained from a Millipore Nanopure system (18.1-18.2 MΩ•cm).

The 59.5 wt% sulfuric acid solution was prepared by diluting 95.6 wt% sulfuric acid with deionized water. The concentration was determined by titration with a standardized sodium hydroxide solution to ± 0.1 wt%. The ammonium bisulfate solution was prepared by dissolving the salt in deionized water and filtering two times through a carbon filter (Carbon-Cap 75, Whatman). The concentration (0.78 ± 0.1 M) was determined spectroscopically using the sulfate vibrational mode at 985 cm^{-1}. The butanol and hexanol solution concentrations used in this study were chosen to reflect different surface excess conditions.[114] The concentrations and their respective uncertainty used in this study were (0.50 ± 0.02) M, (0.0179 ± 0.003) M, and (0.052 ± 0.002) M BuOH and (0.050 ± 0.002) M, (0.045 ±0.002) M, (0.0099 ±0.0003) M, and (0.0051 ±0.0001) M HexOH.

Results

While the VSFG spectra of neat alcohols[108,111,112] are found in the literature, much less work has been done to understand the surface structure of aqueous alcohol solutions. Recently the air-liquid interface of aqueous mixtures of methanol, ethanol, and propanol were investigated with VSFG.[49,79,80] The air-liquid interfaces of the longer, but still miscible alcohols (C4, C6) in aqueous, ammonium bisulfate, and sulfuric acid solutions are the focus of this study.

The butanol and hexanol solution concentrations correspond to three different regions of the surface excess curves of 1-butanol in water and 61.5 wt% sulfuric acid solution, and 1-hexanol in 61.5 wt% sulfuric acid solution.[114] The lowest concentrations correspond to a region of low surface excess, far from full surface coverage. The intermediate concentrations correspond to the region where the surface excess is beginning to level off, slightly less than full surface coverage. The greatest concentrations correspond to the region where the surface excess is constant, full surface coverage. When increasing from the lowest to the highest concentrations used in these studies, the surface excesses of butanol and hexanol double. All concentrations used in this study were below the solubility limits of the alcohols in water: 115 g/L for 1-butanol and 7.9 g/L for 1-hexanol.[115]

Prior to obtaining the VSFG spectra of the 1-alcohol solution mixtures, the spectra of the neat alcohols were investigated. The neat 1-butanol ssp spectrum, shown in Figure 6.1 (a,b), is fit with four component peaks:[108] the CH_2-ss at 2846 cm^{-1}, the CH_3-ss at 2877 cm^{-1}, the CH_2-FR at 2908 cm^{-1}, and the CH_3-FR at 2941 cm^{-1}.

The neat 1-hexanol ssp spectrum, shown in Figure 6.1 (f, g), is fit with six component peaks:[108] the CH_2-ss at 2856 cm^{-1}, the CH_3-ss at 2878 cm^{-1}, three CH_2 Fermi resonances at 2903, 2922, and 2947 cm^{-1}, and the CH_3-FR at 2939 cm^{-1}.

The ppp and sps polarization spectra of both neat butanol and neat hexanol are shown in Figure 6.1 (b,g). The ppp spectra are fit with three component peaks: the CH_3-ss, the CH_2-as, and the CH_3-as. The sps spectra are fit with two component peaks: the CH_2-as and the CH_3-as. The spectra of neat 1-butanol and neat 1-hexanol in this study are consistent with those found in the literature.[108,111]

The VSFG spectra of butanol in water, aqueous ammonium bisulfate, and SA shown in Figures 6.1-6.3 possess four, three and two component peaks for the ssp, ppp, and the sps spectra respectively, excluding addition of a broad band attributed to OH stretching of water in the aqueous butanol spectra. For the VSFG spectra of hexanol in water, aqueous ammonium bisulfate, and SA (also shown in Figures 6.1-6.3), assignments revealed six, three and two component peaks for the ssp, ppp, and the sps spectra respectively. Only the aqueous hexanol solutions included the broad water band, similar to the aqueous butanol solutions. In general, the assignments follow the neat butanol and neat hexanol assignments discussed above. (Peak positions, assignments, and example fits are shown in the Appendix A.) Of major importance here are the CH_2-ss and the CH_3-ss denoted by the first two dashed lines in Figures 6.1-6.3 (b-e and g-j).

Discussion

The ssp, ppp, and sps VSFG spectra of neat, aqueous, aqueous ammonium bisulfate, and 59.5 wt% SA butanol and hexanol solution surfaces are shown in Figures 6.1-6.3. From left to right denoted by dashed lines for Figures 6.1-6.3 (b-e) and Figures 6.1-6.3 (g-j) are the CH_2-ss, the CH_3-ss, the CH_3-FR, and the CH_3-as, respectively. The CH_3-ss peak intensity goes through a maximum in the VSFG spectra for the butanol and hexanol solutions that does not correspond with increasing bulk concentration (or surface excess). Previous studies of short-chain alcohols (C1-C3)[49,80] have shown that the CH_3-ss passes through a maximum at a concentration below the solubility limit, as is observed here. This phenomenon is indicative of organization and orientation differences of the different solution concentrations. For the aqueous solutions (Figure 6.1), the butanol ssp VSFG spectra reaches a maximum at 0.50 M, and the hexanol ssp VSFG spectra go through a maximum at 0.045 M.

The VSFG response, in particular the CH_3-ss peak, for the neat solution surfaces is relatively small when compared to the higher concentration solutions. Previously, orientation differences have been used to explain the anti-correlation of the surface number density and the VSFG intensity of the CH_3-ss.[49] Although this is still thought to be mostly true, the surface structure is more complex. Upon examination of the VSFG

spectra in Figures 6.1-6.3, it is clear that centrosymmetry is playing a role in the reduced VSFG intensity of the CH_3-ss from the neat butanol and neat hexanol surfaces. Orientation calculations (described further below and in Appendix A) do not account for the dramatic loss in VSFG signal intensity relative to the solution spectra in Figures 6.1-6.3. Thus, self-aggregation into surface structures that possess inversion symmetry is likely occurring. Inverse micelle-like structures are quite plausible at the neat alcohol surfaces. The alcohol moieties may form hydrogen-bonded aggregates that possess a certain degree of centrosymmetry. Upon addition of water, the alcohol moieties hydrogen bond preferentially to the solvating water molecules, thereby breaking up the centrosymmetric surface aggregates.

Another plausible explanation for the relatively small intensity of the neat alcohols is centrosymmetry due to formation of layered hydrogen-bonded structures.[116] Simulations of neat octanol show the formation of hydrogen-bonded chains.[116] A molecular dynamics study of the n-octanol/vapor interface[117] show the alkyl chains aligned at the surface. Several layers beneath the interface these molecules are also well aligned due to hydrogen bonding between the hydroxyl groups. The weaker intensity of the neat alcohol ssp VSFG spectra is consistent with alignment of butanol and hexanol several layers into the interface, resulting in a cancellation of VSFG spectral intensity.

Comparing the neat alcohol ssp spectra (Figure 6.1 (a, f)), the CH_3-ss intensity of neat butanol is greater than that of neat hexanol. Perhaps hexanol, closer in length to octanol[117] than butanol, exhibits a stronger tendency to form inverse micelle-like surface structures or is somewhat better at forming multiple layered structures at the surface of its neat liquid. However, the additional presence of the CH_2-ss peak in the neat hexanol spectra (Figure 6.1 (f, g)) makes the neat hexanol structure determination ambiguous.

The influence of solvent on the alcohol surface organization of the butanol and hexanol solution spectra is shown in Figures 6.1-6.3. The most noticeable difference between the aqueous butanol and aqueous hexanol VSFG spectra is the significant presence of the CH_2-ss in the hexanol ssp spectra (Figures 6.1-6.3 (f-j)), and moreover, its near absence in the butanol spectra (Figures 6.1-6.3 (a-e)), with the exception of the anomalous 0.052 M butanol in SA spectrum (Figure 6.3 (a, e)).

Presence of methylene VSFG intensity is an important indicator of gauche conformations, and therefore, ordering, or rigidity, of the alkyl chains.[110] In an all-anti alkyl chain, local inversion centers disallow the SFG response, as is observed in the butanol spectra shown in Figures 6.1-6.3 (except the 0.052 M BuOH in SA). However, gauche defects destroy the local centrosymmetric methylene structures and thereby the CH_2 modes in an alkyl chain become SFG-active. For hexanol, the CH_2-ss is observed in all spectra (Figures 6.1-6.3), indicating that hexanol molecules possess a significant number of gauche defects in their alkyl chains. Hexanol is disordered at the neat, aqueous, aqueous ammonium bisulfate, and 59.5 wt% SA surfaces.

Using the fitted intensities of the CH_3 and CH_2 symmetric stretches in the ssp spectra, the CH_3-ss/CH_2-ss ratios (I_{CH_3}/I_{CH_2}) can be calculated for each butanol and hexanol solution. This ratio (or its inverse) is used as a measure of gauche defects.[118] Large CH_3-ss/CH_2-ss ratios indicate order, whereas small ratios indicate disorder in the alkyl chains. Although this indicator can be convoluted by a methyl orientation effect, it provides additional evidence for order versus disorder. In Table 6.1, hexanol I_{CH_3}/I_{CH_2} ratios and the 0.052 M butanol in SA ratio are shown. The hexanol solutions have ratios less than 20. We were unable to confirm the presence of any VSFG CH_2-ss intensity for the butanol solution spectra, including neat butanol, and therefore, we do not report ratios for these solutions; they are clearly large for the butanol spectra, indicating that surface butanol exists in all-anti conformations (the alkyl chains are well ordered).

Hexanol has two additional methylene groups relative to butanol, and statistically has a greater possibility of producing gauche conformations. Therefore, one might expect additional intensity of the methylenes for hexanol relative to butanol. However, contrary to this statistical argument, self assembled monolayer (SAM) studies have shown that longer chain SAMs tend to order more.[119,120] This finding is counter to the observation here.

A possible explanation to our observation that butanol is significantly more ordered that hexanol at the surface of aqueous solutions stems from potential solvent interactions with butanol versus hexanol. Butanol has a shorter chain, and energetically it should be less favorable for the butanol chain to contain gauche configurations, which would tilt the

terminal methyl group back toward the surface. In hexanol, the conformation with C_3 gauche to the oxygen is the lowest energy conformation.[121] Raman spectroscopy studies showed that the energy differences between all-trans and trans-gauche conformations of 1-pentane are much smaller than the energy differences for 1-butane.[122] Following these results, the energy difference between all-trans and trans-gauche conformations for hexanol chains should then be smaller than that for butanol chains.

The conformational energies of butanol in water have been investigated using ab initio molecular orbital calculations and Raman spectroscopy.[123] Raman spectra revealed that the gauche conformers of butanol dominate in aqueous solutions in order to minimize the butanol surface area that is in contact with water molecules. Using this argument, it is plausible to postulate that at the aqueous surface, butanol prefers an all-trans conformation to minimize the interaction between the alkyl chain and surface water.

Comparison of the butanol spectra in water, aqueous ammonium bisulfate, and most of the SA solutions, reveal that the CH_2-ss remains absent from the spectra. The butanol molecules stay in their all-trans conformation even at low surface excess. Orientation calculations using the ssp and ppp spectral intensities also reveal that the chain tilt angles are between 4° and 13° from the surface normal for butanol in aqueous, in aqueous ammonium bisulfate, and in SA solutions (except the 0.052 M BuOH in SA). (Orientation calculation data is available in Appendix A.) Butanol molecules do not change their orientation or surface organization to any significant extent with solvent variation. There may be self-aggregation at the surface of these butanol solutions that stabilizes the rigid butanol structures. This is in contrast to the individual alcohol molecules spreading out in an isolated fashion evenly over the entire surface. Consistent with this hypothesis, propanol studies show that even at very low concentrations, the alcohol molecules self-aggregate into clusters.[124] Additionally, an investigation of a saturated butanol-water solution showed that both self-aggregated clusters and butanol clusters with hydrogen bonded water molecules exist.[125]

Molecular modeling of the water-butanol surface predict that the alkyl chains of butanol are aligned upright, and that the presence of water enhances ordering compared to that of neat butanol.[104] We observe a significant difference in the neat (21.5°) versus

solution butanol chain orientation (4° to 13°), consistent with Chen et al.[104] Electric surface potential measurements[126] suggest that n-butanol molecules adsorbed to the surface of water are nearly perpendicular in order to prevent the hydrophobic chain from coming into contact with the water. These experimental and theoretical results as discussed above are consistent with the findings and interpretation presented here.

The ratios in Table 6.1 reveal that hexanol is disordered at its solution surfaces. In the low concentration regime in water (0.0051 M and 0.0099 M), the I_{CH_3}/I_{CH_2} values are in the single digits, indicative of disorder. Ratios in the full surface coverage concentration regime (0.045 M and 0.052 M) become larger by about a factor of two, indicating that the increased surface coverage helps to minimize the existing gauche conformations, stabilizing the hexanol alkyl chain to some extent. This is not observed in the aqueous ammonium bisulfate or SA solutions for hexanol, revealing that the solvent is playing a significant role in the surface ordering, or lack thereof, for hexanol. Chain tilt angle calculations will be inaccurate for these solutions since the methyl tilt angle is not representative of the chain tilt due to the gauche conformations in the hexanol chains.

As discussed above, ordering of the butanol molecules at the surface of the various solutions is constant and well ordered, quite different relative to hexanol surfaces. However, the 0.052 M butanol in 59.5 wt% SA has a I_{CH_3}/I_{CH_2} of 2.5, close to the I_{CH_3}/I_{CH_2} from hexanol at the surface of the 0.045 M hexanol in 59.5 wt % SA, revealing that these surfaces are the most disordered of the alcohol surfaces studied here.

To understand how these alcohols could organize at the surface of sulfate-containing atmospheric aerosols, the differences in surface structure with water versus ammonium bisulfate versus SA solution as solvent is examined. The presence of salts in aqueous solutions can reduce the solubility of organic compounds such as alcohols. This is known as the salting out effect.[127,128] Previous surface tension experiments of 1-propanol in aqueous NaCl solutions show a greater decrease in surface tension at low propanol and high salt concentrations, indicating that salting out occurs.[129] Here, the VSFG spectra of the two lowest surface excess concentrations shown in Figure 6.4 (a, b) show evidence for salting out of butanol and hexanol. The CH_3 symmetric stretches are more intense in

the ammonium bisulfate solutions than in the water solutions.

The intensity of the 59.5 wt% SA solutions is lower than that of the water solutions as is shown in Figure 6.4 (a, b) (other concentration spectra are shown in Appendix A). Unlike for the water solutions, no solubility limit for butanol and hexanol in SA was observed, both in this work and in previous studies.[60] In 60 wt% SA solution, using the pK_a of ethanol (–1.94)[94] and a value of H_{ROH} of –1.59[94] and assuming an equilibrium constant of 0.31[130] we calculate a distribution of 57% BuOH (HexOH), 25% $BuOH_2^+$ ($HexOH_2^+$), and 18% $BuOSO_3H/BuOSO_3^-$ ($HexOSO_3H/HexOSO_3^-$). However, this does not appear to affect the surface CH_3-ss vibrational frequency. The calculated surface excess for butanol in SA is lower than that for butanol in water,[114] and it is likely that this is the case for hexanol as well. The surface structure of the 0.052 M butanol in SA solution is different from the other butanol solutions. This is apparent from the presence of the CH_2-ss in the ssp spectrum. This may indicate that the butanol is not aggregating to the same extent as at the other solution surfaces.

Conclusions

The organization of 1-butanol and 1-hexanol molecules at the air-liquid interface of water, aqueous NH_4HSO_4, and 59.5 wt% sulfuric acid solutions was investigated using vibrational broad bandwidth sum frequency generation spectroscopy. The VSFG spectra strongly suggest that aggregation into somewhat centrosymmetric structures of the neat butanol and neat hexanol molecules is occurring at the neat surfaces. Butanol is relatively rigid, with all-trans chains for all solution surfaces investigated, with the exception of low concentration butanol in sulfuric acid. Hexanol, on the other hand, appears to contain gauche defects in its chain for all solution surfaces investigated. Butanol may self-aggregate at the solution surfaces to help maintain its rigid surface structure; however, energetically, butanol is more likely to be in all-trans conformations relative to hexanol at the solution surfaces due to potential and unfavorable solvent interactions.

	Neat HexOH	0.050 M HexOH	0.045 M HexOH	0.0099 M HexOH	0.0051 M HexOH	0.052 M BuOH
		In water				
I_{CH_3}/I_{CH_2}	7.3	14.0	18.0	9.2	9.0	
		In 0.78 M NH_4HSO_4				
I_{CH_3}/I_{CH_2}		7.3		5.7	5.3	
		In 59.5 wt % SA				
I_{CH_3}/I_{CH_2}		6.5	3.0	12.1	7.2	2.5

Table 6.1. Calculated I_{CH_3}/I_{CH_2} ratio for the 1-hexanol solutions and the 0.052 M 1-butanol in SA solution.

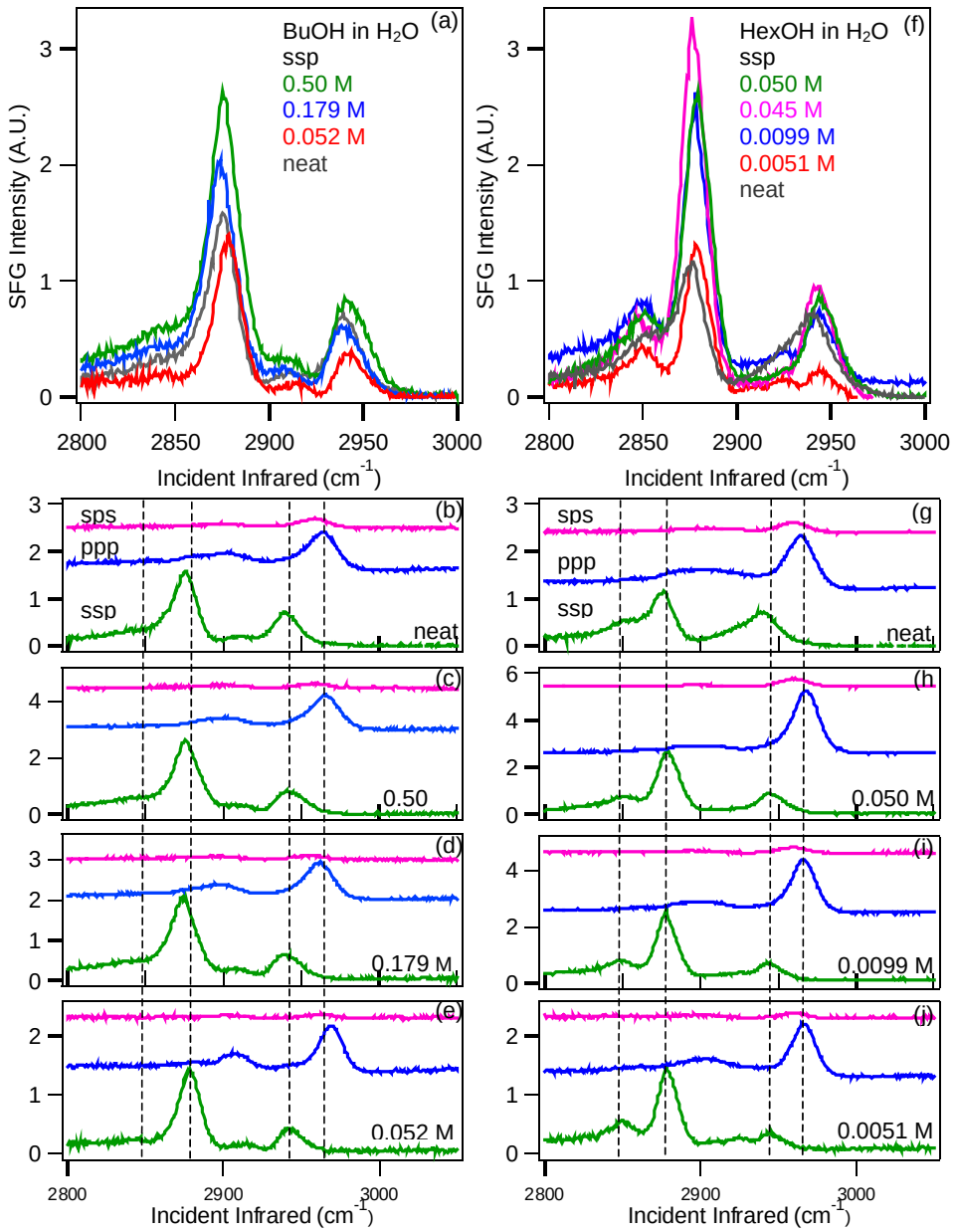

Figure 6.1. VSFG spectra of the CH stretching region of the (a) - (e) 1-butanol - water mixtures and (f) - (j) 1-hexanol-water mixtures. In (b) - (e) and (g) - (j) the ssp spectra are shown in green, the ppp spectra are shown in blue, and the sps spectra are shown in pink. The dashed lines are guides for the eye showing peak position variation; from left to right for b-e and g-j are the CH_2-ss, the CH_3-ss, the CH_3-FR, and the CH_3-as, respectively.

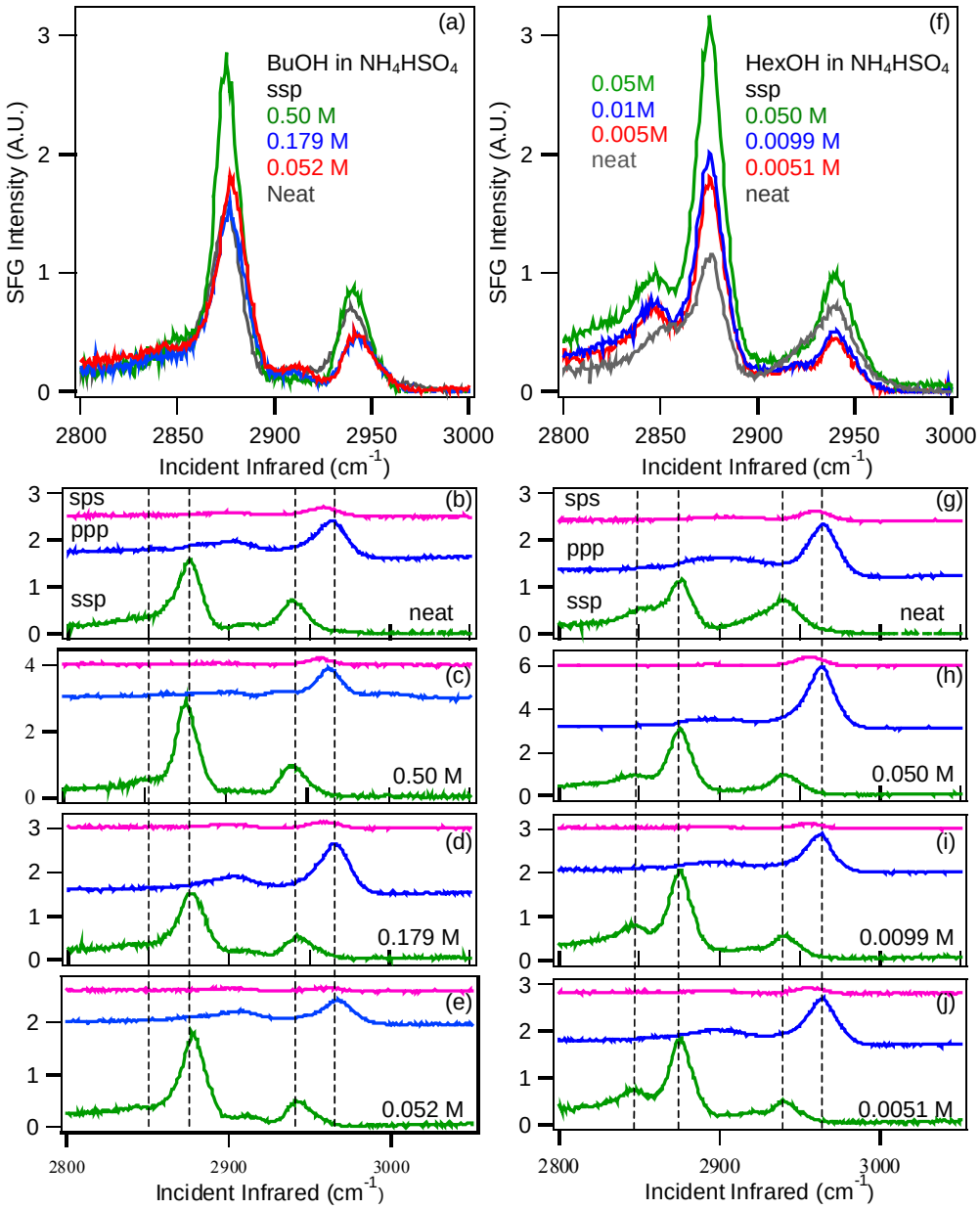

Figure 6.2. VSFG spectra of the CH stretching region of the (a) - (e) 1-butanol - 0.78 M NH_4HSO_4 mixtures and (f) - (j) 1-hexanol - 0.78 M NH_4HSO_4 mixtures. In (b) - (e) and (g) - (j) the ssp spectra are shown in green, the ppp spectra are shown in blue, and the sps spectra are shown in pink. The dashed lines are guides for the eye showing peak position variation; from left to right for b-e and g-j are the CH_2-ss, the CH_3-ss, the CH_3-FR, and the CH_3-as, respectively.

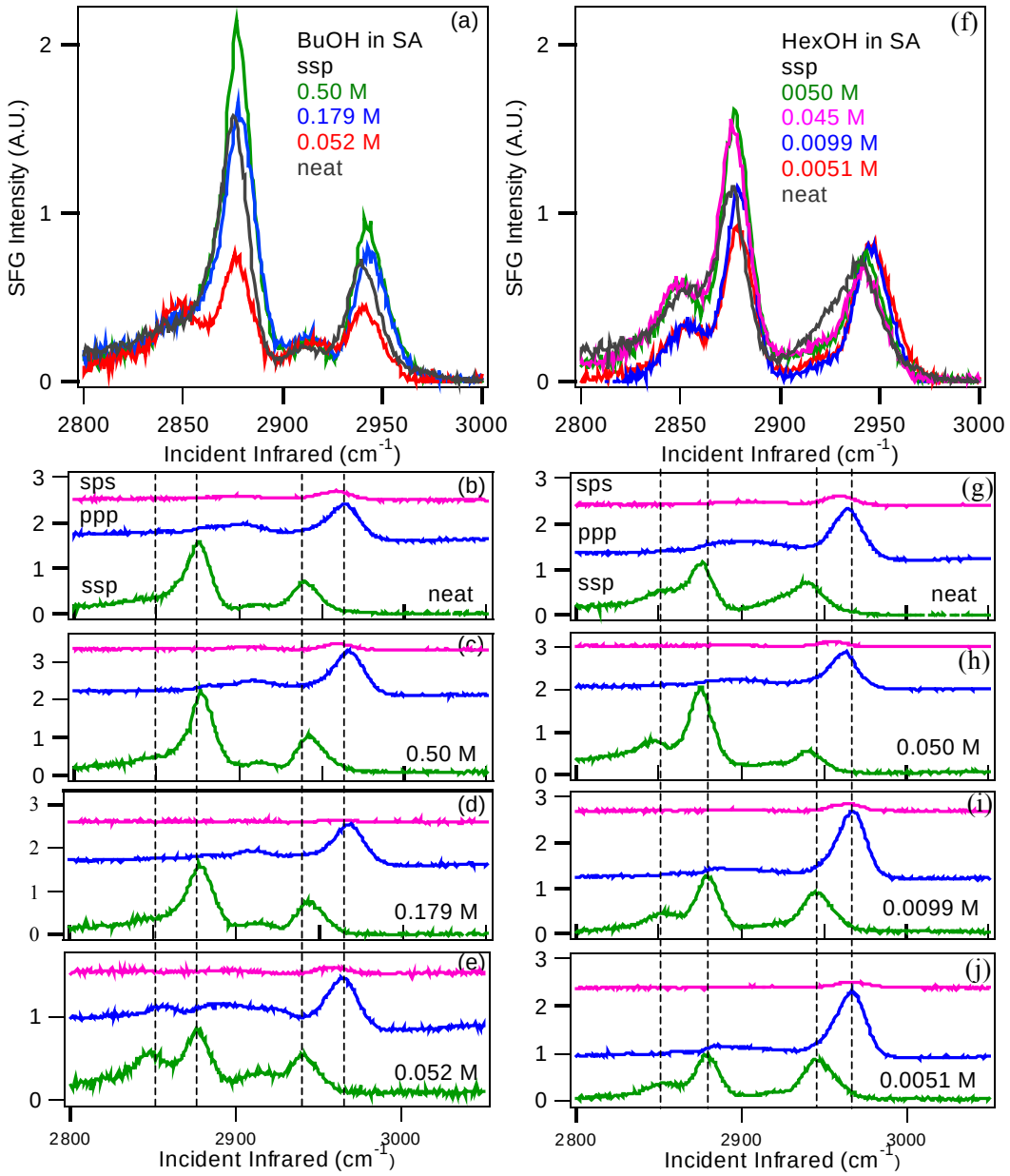

Figure 6.3. VSFG spectra of the CH stretching region of the (a) - (e) 1-butanol - 59.5 wt % SA mixtures and (f) - (j) 1-hexanol - 59.5 wt % SA mixtures. In (b) - (e) and (g) - (j) the ssp spectra are shown in green, the ppp spectra are shown in blue, and the sps spectra are shown in pink. The dashed lines are guides for the eye showing peak position variation; from left to right for b-e and g-j are the CH_2-ss, the CH_3-ss, the CH_3-FR, and the CH_3-as, respectively.

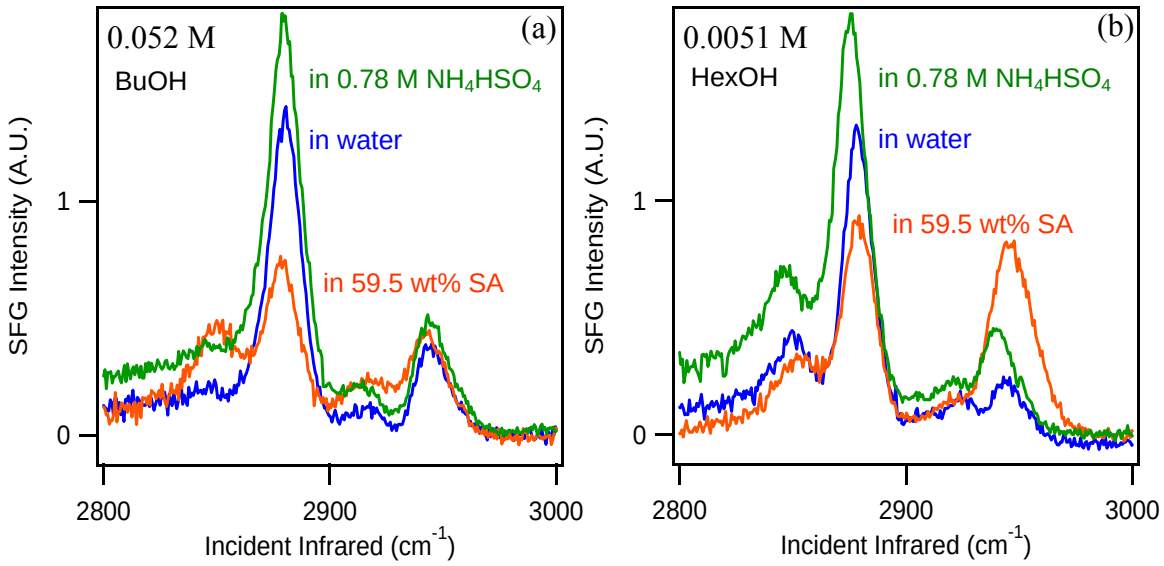

Figure 6.4. VSFG ssp polarization spectra of (a) 0.052 M 1-butanol solution and (b) 0.0051 M 1-hexanol solution. The water solutions are shown in blue, the 0.78 M NH_4HSO_4 solutions are shown in green, and the 59.5 wt % SA solutions are shown in orange.

CHAPTER 7

CONCLULSIONS AND ATMOSPHERIC IMPLICATIONS

The work presented in this thesis was motivated by an interest in understanding the formation of secondary organic aerosols and the likelihood for this to be a contributor to the growth of acidic sulfate aerosols. The uptake of methanol (MeOH) by sulfuric acid (SA) solutions and the formation of methyl sulfate were investigated to determine the feasibility of this reaction contributing to aerosol growth. For aerosol growth to occur by the uptake of volatile organic compounds, there must be a reduction in the volatility of the organic compound. The reaction of MeOH with SA forms methyl hydrogen sulfate (MHS), a non-volatile compound. With this reduction in volatility, MeOH could be contributing to the growth of acidic sulfate aerosols, through the formation of a secondary organic aerosol. However, transformation of MeOH to MHS is highly dependent on the acid concentration, with the 20+ % MHS being formed only in very acidic SA solution (70+ wt%).

The formation of MHS requires an acidic sulfate solution. The reaction was investigated using both Raman and vibrational sum frequency generation (VSFG) spectrosocopies. The appearance of a peak at 800 cm^{-1} in the Raman spectra indicates the presence of MHS in the solution. MHS was first detected in 51.4 wt% SA solutions, in SA solutions below 51.4 wt%, any MHS formed is beneath the experimental detection limits. Using equilibrium constants, the fraction of MHS in a 51.4 wt% SA solution is 14.2 %. Increasing to 68.3 wt% SA increases the fraction of MHS to 20.4 %. The conversion is (95 ± 5)% complete in 96.6 wt% SA solution. These results suggest that a minor component of methanol will be transformed to MHS in atmospheric

sulfate aerosols. The majority of methanol that is taken by atmospheric aerosols remains as MeOH or protonated methanol, $MeOH_2^+$, which are expected to remain volatile. However, MeOH is the dominant oxygenated species present in the atmosphere, and so, it is not inconceivable that MeOH is continually adsorbing to sulfate aerosols. Therefore, the uptake of MeOH can, over time, contribute to aerosol growth.

Atmospheric aerosols are partially neutralized through the uptake of ammonia. Partially neutralized SA solutions are still acidic, but no evidence for MHS was found when NH_4HSO_4 solutions were used to represent these partially neutralized aerosols. This is due to the presence of water in the solutions, pushing the reaction equilibrium back to the starting products. Sulfate aerosols will take up water with time, and so this result suggests that the formation of sulfate esters will not contribute to the growth of aging aerosols due to the presence of water.

The uptake of MeOH as a contributor to sulfate aerosol growth can only occur if MeOH, $MeOH_2^+$, and MHS diffuse into the aerosol. The uptake and diffusion of the three methyl species into 40 to 96.5 wt% SA solutions was investigated by flowing MeOH vapor over the solution surfaces. The VSFG spectra indicate that the interfacial region reaches equilibrium after 20 minutes. However, diffusion into the SA solutions occurs over many hours, making the uptake of methanol vapor by sulfate aerosols, and the subsequent growth of these aerosols diffusion limited.

Finally, the organization of longer alcohols, 1-butanol and 1-hexanol on aqueous, NH_4HSO_4, and 59.5 wt% SA solutions was investigated using VSFG spectroscopy. Differences were observed in the surface structures of the two alcohols. The VSFG spectra of the HexOH solution interfaces showed contribution from the ν_{CH_2}-ss while the BuOH solutions, except for the 0.05 M in 59.5 wt% SA, did not show ν_{CH_2}-ss contribution. The presence of ν_{CH_2}-ss in the HexOH spectra indicates that the chains have gauche defects, while BuOH is in a predominantly trans configuration. This difference could result in different growth behavior of aerosols with long versus short chain compounds present at the surface. The presence of organic compounds with chain-lengths longer than butanol at the surface of atmospheric aerosols is expected to impede uptake

of volatile compounds by the aerosol, resulting in a reduced growth rate of the aerosols.

The results of this work suggest that although volatile alcohol compounds are taken up by SA solutions, the uptake will be diffusion limited, reducing the possible growth of acidic aerosols. Also, the uptake of compounds longer than BuOH will impede further uptake of volatile compounds, again reducing the rate of aerosol growth. Most importantly, the uptake of volatile organic compounds by acidic sulfate aerosols will be dependent on the aerosol acidity. In conclusion, newer aerosols with higher SA concentrations are expected to have higher growth rates from the uptake and transformation of volatile organic compounds.

APPENDIX A

VSFG FITTING PARAMETERS WITH EXAMPLES

Fitting of the VSFG spectra

The ssp VSFG spectra of the BuOH solutions were fit with four, five (to include a contribution from water), and six (to include ν_{CH3}-as) component peaks to determine the best overall fit. The 0.50 M BuOH in water ssp SFG spectrum is shown in Figure A.1 three times to show the differences in the fits. The four-component peak fit (a) considers only the expected BuOH peaks. The five-component peak fit (b) gave the best overall fit by including a contribution from water. Adding a sixth component peak to include a contribution from the methyl asymmetric stretch (c) did not improve the overall fit. The 0.050 M HexOH in water ssp SFG spectrum is also shown in Figure A.1 fit with (d) six and (e) seven component peaks. The six-component peak fit comprises only the expected HexOH peaks. Allowing for a water contribution, using seven component peaks gave the best overall fit.

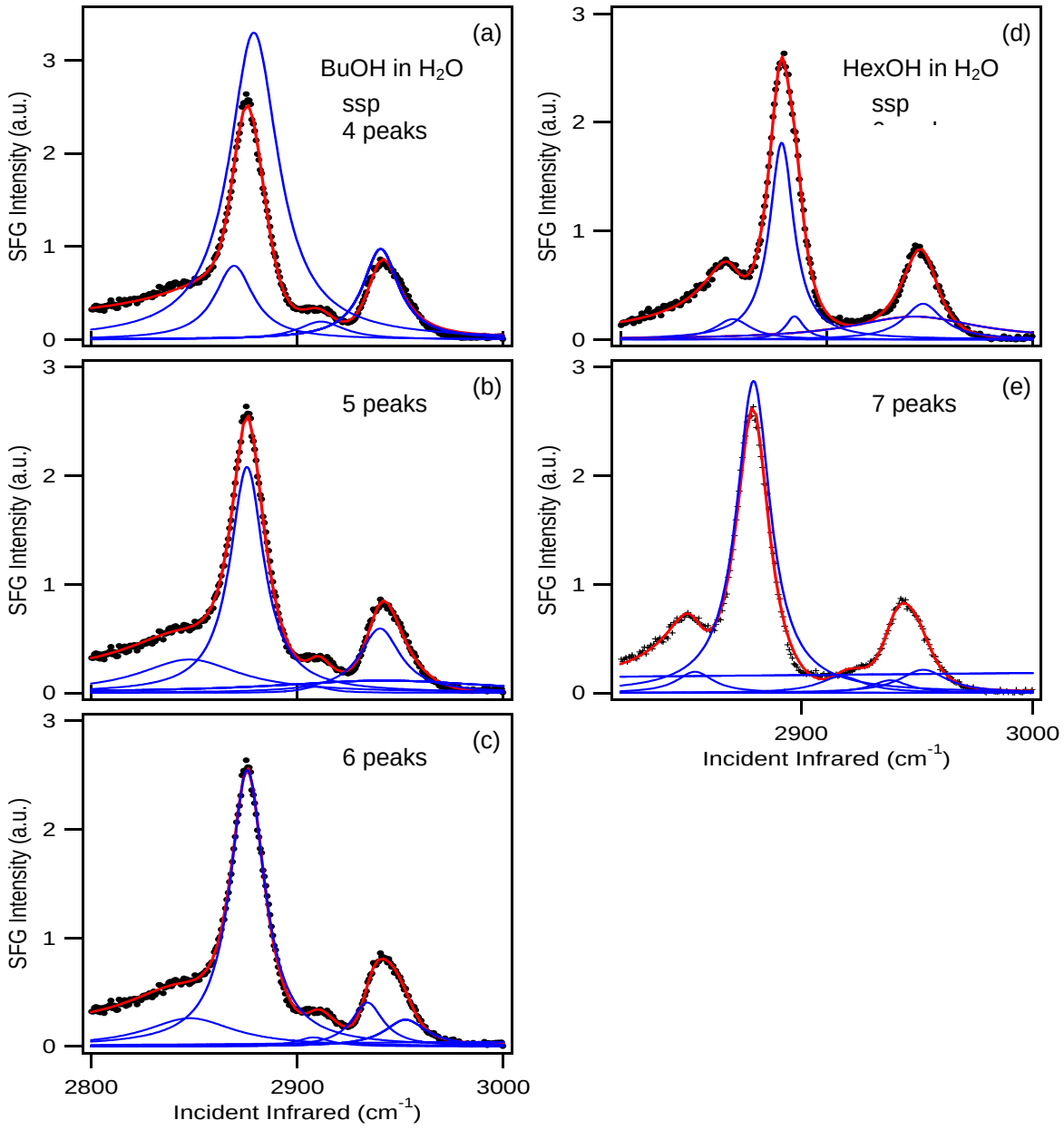

Figure A.1. Peak fits of (a-c) the ssp VSFG spectrum of 0.50 M BuOH in H_2O with (a) four, (b) five, and (c) six component peaks, and (d-e) the ssp VSFG spectrum of 0.050 M HexOH in H_2O with (d) six, and (e) seven component peaks. The original spectrum is shown as black data points, the overall fit is shown as the red line going through the data points, and the component peaks are shown in blue.

To determine the peak positions of each vibrational mode, the ssp, ppp, and sps VSFG spectra were fit with the appropriate component peaks. If a peak contribution was very small, i.e., the CH_3-ss in the ppp spectra, the position was held (see Tables A.1-A.4). The fitted 0.50 M BuOH in water ssp, ppp, and sps VSFG spectra are shown in Figure A.2. The ssp spectrum (a) is fit with five peaks, the ppp spectrum (b) is fit with three peaks, and the sps spectrum (c) is fit with two peaks. The fitted peak positions and assignments are shown in Tables A.1-A.4.

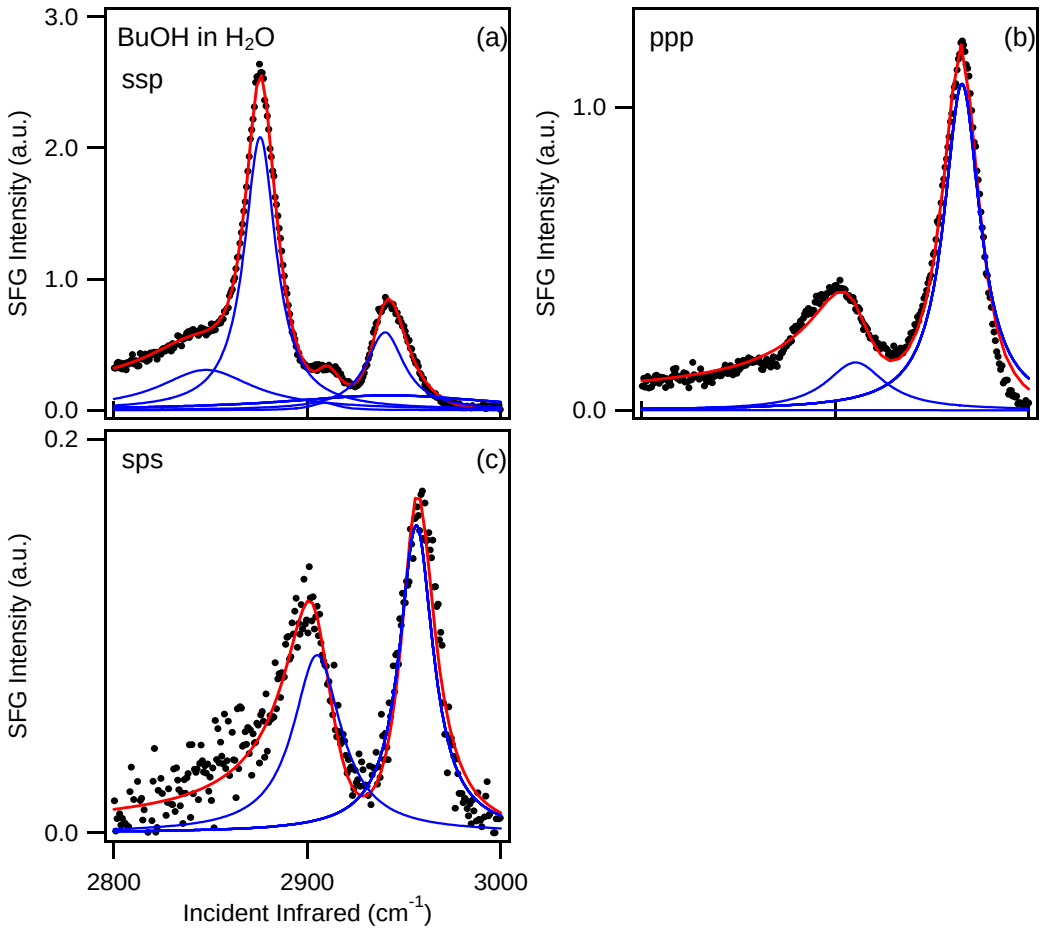

Figure A.2. Fitting of the (a) ssp, (b) ppp, and (c) sps SFG spectrum of 0.50 M BuOH in H_2O. The original spectrum is shown as black data points, the overall fit is shown in red,

and the component peaks are shown in blue.

	ν_{CH_2}-ss	ν_{CH_3}-ss	ν_{CH_2}-as	CH_2-FR	CH_3-FR	ν_{CH_3}-as
1-Butanol						
ssp	2846	2877		2908	2941	
ppp		2880(h)	2909			2966
sps			2889			2961
1-Hexanol						
ssp	2856	2878		2903/2922/2947	2939	
ppp		2880(h)	2920			2970
sps			2915			2961

Table A.1. Vibrational mode assignments for neat BuOH and neat HexOH with fitted peak positions. Peak positions held during the spectral fitting are indicated by (h).

	ν_{CH_2}-ss	ν_{CH_3}-ss	ν_{CH_2}-as	CH_2-FR	CH_3-FR	ν_{CH_3}-as
1-Butanol						
0.50 M						
ssp	2833	2879		2914	2941	
ppp		2885	2913			2973
sps			2908			2965
0.179 M						
ssp	2836	2876		2907	2938	
ppp		2880(h)	2910			2968
sps			2901			2955
0.052 M						
ssp	2848	2876		2919	2940	
ppp		2887(h)	2910			2965
sps			2905			2956
1-Hexanol						
0.050 M						
ssp	2854	2879	2917/2931/2953	2938		
ppp		2880(h)	2912			2969
0.0099 M						
ssp	2850	2879	2912/2925/2946	2938		
ppp		2880(h)	2912			2966
0.0051 M						
ssp	2852	2880	2909/2924/2947	2941		
ppp		2880(h)	2914			2966

Table A.2. Vibrational mode assignments for BuOH and HexOH solutions in water with fitted peak positions. Peak positions held during the spectral fitting are indicated by (h).

	ν_{CH_2}-ss	νCH_3-ss	ν_{CH_2}-as	CH_2-FR	CH_3-FR	ν_{CH_2}-as
1-Butanol						
0.50 M						
ssp	2835	2880		2912	2943	
ppp		2877	2902		2940	2962
sps			2905			2958
0.179 M						
ssp	2841	2878		2905 (h)	2941	
ppp		2880(h)	2916			2974
sps			2906			2956
0.052 M						
ssp	2835	2880		2912	2943	
ppp		2880(h)	2908			2969
sps			2905			2958
1-Hexanol						
0.050 M ssp	2852	2876		2881/2912/2974	2938	
0.0099 M ssp	2852	2876		2883/2912/2951	2937	
0.0051M ssp	2853	2876		2883/2914/2951	2937	

Table A.3. Vibrational mode assignments for BuOH and HexOH solutions in 0.78 M NH_4HSO_4 with fitted peak positions. Peak positions held during the spectral fitting are indicated by (h).

	ν_{CH_2}-ss	ν_{CH_3}-ss	ν_{CH_2}-as	CH_2-FR	CH_3-FR	ν_{CH_3}-as
1-Butanol						
0.50 M						
ssp	2848	2879		2912	2941	
ppp		2880(h)	2918			2969
sps			2911			2962
0.179 M						
ssp	2848(h)	2884		2915	2946	
ppp		2880(h)	2923			2970
sps			2920			2965
0.052 M						
ssp	2853	2879		2915	2939	
ppp	2866	2885(h)	2898		2925	2969
sps			2908			2970
1-Hexanol						
0.050 M ssp	2853	2878		2885/2903/2915	2945	
0.0099 M ssp	2858	2880		2885/2919/2952	2940	
0.0051 M ssp	2858	2878		2884/2901/2913	2946	

Table A.4. Vibrational mode assignments for BuOH and HexOH solutions in 59.5 wt% SA with fitted peak positions. Peak positions held during the spectral fitting are indicated by (h).

Normalization of spectra to methyl symmetric stretch

The butanol and hexanol solution ssp spectra were normalized to the most intense methyl symmetric stretch to compare spectral differences. The normalized spectra are shown in Figure A.3.

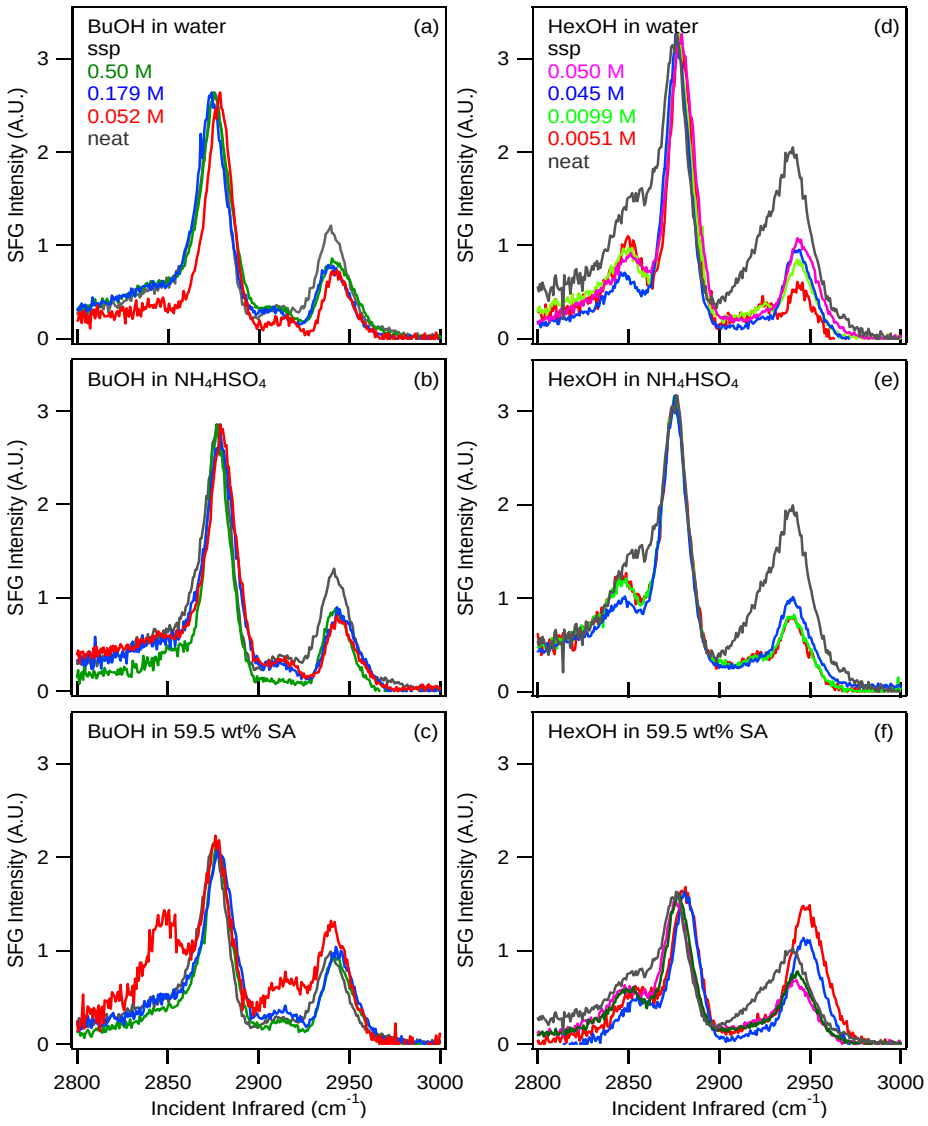

Figure A.3. VSFG ssp spectra of BuOH (a-c) and HexOH (d-f) solutions in

water, 0.78 M NH_4HSO_4, and 59.5 wt% SA normalized to the CH_3-ss.

Comparison of solvents

The differences in the ssp polarization spectra for each concentration of BuOH and HexOH were examined as a function of solvent. The spectra are shown in Figure A.4.

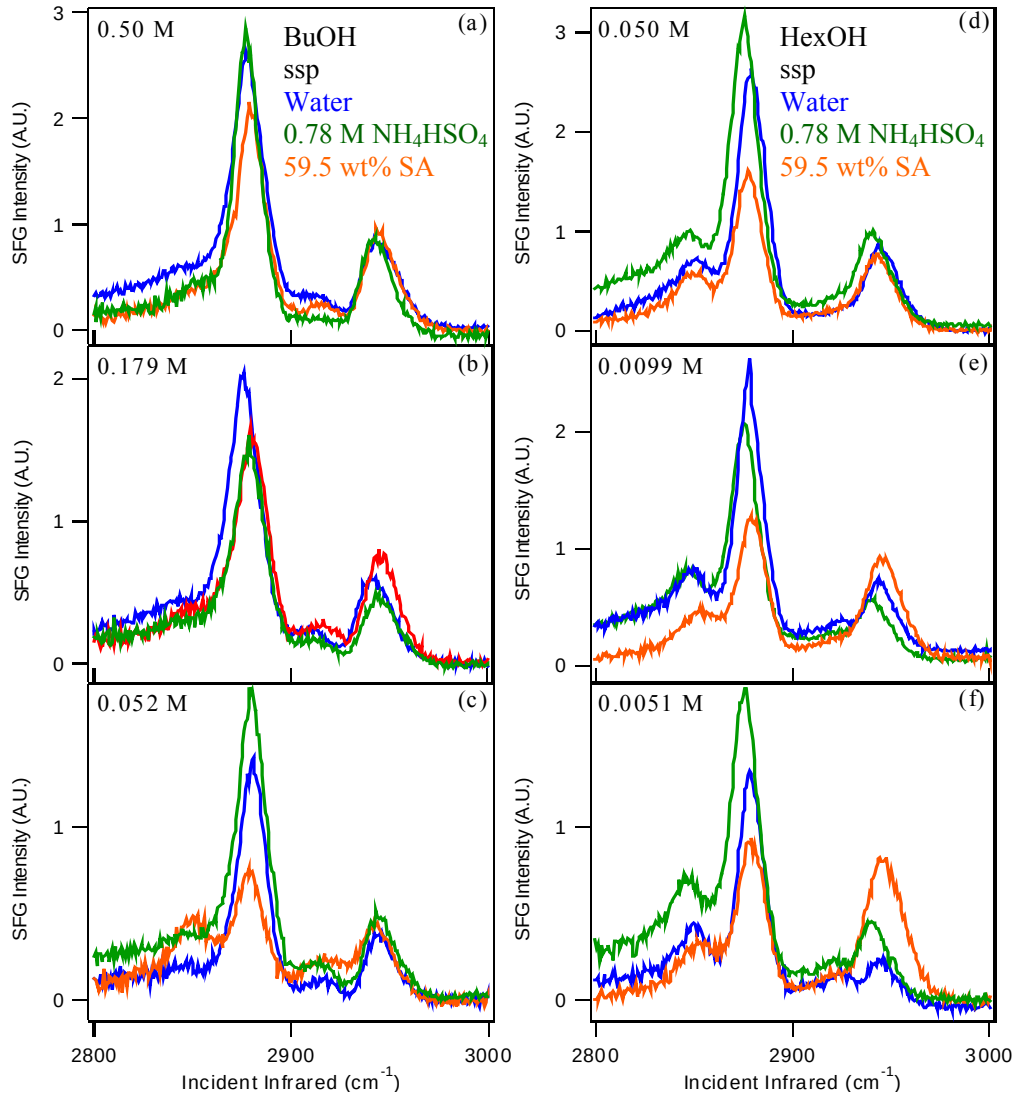

Figure A.4. VSFG ssp polarization spectra of (a-c) BuOH solution and (d-f) HexOH solution. The water solutions are shown in blue, the 0.78 M NH4HSO4 solutions

are shown in green, and the 59.5 wt% SA solutions are shown in orange.

Parameters for determination of θ

For a vibrational mode assigned to the terminal methyl group that is present in both the ssp and ppp SFG polarization spectra, the intensity ratio, $\sqrt{\frac{I_{ssp,ss}}{I_{ppp,ss}}}$, can be used to determine the orientation angle of the moiety. The intensity of the signal is proportional to the effective molecular susceptibility, $\chi_{eff}^{(2)}$, equation A.1.

$$I_{SFG} \propto |\chi^{(2)}|^2 I(\omega_{IR}) I(\omega_{800}) \qquad \text{(A.1)}$$

Since the same frequency is being probed with both polarization combinations, only $\chi_{eff}^{(2)}$ changes so that the ratio of intensity is proportional to the ratio of $\chi_{eff,ssp}/\chi_{eff,ppp}$, equation A.2.

$$\sqrt{\frac{I_{ssp,ss}}{I_{ppp,ss}}} = \frac{\chi_{eff,ssp\_ss(\vartheta)}}{\chi_{eff,ppp\_ss(\vartheta)}} \qquad \text{(A.2)}$$

By solving $\chi_{effssp}/\chi_{eff,ppp}$ for θ = (0–90)°,and comparing it to the intensity ratio, the angle of the terminal methyl group, relative to the surface normal, can be determined, assuming that the methyl group distribution is a delta function, that the surface is isotropic, and that the methyl group has C_{3v} symmetry.

An example of the Mathcad file (Mathcad Professional 2000) used to determine the terminal methyl angles is found at the end of this appendix. The file was modified for each solution investigated with the appropriate values for the required parameters. The orientation calculations require the input of several system-dependant variables, including the indices of refraction, the input beam wavelengths and incident angles, and the hyperpolarizability ratio (R) for the functional group being studied. The index of refraction of neat butanol used was n = 1.3973.[131] The index of refraction for each BuOH-water solution was extrapolated from data found in the literature.[132] The BuOH-NH_4HSO_4 solutions were assumed to have the same indices of refraction as the comparable water solutions. The value of n for the sulfuric acid solutions used was

the index of refraction for 60 wt% SA at 2880 cm^{-1}.[133] All of the values for n used are found in Table A.5. The visible beam wavelength was 799.8 nm. The IR peak chosen was the CH_3-ss at 2880 cm^{-1}. The hyperpolarizability ratio for the methyl group used was R = 3.4.[112] The experimental incident angles are also found in Table A.5. From this information the χ_{eff}(ssp) and χ_{eff}(ppp) for the symmetric stretch are calculated as a function of orientation angle, θ. The plots of the ratio of $\frac{\chi_{effective\_ssp\_SS(\theta)}}{\chi_{effective\_ppp\_SS(\theta)}}$ versus θ used are shown in Figure A.5. The ratio of the square root of the intensities of the CH_3-ss in the ssp and ppp spectra, $\sqrt{\frac{I_{ssp,ss}}{I_{ppp,ss}}}$, is calculated. From the plot, the angle corresponding to that ratio is the terminal methyl orientation angle. Once the orientation angle is known, the chain tilt angle can also be calculated as $\alpha = \left|35.5 - \theta_{CH_3}\right|$. The calculated BuOH methyl orientation angles and chain tilt angles are found in Table A.6.

θ_{vis}= 58°	n_{neat}[131] = 1.3973	$n_{0.052\ in\ H2O}$ = 1.3325
θ_{IR} = 66°	n_{SA}[133] =1.37624	$n_{0.179\ in\ H2O}$ = 1.3334
		$n_{0.50\ in\ H2O}$ = 1.3358

Table A.5. Variables used in the calculation of the methyl orientation angle, θ.

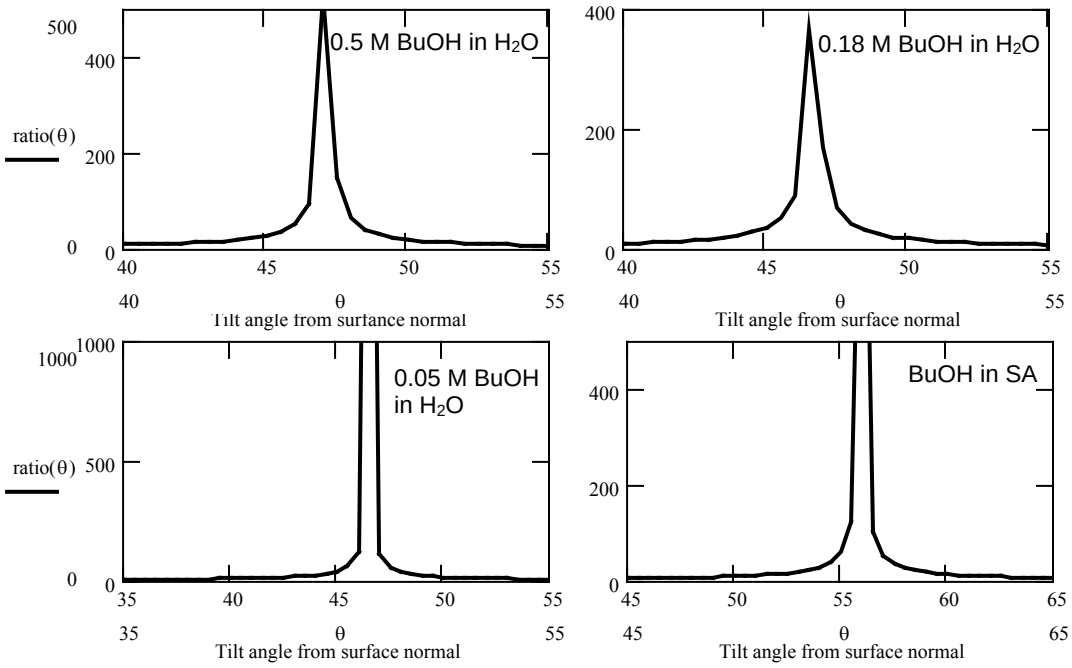

Figure A.5. Plots of $\frac{\chi_{effective\_ssp\_SS(\theta)}}{\chi_{effective\_ppp\_SS(\theta)}}$ versus θ for each solution. The terminal methyl orientation angle, θ, is read off the plot for the appropriate value(s) of the ratio.

	θ_{CH_3}	α		θ_{CH_3}	α		θ_{CH_3}	α
neat	57	21.5						
Water			59.5 wt% SA			0.78 M NH_4HSO_4		
0.50 M	44.5	9	0.50 M	46.5	11	0.50 M	47	9.5
0.179 M	39.5	4	0.179 M	48.5	13	0.179 M	42.5	7
0.052 M	46.5	11	0.052 M	67	31.5	0.052 M	41	5.5

Table A.6. Calculated orientation angles for the 1-butanol methyl group, θ_{CH_3}, and the butanol chain tilt angles, α.

Mathcad file used to determine methyl orientation angles:

Note:
1. The following program is for orientational analysis of methyl group.
2. For different chemical systems, values of n1, n2, n3, and r should be modified.

Here are some definitions for some parameters used in this program:

ω=SFG; ω1=vis; ω2=IR

n1 is the refractive index of air.
n2 is the refractive index of the solution.
n3 is the refractive index of interfacial region

n1ω is the refractive index of air at the wavelength of SFG
n2ω is the refractive index of water at the wavelength of SFG
n3ω is the refractive index of interfacial region at the wavelength of SFG
n1ωιis the refractive index of air at the wavelength of visible
n2ωι is the refractive index of the solution at the wavelength of visible
n3ωι is the refractive index of interfacial region at the wavelength of visible
n1ω2 is the refractive index of air at the wavelength of IR
n2ω2 is the refractive index of the solution at the wavelength of IR
n3ω2 is the refractive index of interfacial region at the wavelength of IR

β is the incident angle; γ is the refraction angle

βω is the incident angle for SFG; **βωι** is the Vis incident angle; **βω2** is the IR incident angle

γω is the incident angle for SFG; **γωι** is the Vis incident angle; γω2 is the IR incident angle

L is the Fresnel factor

χ is the 2nd order susceptibility

βaac and βccc are the molecular hyperpolarizabilities

$n1\omega 1 := 1$

$n1\omega 2 := 1$

$n1\omega := 1$

actual peak position of 800nm (nm)

$\omega 1 := 799.8$

$n2\omega 1 := 1.3325$

using n values calculated for the appropriate solution

actual peak position of IR (cm-1)

$\omega 2 := 2880$

$n2\omega 2 := 1.3325$

$$\omega := \frac{10000000}{\left(\omega 2 + \frac{10000000}{\omega 1}\right)}$$

calculated peak position of SFG (nm)

$\omega = 650.063$

$$n2\omega := -4.889045910^{-15}\cdot\omega^{6} + 2.0305040410^{-11}\cdot\omega^{5} - 3.506514410^{-8}\cdot\omega^{4} + 3.2229884110^{-5}\cdot\omega^{3} \ldots$$
$$+ -0.0166297664\omega^{2} + 4.56708627\omega - 520.231783$$

$n2\omega = 1.331$

incident angles of 800nm and IR (degree)

$\beta\omega 1 := 58$

$\beta\omega 2 := 66$

$$\beta\omega := \frac{180\cdot\operatorname{asin}\left(\frac{\omega}{\omega 1}\cdot\sin\left(\beta\omega 1\frac{\pi}{180}\right) + \frac{\omega 2\cdot\omega}{10^{7}}\cdot\sin\left(\beta\omega 2\frac{\pi}{180}\right)\right)}{\pi}$$

calculated incident angle of SFG (degree)

$\beta\omega = 59.351$

calculated refractive angle of 800nm (degree)

$$\gamma\omega 1 := 180\frac{\operatorname{asin}\left(\frac{n1\omega 1}{n2\omega 1}\cdot\sin\left(\beta\omega 1\frac{\pi}{180}\right)\right)}{\pi}$$

$\gamma\omega 1 = 39.526$

calculated refractive angle of IR (degree)

$$\gamma\omega 2 := 180\frac{\operatorname{asin}\left(\frac{n1\omega 2}{n2\omega 2}\cdot\sin\left(\beta\omega 2\frac{\pi}{180}\right)\right)}{\pi}$$

$\gamma\omega 2 = 43.282$

calculated refractive angle of SFG (degree)

$$\gamma\omega := 180\frac{\operatorname{asin}\left(\frac{n1\omega}{n2\omega}\cdot\sin\left(\beta\omega\frac{\pi}{180}\right)\right)}{\pi}$$

$\gamma\omega = 40.271$

calculated interfacial refractive index n3 of 800nm

$$n3\omega 1 := \sqrt{\frac{\left(n2\omega 1^4 + 5 \cdot n2\omega 1^2\right)}{4 \cdot n2\omega 1^2 + 2}}$$

$$n3\omega 1 = 1.15$$

calculated interfacial refractive index n3 of IR

$$n3\omega 2 := \sqrt{\frac{\left(n2\omega 2^4 + 5 \cdot n2\omega 2^2\right)}{4 \cdot n2\omega 2^2 + 2}}$$

$$n3\omega 2 = 1.15$$

calculated interfacial refractive index n3 of SFG

$$n3\omega := \sqrt{\frac{\left(n2\omega^4 + 5 \cdot n2\omega^2\right)}{4 \cdot n2\omega^2 + 2}}$$

$$n3\omega = 1.149$$

Fresnel factors for SFG beam

$$Lxx\omega := \frac{\left(2 \cdot n1\omega \cdot \cos\left(\gamma\omega \cdot \frac{\pi}{18}\right)\right)}{n1\omega \cdot \cos\left(\gamma\omega \cdot \frac{\pi}{180}\right) + n2\omega \cdot \cos\left(\beta\omega \cdot \frac{\pi}{180}\right)}$$

$$Lxx\omega = 1.02$$

$$Lyy\omega := \frac{\left(2 \cdot n1\omega \cdot \cos\left(\beta\omega \cdot \frac{\pi}{180}\right)\right)}{n1\omega \cdot \cos\left(\beta\omega \cdot \frac{\pi}{180}\right) + n2\omega \cdot \cos\left(\gamma\omega \cdot \frac{\pi}{180}\right)}$$

$$Lyy\omega = 0.668$$

$$Lzz\omega := \frac{\left(2 \cdot n2\omega \cdot \cos\left(\beta\omega \cdot \frac{\pi}{180}\right)\right) \cdot \left(\frac{n1\omega}{n3\omega}\right)^2}{n1\omega \cdot \cos\left(\gamma\omega \cdot \frac{\pi}{180}\right) + n2\omega \cdot \cos\left(\beta\omega \cdot \frac{\pi}{180}\right)}$$

$$Lzz\omega = 0.713$$

Fresnel factors for 800nm beam

$$Lxx\omega 1 := \frac{\left(2 \cdot n1\omega 1 \cdot \cos\left(\gamma\omega 1 \cdot \frac{\pi}{18}\right)\right)}{n1\omega 1 \cdot \cos\left(\gamma\omega 1 \cdot \frac{\pi}{180}\right) + n2\omega 1 \cdot \cos\left(\beta\omega 1 \cdot \frac{\pi}{180}\right)}$$

$$Lxx\omega 1 = 1.105$$

$$Lyy\omega 1 := \frac{\left(2 \cdot n1\omega 1 \cdot \cos\left(\beta\omega 1 \cdot \frac{\pi}{180}\right)\right)}{n1\omega 1 \cdot \cos\left(\beta\omega 1 \cdot \frac{\pi}{180}\right) + n2\omega 1 \cdot \cos\left(\gamma\omega 1 \cdot \frac{\pi}{180}\right)}$$

$$Lyy\omega 1 = 0.68$$

$$Lzz\omega 1 := \frac{\left(2 \cdot n2\omega 1 \cdot \cos\left(\beta\omega 1 \frac{\pi}{180}\right)\right) \cdot \left(\frac{n1\omega 1}{n3\omega 1}\right)^2}{n1\omega 1 \cdot \cos\left(\gamma\omega 1 \frac{\pi}{180}\right) + n2\omega 1 \cdot \cos\left(\beta\omega 1 \frac{\pi}{180}\right)}$$

$Lzz\omega 1 = 0.723$

Fresnel factors for IR beam

$$Lxx\omega 2 := \frac{\left(2 \cdot n1\omega 2 \cdot \cos\left(\gamma\omega 2 \frac{\pi}{18}\right)\right)}{n1\omega 2 \cdot \cos\left(\gamma\omega 2 \frac{\pi}{180}\right) + n2\omega 2 \cdot \cos\left(\beta\omega 2 \frac{\pi}{180}\right)}$$

$Lxx\omega 2 = 0.465$

$$Lyy\omega 2 := \frac{\left(2 \cdot n1\omega 2 \cdot \cos\left(\beta\omega 2 \frac{\pi}{180}\right)\right)}{n1\omega 2 \cdot \cos\left(\beta\omega 2 \frac{\pi}{180}\right) + n2\omega 2 \cdot \cos\left(\gamma\omega 2 \frac{\pi}{180}\right)}$$

$Lyy\omega 2 = 0.591$

$$Lzz\omega 2 := \frac{\left(2 \cdot n2\omega 2 \cdot \cos\left(\beta\omega 2 \frac{\pi}{180}\right)\right) \cdot \left(\frac{n1\omega 2}{n3\omega 2}\right)^2}{n1\omega 2 \cdot \cos\left(\gamma\omega 2 \frac{\pi}{180}\right) + n2\omega 2 \cdot \cos\left(\beta\omega 2 \frac{\pi}{180}\right)}$$

$Lzz\omega 2 = 0.646$

orientation angle θ of methyl group

$\theta := 0, 0.5 .. 90$

$\theta =$

0
0.5
1
1.5

$r := 3.4$

$\beta ccc := 1$

$Ns := 1$

For CH3-SS, the components of χ are given by:

$$\chi yyz\_SS(\theta) := \frac{1}{2} \cdot Ns \cdot \beta ccc \cdot \left[(1 + r) \cdot \cos\left(\theta \frac{\pi}{180}\right) - (1 - r) \cdot \left(\cos\left(\theta \frac{\pi}{180}\right)\right)^3\right]$$

$$\chi yzy\_SS(\theta) := \frac{1}{2} \cdot Ns \cdot \beta ccc \cdot (1 - r) \cdot \left[\cos\left(\theta \frac{\pi}{180}\right) - \left(\cos\left(\theta \frac{\pi}{180}\right)\right)^3\right]$$

Xxxz is equal to Xyyz

Xxzx is equal to Xyzy is equal to Xzxx is equal to Xzyy

$$\chi zzz\_SS(\theta) := Ns \cdot \beta ccc \cdot \left[r \cdot \cos\left(\theta \frac{\pi}{180}\right) + (1 - r) \cdot \left(\cos\left(\theta \frac{\pi}{180}\right)\right)^3 \right]$$

$$\chi effective\_ssp\_SS(\theta) := Lyy\omega \cdot Lyy\omega 1 \cdot Lzz\omega 2 \cdot \sin\left(\beta\omega 2 \frac{\pi}{180}\right) \cdot \chi yyz\_SS(\theta)$$

$$\begin{aligned}\chi effective\_ppp\_SS(\theta) := & -Lxx\omega \cdot Lxx\omega 1 \cdot Lzz\omega 2 \cdot \cos\left(\beta\omega \frac{\pi}{180}\right) \cdot \cos\left(\beta\omega 1 \frac{\pi}{180}\right) \cdot \sin\left(\beta\omega 2 \frac{\pi}{180}\right) \cdot \chi yyz\_SS(\theta) \ldots \\ & + Lxx\omega \cdot Lzz\omega 1 \cdot Lxx\omega 2 \cdot \cos\left(\beta\omega \frac{\pi}{180}\right) \cdot \sin\left(\beta\omega 1 \frac{\pi}{180}\right) \cdot \cos\left(\beta\omega 2 \frac{\pi}{180}\right) \cdot \chi yzy\_SS(\theta) \ldots \\ & + Lzz\omega \cdot Lxx\omega 1 \cdot Lxx\omega 2 \cdot \sin\left(\beta\omega \frac{\pi}{180}\right) \cdot \cos\left(\beta\omega 1 \frac{\pi}{180}\right) \cdot \cos\left(\beta\omega 2 \frac{\pi}{180}\right) \cdot \chi yzy\_SS(\theta) \ldots \\ & + Lzz\omega \cdot Lzz\omega 1 \cdot Lzz\omega 2 \cdot \sin\left(\beta\omega \frac{\pi}{180}\right) \cdot \sin\left(\beta\omega 1 \frac{\pi}{180}\right) \cdot \sin\left(\beta\omega 2 \frac{\pi}{180}\right) \cdot \chi zzz\_SS(\theta)\end{aligned}$$

$$\chi effective\_sps\_SS(\theta) := Lyy\omega \cdot Lzz\omega 1 \cdot Lyy\omega 2 \cdot \sin\left(\beta\omega 1 \frac{\pi}{180}\right) \cdot \chi yzy\_SS(\theta)$$

$\chi 2ssp\_SS(\theta) := \left(\left|\chi effective\_ssp\_SS(\theta)\right|\right)^2$

$\chi 2ppp\_SS(\theta) := \left(\left|\chi effective\_ppp\_SS(\theta)\right|\right)^2$

$\chi 2sps\_SS(\theta) := \left(\left|\chi effective\_sps\_SS(\theta)\right|\right)^2$

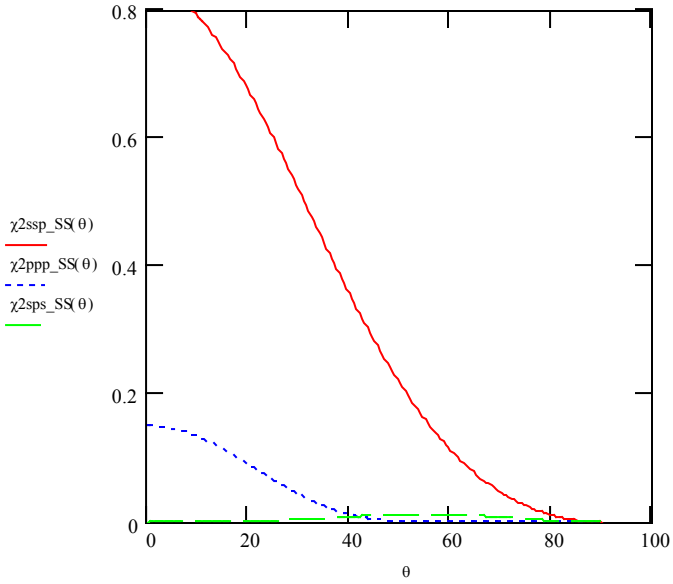

$ratio(\theta) := \dfrac{\left(\left|\chi effective\_ssp\_SS(\theta)\right|\right)}{\left(\left|\chi effective\_ppp\_SS(\theta)\right|\right)}$

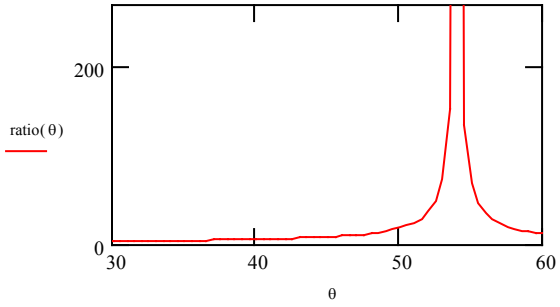

For CH3-AS, the components of χ are given by:

$$\beta aca := 1$$

$$\chi yyz\_AS(\theta) := (-1) \cdot Ns \cdot \beta aca \cdot \left[\cos\left(\theta \frac{\pi}{180}\right) - \left(\cos\left(\theta \frac{\pi}{180}\right)\right)^3 \right]$$

$$\chi yzy\_AS(\theta) := Ns \cdot \beta aca \cdot \left(\cos\left(\theta \frac{\pi}{180}\right)\right)^3$$

Xxxz is equal to Xyyz

Xxzx is equal to Xyzy is equal to Xzxx is equal to Xzyy

$$\chi zzz\_AS(\theta) := Ns \cdot \beta aca \cdot \left[\cos\left(\theta \frac{\pi}{180}\right) - \left(\cos\left(\theta \frac{\pi}{180}\right)\right)^3 \right]$$

$$\chi effective\_ssp\_AS(\theta) := Lyy\omega \cdot Lyy\omega 1 \cdot Lzz\omega 2 \cdot \sin\left(\beta\omega 2 \frac{\pi}{180}\right) \cdot \chi yyz\_AS(\theta)$$

$$\begin{aligned} \chi effective\_ppp\_AS(\theta) := & -Lxx\omega \cdot Lxx\omega 1 \cdot Lzz\omega 2 \cdot \cos\left(\beta\omega \frac{\pi}{180}\right) \cdot \cos\left(\beta\omega 1 \frac{\pi}{180}\right) \cdot \sin\left(\beta\omega 2 \frac{\pi}{180}\right) \cdot \chi yyz\_AS(\theta) \ldots \\ & + Lxx\omega \cdot Lzz\omega 1 \cdot Lxx\omega 2 \cdot \cos\left(\beta\omega \frac{\pi}{180}\right) \cdot \sin\left(\beta\omega 1 \frac{\pi}{180}\right) \cdot \cos\left(\beta\omega 2 \frac{\pi}{180}\right) \cdot \chi yzy\_AS(\theta) \ldots \\ & + Lzz\omega \cdot Lxx\omega 1 \cdot Lxx\omega 2 \cdot \sin\left(\beta\omega \frac{\pi}{180}\right) \cdot \cos\left(\beta\omega 1 \frac{\pi}{180}\right) \cdot \cos\left(\beta\omega 2 \frac{\pi}{180}\right) \cdot \chi yzy\_AS(\theta) \ldots \\ & + Lzz\omega \cdot Lzz\omega 1 \cdot Lzz\omega 2 \cdot \sin\left(\beta\omega \frac{\pi}{180}\right) \cdot \sin\left(\beta\omega 1 \frac{\pi}{180}\right) \cdot \sin\left(\beta\omega 2 \frac{\pi}{180}\right) \cdot \chi zzz\_AS(\theta) \end{aligned}$$

$$\chi effective\_sps\_AS(\theta) := Lyy\omega \cdot Lzz\omega 1 \cdot Lyy\omega 2 \cdot \sin\left(\beta\omega 1 \frac{\pi}{180}\right) \cdot \chi yzy\_AS(\theta)$$

$\chi 2ssp\_AS(\theta) := \left(\left|\chi effective\_ssp\_AS(\theta)\right|\right)^2$

$\chi 2ppp\_AS(\theta) := \left(\left|\chi effective\_ppp\_AS(\theta)\right|\right)^2$

$\chi 2sps\_AS(\theta) := \left(\left|\chi effective\_sps\_AS(\theta)\right|\right)^2$

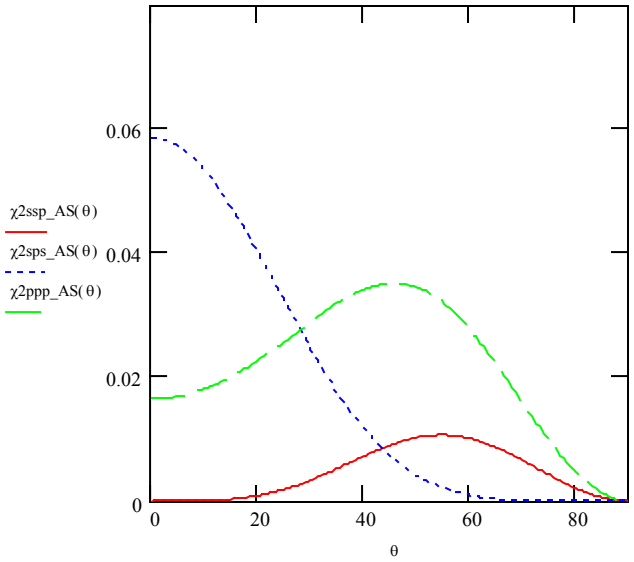

$$\frac{(|\chi_{effective\_ppp\_A\$}(\theta)|)}{(|\chi_{effective\_sps\_A\$}(\theta)|)}$$

0.53
0.53
0.53
0.531
0.532
0.533
0.534
0.536
0.538
0.54
0.542
0.545
0.548
0.551
0.555
0.558

$$\frac{(|\chi_{effective\_ppp\_AS}(\theta)|)}{(|\chi_{effective\_sps\_AS}(\theta)|)}$$

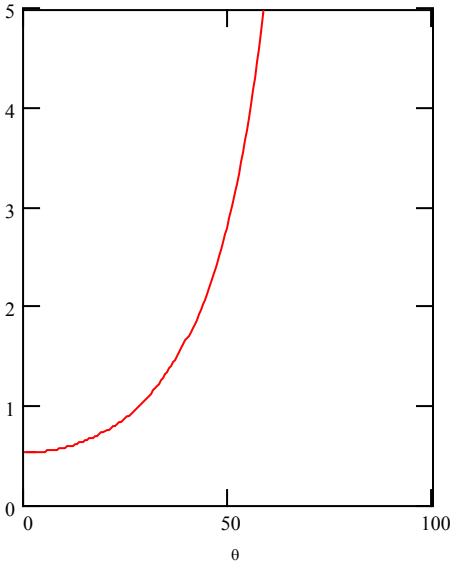

APPENDIX B

DIFFUSION INTO A SLAB WITH ONE OPEN BOUNDARY

Fick's second law of diffusion, equation B.1, relates the change in concentration as a function of time with the change in concentration as a function of depth.

$$\frac{\partial u}{\partial t} = D\frac{\partial^2 u}{\partial z^2} \qquad \text{(B.1)}$$

where u is the concentration, and D is the diffusion coefficient. Each side of the equation B.1 considers only time, t, or position, z, each side.

To solve equation B.1 for the concentration u, let the solution have two parts, one dependent on position, Z, and one dependent on time, T, equation B.2

$$u=ZT \qquad \text{(B.2)}$$

solving the partial differential equations

$$\frac{1}{DT}\frac{\partial T}{dt} = \frac{1}{Z}\frac{\partial^2 Z}{\partial z^2} \qquad \text{(B.3)}$$

The two sides of the equation can be separated and set equal to a constant, $-\mu^2$.

$$\frac{1}{DT}\frac{\partial T}{dt} = -\mu^2 \qquad \text{(B.4)}$$

and

$$\frac{1}{X}\frac{\partial^2 Z}{\partial x^2} = -\mu^2 \qquad \text{(B5)}$$

Setting each equal to 0 gives

$$\frac{\partial T}{\partial t} + \mu^2 DT = 0 \qquad \text{(B.6)}$$

$$\frac{\partial Z}{\partial z} + \mu^2 Z = 0 \qquad \text{(B.7)}$$

The general solutions to equations B.6 and B.7 are

$$T = C\exp[-\mu^2 DT] \qquad \text{(B.8)}$$

and

$$Z = A\sin \mu z + B\cos \mu z \qquad \text{(B.9)}$$

Substituting these solutions back into equation B.2 gives two solutions, B.10 and B.11

$$u = a\sin \mu \exp[-\mu^2 Dt] \qquad \text{(B.10)}$$

$$u = b\cos \mu \exp[-\mu^2 Dt] \qquad \text{(B.11)}$$

To correctly solve equation B.1, the correct boundary conditions must be chosen for the experimental setup. For diffusion into a finite slab with one open boundary, Figure B.1:

The starting condition is

1. u=0 at t<=0

The boundary conditions are

2. u=0 for 0<z<L
3. $u=u_0$ for z=0 because the open boundary is at the top of the experimental system.
4. $\partial u/\partial z=0$ at z=L because the closed boundary is at the bottom of the system.

$$u = u_0\{1 - \frac{4}{\pi}\sum_{\nu=0}^{\nu=\infty}(\frac{1}{(2\nu+1)}\sin\frac{(2\nu+1)\pi x}{2L}\exp[\frac{-(2\nu+1)^2\pi^2 Dt}{4L^2}]\} \qquad \text{(B.12)}$$

In equation B.12, u is the concentration, u_0 is the surface concentration, ν is an integer, L is the solution thickness (cm), and x is the probe position beneath the surface (cm), and t is time (seconds). D is the diffusion coefficient (cm^2/s), and it is assumed to be independent of concentration.

The summation was evaluated to determine the number of terms required for the expansion. The limit was set at a change of 1% or less with the addition of another term. With this limit, it was found that the expansion series requires ν=0 to ν=6.

In Raman spectroscopy the peak area is proportional to the concentration. To minimize the amount of error in the returned diffusion coefficient, peak areas and not concentrations were used in the fit, equation B.13.

$$A = A_0\{1 - \frac{4}{\pi}\sum_{\nu=0}^{\nu=\infty}(\frac{1}{(2\nu+1)}\sin\frac{(2\nu+1)\pi x}{2L}\exp[\frac{-(2\nu+1)^2\pi^2 Dt}{4L^2}]\} \qquad \text{(B.13)}$$

In equation B.13, A is the peak area and A_0 is the "surface area." When determining the peak areas, care was taken to keep the Voigt shape similar within an experiment.

The data was fit using a weighted fit to include the standard deviations of the peak areas. The fitting requires user input for the following parameters: the surface area, A0, the solution thickness, L (held constant), the probe depth, x (held constant), and the diffusion coefficient, D. After fitting, the best values for the diffusion coefficient and surface "peak area" are returned by the software. To confirm that the expansion to ν=6 was valid, the number of expansion terms was changed to ν=10 for one experiment. No change in the value for the diffusion coefficient and no improvement in the standard deviation were noted.

A fitting function was written for use in IgorPro 4.05 to solve equation B.13 for D and A_0:

```
#pragma rtGlobals=1                    // Use modern global access method.

function diffusion(w,t) : fitfunc
        wave w
        variable t  //time
        variable h=2.4, x=0.35
        variable n=0, total=0
do
```

```
  total+=1/(2*n+1)*sin((2*n+1)/w[3]*Pi*w[2])*exp(((2*n+1)/w[3]*Pi)*((2*n+1)/w[3]*
Pi)*w[0]*t)

  n+=1
  while (n<=6) //change for number of terms needed

      variable C=w[1]*(1-4/Pi*total)
      return C

  End
```

Initial starting guesses for the following parameters are provided by the user:

w[0] is the diffusion coefficient, D (allowed to vary).

w[1] is surface area, A0 (allowed to vary).

w[2] is the 2*slab depth, 2L (held constant).

w[3] is the probe position beneath the surface, x (held constant).

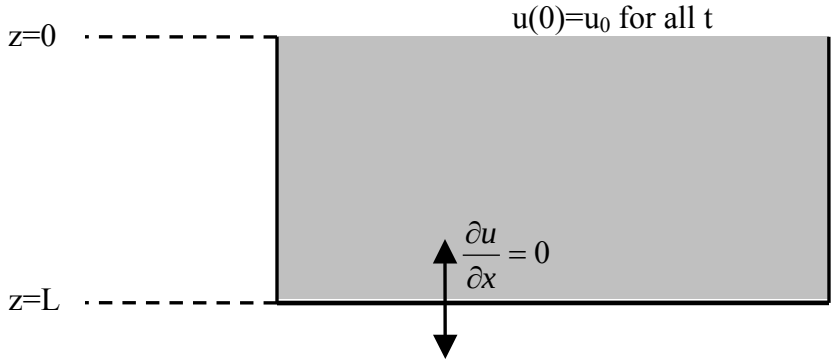

Figure B.1. Diffusion into a slab: Boundary conditions.

REFERENCES

(1) Kerminen, V.-M.; Anttila, T.; Lehtinen, K. E. J.; Kulmala, M. *Aerosol Sci. Tech.* **2004**, *38*, 1001-1008.

(2) Facchini, M. C.; Decesari, S.; Mircea, M.; Fuzzi, S.; Loglio, G. *Atmos. Environ.* **2000**, *34*, 4853-4857.

(3) Facchini, M. C.; Mircea, M.; Fuzzi, S.; Charlson, R. J. *Nature* **1999**, *401*, 257-259.

(4) Murphy, D. M.; Thomson, D. S.; Mahoney, M. J. *Science* **1998**, *282*, 1664-1669.

(5) Singh, H.; Chen, Y.; Staudt, A.; Jacob, D.; Blake, D.; Heikes, B.; Snow, J. *Nature* **2001**, *410*, 1078 - 1081.

(6) Donaldson, D. J.; Vaida, V. *Chem. Rev.* **2006**, *106*, 1445-1461.

(7) Noziere, B.; Esteve, W. *Geophys. Res. Lett.* **2005**, *32*, L03812, doi:10.1029/2004GL021942.

(8) Anttila, T.; Kerminen, V.-M. *J. Geophys. Res.* **2002**, *107*, AAC 12.

(9) Anttila, T.; Kerminen, V.-M. *J. Geophys. Res.* **2003**, *108*, AAC 1.

(10) Kumar, P. P.; Broekhuizen, K.; Abbatt, J. P. D. *Atmos. Chem. Phys.* **2003**, *3*, 509-520.

(11) Yu, S. *Atmos. Res.* **2000**, *53*, 185-217.

(12) Zhang, K. M.; Wexler, A. S. *J. Geophys. Res.* **2002**, *107*, AAC15-1-15-6.

(13) Romero, F.; Oehme, M. *J. Atmos. Chem.* **2005**, *52*, 283-294.

(14) Surratt, J. D.; Kroll, J. H.; Kleindienst, T. E.; Edney, E. O.; Claeys, M.; Sorooshian, A.; Ng, N. L.; Offenberg, J. H.; Lewandowski, M.; Jaoui, M.; Flagan, R. C.; Seinfeld, J. H. *Environ. Sci. Technol.* **2007**, *41*, 517-527.

(15) Liggio, J.; Li, S.-M. *Geophys. Res. Lett.* **2006**, *33*, L13808.

(16) Jang, M.; Lee, S.; Kamens, R. M. *Atmos. Environ.* **2003**, *37*, 2125-2138.

(17) Liggio, J.; Li, S.-M.; McLaren, R. *Environ. Sci. Technol.* **2005**, *39*, 1532-1541.

(18) Zhao, J.; Levitt, N. P.; Zhang, R.; Chen, J. *Environ. Sci. Technol.* **2006**, *40*, 7682-7687.

(19) Galbally, I. E.; Kirstine, W. *J. Atmos. Chem.* **2002**, *43*, 195-229.

(20) Tie, X.; Guenther, A.; Holland, E. *Geophys. Res. Lett.* **2003**, *30*, 1881.

(21) Heikes, B. G.; Chang, W.; Pilson, M. E. Q.; Swift, E.; Singh, H. B.; Guenther, A.; Jacob, D. J.; Field, B. D.; Fall, R.; Riemer, D.; Brand, L. *Global Biogeochem. Cycles* **2002**, *16*, 80-1-80-13.

(22) Singh, H. B.; Salas, L. J.; Chatfield, R. B.; Czech, E.; Fried, A.; Walega, J.; Evans, M. J.; Field, B. D.; Jacob, D. J.; Blake, D.; Heikes, B.; Talbot, R.; Sachse, G.; Crawford, J. H.; Avery, M. A.; Sandholm, S.; Fuelberg, H. *J. Geophys. Res.* **2004**, *109*, D15S07, doi:10.1029/2003JD003883.

(23) Scheeren, H. A.; Lelieveld, J.; Roelofs, G. J.; Williams, J.; Fischer, H.; de Reus, M.; de Gouw, J. A.; Warneke, C.; Holzinger, R.; Schlager, H.; Klupfel, T.; Bolder, M.; van der Veen, C.; Lawrence, M. *Atmos. Chem. Phys.* **2003**, *3*, 1589-1608.

(24) Fischer, H.; de Reus, M.; Traub, M.; Williams, J.; Lelieveld, J.; de Gouw, J.; Warneke, C.; Schlager, H.; Minikin, A.; Scheele, R.; Siegmund, P. *Atmos. Chem. Phys.* **2003**, *3*, 739-745.

(25) Fall, R. *Chem. Rev.* **2003**, *103*, 4941-4951.

(26) Karl, T.; Potosnak, M.; Guenther, A. *J. Geophys. Res.* **2004**, *109*, D18306, doi:10.1029/2004JD004738.

(27) Mao, H.; Talbot, R.; Nielsen, C.; Sive, B. *Geophys. Res. Lett.* **2006**, *33*, L02803.

(28) Schade, G. W.; Goldstein, A. H. *Global Biogeochem. Cycles* **2006**, *20*, GB1011.

(29) Lathiere, J.; Hauglustaine, D. A.; Friend, A. D.; De Noblet-Ducoudre, N.; Viovy, N.; Folberth, G. A. *Atmos. Chem. Phys.* **2006**, *6*, 2129–2146.

(30) Holzinger, R.; Williams, J.; Salisbury, G.; Klüpfel, T.; de Reus, M.; Traub, M.; Crutzen, P.; Lelieveld, J. *Atmos. Chem. Phys.* **2005**, *5*, 39-46.

(31) Lewis, A. C.; Hopkins, J. R.; Carpenter, L. J.; Stanton, J.; Read, K. A.; Pilling, M. J. *Atmos. Chem. Phys.* **2005**, *5*, 1963-1974.

(32) de Gouw, J. A.; Warneke, C.; Stohl, A.; Wollny, A. G.; Brock, C. A.; Cooper, O. R.; Holloway, J. S.; Trainer, M.; Fehsenfeld, F. C.; Atlas, E. L.; Donnelly, S. G.; Stroud, V.; Lueb, A. *J. Geophys. Res.* **2006**, *111*, D10303, doi:10.1029/2005JD006175.

(33) Singh, H. B.; Tabazadeh, A.; Evans, M. J.; Field, B. D.; Jacob, D. J.; Sachse, G.; Crawford, J. H.; Shetter, R.; Brune, W. H. *Geophys. Res. Lett.* **2003**, *30*, 1862 doi:10.1029/2003GL017933.

(34) Jacob, D. J.; Field, B. D.; Li, Q.; Blake, D. R.; de Gouw, J.; Warneke, C.; Hansel, A.; Wisthaler, A.; Singh, H. B.; Guenther, A. *J. Geophys. Res.* **2005**, *110*, D08303, doi:10.1029/2004JD005172.

(35) Finlayson-Pitts, B. J.; Pitts, J., James N. *Chemistry of the Upper and Lower Atmosphere*; Academic Press: San Diego, CA, 2000.

(36) Brock, C. A.; Wilson, J. C.; Honsson, H. H. *Science* **1995**, *270*, 1650-1653.

(37) Kusaka, I.; Wang, Z.-G.; Seinfeld, J. H. *J. Chem. Phys.* **1998**, *108*, 6829-6848.

(38) Brandt, C.; van Eldik, R. *Chem. Rev.* **1995**, *95*, 119-190.

(39) Johnson, C. M.; Tyrode, E. *Phys. Chem. Chem. Phys.* **2005**, *7*, 2635-2640.

(40) Shultz, M. J.; Baldelli, S.; Schnitzer, C.; Simonelli, D. *J. Phys. Chem. B* **2002**, *106*, 5313-5324.

(41) Tarbuck, T. L.; Richmond, G. L. *J. Am. Chem. Soc.* **2006**, *128*, 3256-3267.

(42) Van Loon, L. L.; Allen, H. C. *J. Phys. Chem. B* **2004**, *108*, 17666-17674.

(43) Voss, L. F.; Hadad, C. M.; Allen, H. C. *J. Phys. Chem. B* **2006**, *110*, 19487-19490.

(44) Lambert, A. G.; Davies, P. B.; Neivandt, D. J. *Appl. Spectrosc. Rev.* **2005**, *40*, 103-145.

(45) Moad, A. J.; Simpson, G. J. *J. Phys. Chem. B* **2004**, *108*, 3548-3562.

(46) Shen, Y.-R. *Surf. Sci.* **1994**, *299-300*, 551-562.

(47) Zhuang, X.; Miranda, P. B.; Kim, D.; Shen, Y.-R. *Phys. Rev. B* **1999**, *59*, 12632-12640.

(48) Hommel, E. L.; Ma, G.; Allen, H. C. *Anal. Sci.* **2001**, *17*, 137-139.

(49) Ma, G.; Allen, H. C. *J. Phys. Chem. B* **2003**, *107*, 6343-6349.

(50) Ma, G.; Allen, H. C. *Photchem. Photobiol.* **2006**, *82*, 1517-1529.

(51) McCreery, R. L. *Raman Spectroscopy for Chemical Analysis*; John Wiley & Sons, Inc.: New York, 2000.

(52) Iraci, L. T.; Essin, A. M.; Golden, D. M. *J. Phys. Chem. A* **2002**, *106*, 4054 - 4060.

(53) Kane, S. M.; Leu, M.-T. *J. Phys. Chem. A* **2001**, *105*, 1411-1415.

(54) Deno, N. C.; Newman, M. S. *J. Am. Chem. Soc.* **1950**, *72*, 3852-3856.

(55) Frisch, M. J.; Trucks, G. W.; Schlegel, H. B.; Scuseria, G. E.; Robb, M. A.; Cheeseman, J. R.; J. A. Montgomery, J.; Vreven, T.; Kudin, K. N.; Burant, J. C.; Millam, J. M.; Iyengar, S. S.; Tomasi, J.; Barone, V.; Mennucci, B.; Cossi, M.; Scalmani, G.; Rega, N.; Petersson, G. A.; Nakatsuji, H.; Hada, M.; Ehara, M.; K. Toyota; Fukuda, R.; Hasegawa, J.; Ishida, M.; Nakajima, T.; Honda, Y.; Kitao, O.; Nakai, H.; Klene, M.; Li, X.; Knox, J. E.; Hratchian, H. P.; Cross, J. B.; Adamo, C.; Jaramillo, J.; Gomperts, R.; Yazyev, R. E. S.; Austin, A. J.; Cammi, R.; Pomelli, C.; Ochterski, J. W.; Ayala, P. Y.; Morokuma, K.; Voth, G. A.; Salvador, P.; Dannenberg, J. J.; Zakrzewski, V. G.; Dapprich, S.; Daniels, A. D.; Strain, M. C.; Farkas, O.; Malick, D. K.; Rabuck, A. D.; Raghavachari, K.; Foresman, J. B.; Ortiz, J. V.; Cui, Q.; Baboul, A. G.; Clifford, S.; Cioslowski, J.; Stefanov, B. B.; Liu, G.; Liashenko, A.; Piskorz, P.; Komaromi, I.; Martin, R. L.; Fox, D. J.; Keith, T.; Al-Laham, M. A.; Peng, C. Y.; Nanayakkara, A.; Challacombe, M.; Gill, P. M. W.; Johnson, B.; Chen, W.; Wong, M. W.; Gonzalez, C.; Pople, J. A. Gaussian 03, Revision B.04; Gaussian, Inc.: Pittsburgh, PA, 2003.

(56) Whitfield, D. M.; Tang, T.-H. *J. Am. Chem. Soc.* **1993**, *115*, 9648-9654.

(57) Walrafen, G. E.; Yang, W.-H.; Chu, Y. C.; Hokmabadi, M. S. *J. Solution Chem.* **2000**, *29*, 905-936.

(58) Weston Jr, R. E.; Ehrenson, S.; Heinzinger, K. *J. Am. Chem. Soc.* **1967**, *89*, 481 - 486.

(59) Solkan, V. N.; Kuz'min, I. V.; Kazanskii, V. B. *Kinet. Catal.* **2001**, *42*, 411-417.

(60) Torn, R. D.; Nathanson, G. M. *J. Phys. Chem. B* **2002**, *106*, 8064.

(61) Christe, K. O.; Curtis, E. C. *Spectrochim. Acta* **1972**, *28A*, 1889-1898.

(62) Tomikawa, K.; Kanno, H. *J. Phys. Chem. A* **1998**, *102*, 6082-6088.

(63) Batamack, P.; Fraissard, J. *Colloids Surf., A* **1999**, *158*, 207-210.

(64) Marziano, N. C.; Tomasin, A.; Tortato, C.; Isandelli, P. *J. Chem. Soc., Perkin Trans. 2* **1998**, 2535-2540.

(65) Vinnik, M. I.; Kislina, I. S.; Kitaigorodskii, A. N.; Nikitaev, A. T. *Izvestiya Akademii Nauk SSSR, Seriya Khimicheskaya* **1987**, 2447-2453.

(66) Song, J.; Lu, T.; Mao, C. Preparation of dimethyl sulfate from low concentration sulfur trioxide.; Xinghua Pharmaceutical Factory, Shangdong Province, Peop. Rep. China: China, 1987.

(67) Xu, F. *Pige Huagong* **2000**, *17*, 39-40.

(68) Guldan, E. D.; Schindler, L. R.; Roberts, J. T. *J. Phys. Chem.* **1995**, *99*, 16059-16066.

(69) Hore, D. K.; Beaman, D. K.; Richmond, G. L. *J. Am. Chem. Soc.* **2005**, *127*, 9356-9357.

(70) Bertie, J. E.; Zhang, S. L. *J. Molec. Struct.* **1997**, *413-414*, 333-363.

(71) Gillespie, R. J.; Robinson, E. A. *Can. J. Chem.* **1962**, *40*, 658-674.

(72) Goypiron, A.; de Villepin, J.; Novak, A. *J. Chim. Phys.* **1978**, *75*, 889-894.

(73) Givan, A.; Larsen, L. A.; Loewenschuss, A.; Nielsen, C. J. *J. Molec. Struct.* **1999**, *509*, 35-47.

(74) Nash, K. L.; Sully, K. J.; Horn, A. B. *J. Phys. Chem. A* **2001**, *105*, 9422-9426.

(75) Bertoluzza, A.; Fagnano, C.; Morelli, M. A.; Tosi, R. *J. Raman. Spec.* **1987**, *18*, 77-81.

(76) Okabayashi, H.; Okuyama, M.; Kitagawa, T.; Miyazawa, T. *Bull. Chem. Soc. Jap.* **1974**, *47*, 1075-1077.

(77) Hilton, M.; Lettington, A. H.; Mills, I. M. *Meas. Sci. Technol.* **1995**, *6*, 1236-1241.

(78) Rothman, L. S.; Jacquemart, D.; Barbe, A.; Benner, D. C.; Birk, M.; Brown, L. R.; Carleer, M. R.; Chackerian Jr., C.; Chance, K.; Coudert, L. H.; Dana, V.; Devi, V. M.; Flaud, J.-M.; Gamache, R. R.; Goldman, A.; Hartmann, J.-M.; Jucks, K. W.; Maki, A. G.; Mandin, J.-Y.; Massie, S. T.; Orphal, J.; Perrin, A.; Rinsland, C. P.; Smith, M. A. H.; Tennyson, J.; Tolchenov, R. N.; Toth, R. A.; Auwera, J. V.; Varanasi, P.; Wagner, G. *J. Quant. Spect. Ra.* **2005**, *96*, 139-204.

(79) Chen, H.; Gan, W.; Lu, R.; Guo, Y.; Wang, H.-f. *J. Phys. Chem. B* **2005**, *109*, 8064-8075.

(80) Sung, J.; Park, K.; Kim, D. *J. Phys. Chem. B* **2005**, *109*, 18507-18514.

(81) Van Loon, L. L.; Allen, H. C. *J. Phys. Chem. A* **2007**, *Submitted*.

(82) Perdoncin, G.; Scorrano, G. *J. Am. Chem. Soc.* **1977**, *99*, 6983-6986.

(83) Davidovits, P.; Kolb, C.; Williams, L.; Jayne, J.; Worsnop, D. *Chemical reviews* **2006**, *106*, 1323-1354.

(84) Kleno, J. G.; Kristiansen, M. W.; Nielsen, C. J.; Pederson, E. J.; Williams, L. R.; Pederson, T. *J. Phys. Chem. A* **2001**, *105*, 8440-8444.

(85) Klassen, J. K.; Hu, Z.; Williams, L. R. *J. Geophys. Res.* **1998**, *103*, 16197-16202.

(86) Langenberg, S.; Proksch, V.; Schurath, U. *Atmos. Environ.* **1998**, *32*, 3129-3137.

(87) Van Loon, L. L.; Allen, H. C. *In preparation* **2007**.

(88) Bardow, A.; Goke, V.; Koss, H.-J.; Lucas, K.; Marquardt, W. *Fluid Phase Equil.* **2005**, *228-229*, 357-366.

(89) Jacobs, M. *Diffusion Processes*; Springer-Verlag New York:, 1967.

(90) Jost, W. *Diffusion in Solids, Liquids, Gases*; Academic Press New York:, 1960.

(91) Lee, Y. E.; Li, S. F. Y. *J. Chem. Eng. Data* **1991**, *36*, 240-243.

(92) Matthews, M. A.; Akgerman, A. *J. Chem. Eng. Data* **1988**, *33*, 122-123.

(93) Reid, R. C.; Prausnitz, J. M.; Poling, B. E. *The Properties of Gases and Liquids (4th)*; McGraw-Hill, Inc.: New York, 1987.

(94) Lee, D. G.; Cameron, R. *J. Am. Chem. Soc.* **1971**, *93*, 4724 - 4728.

(95) Knopf, D. A.; Luo, B. P.; Krieger, U. K.; Koop, T. *J. Phys. Chem. A* **2003**, *107*, 4322-4332.

(96) Lund Myhre, C. E.; Christensen, D. H.; Nicolaisen, F. M.; Nielsen, C. J. *J. Phys. Chem. A* **2003**, *107*, 1979-1991.

(97) Viscosity of Liquids. In *CRC Handbook of Chemistry and Physics, Internet Version (87th Edition)*; Lide, D. R., Ed.; Taylor and Francis: Boca Raton, FL, 2007.

(98) Williams, L. R.; Long, F. S. *J. Phys. Chem. A* **1995**, *99*, 3748-3751.

(99) http://www.inorganics.basf.com/.

(100) Alexander, A. *Rep. Prog. Phys.* **1942**, *9*, 158-176.

(101) Alexander, A. *P. Roy. Soc. of Lond. Ser-A* **1942**, *179*, 486-499.

(102) Glass, S. V.; Park, S.-C.; Nathanson, G. M. *J. Phys. Chem. A* **2006**, *110*, 7593-7601.

(103) Gao, J.; Jorgensen, W. L. *J. Phys. Chem.* **1988**, *92*, 5813-5822.

(104) Chen, B.; Siepmann, J. I.; Klein, M. L. *J. Am. Chem. Soc.* **2002**, *124*, 12232-12237.

(105) Lawrence, J. R.; Glass, S. V.; Nathanson, G. M. *J. Phys. Chem. A* **2005**, *109*, 7449-7457.

(106) Lawrence, J. R.; Glass, S. V.; Park, S.-C.; Nathanson, G. M. *J. Phys. Chem. A* **2005**, *109*, 7458-7465.

(107) Thornton, J. A.; Abbatt, J. P. D. *J. Phys. Chem. A* **2005**, *109*, 10004-10012.

(108) Lu, R.; Gan, W.; Wu, B.; Zhang, Z.; Guo, Y.; Wang, H. *J. Phys. Chem. B* **2005**, *109*, 14118-14129.

(109) Hirose, C.; Akamatsu, N.; Domen, K. *Appl. Spectrosc.* **1992**, *46*, 1051-1072.

(110) Ma, G.; Allen, H. C. *Langmuir* **2006**, *22*, 5341-5349.

(111) Stanners, C. D.; Du, Q.; Chin, R. P.; Cremer, P.; Somorjai, G. A.; Shen, Y.-R. *Chem. Phys. Lett.* **1995**, *232*, 407-413.

(112) Wang, H.-f.; Gan, W.; Lu, R.; Rao, Y.; Wu, B.-H. *Int. Rev. Phys. Chem.* **2005**, *24*,

191-256.

(113) Ye, S.; Noda, H.; Nishida, T.; Morita, S.; Osawa, M. *Langmuir* **2004**, *20*, 357-365.

(114) Nathanson, G. M., Personal Communication.

(115) Aqueous Solubility and Henry's Law Constants of Organic Compounds. In *CRC Handbook of Chemistry and Physics, Internet Version (87th Edition)*; Lide, D. R., Ed.; Taylor and Francis: Boca Raton, FL, 2007.

(116) MacCallum, J. L.; Tieleman, D. P. *J. Am. Chem. Soc.* **2002**, *124*, 15085-15093.

(117) Napoleon, R. L.; Moore, P. B. *J. Phys. Chem. B* **2006**, *110*, 3666-3673.

(118) Conboy, J. C.; Messmer, M. C.; Richmond, G. L. *J. Phys. Chem. B* **1997**, *101*, 6724-6733.

(119) Dubowski, Y.; Vieceli, J.; Tobias, D. J.; Gomez, A.; Lin, A.; Nizkorodov, S. A.; McIntire, T. M.; Finlayson-Pitts, B. J. *J. Phys. Chem. A* **2004**, *108*, 10473-10485.

(120) Porter, M. D.; Bright, T. B.; Allara, D. L.; Chidsey, C. E. D. *J. Am. Chem. Soc.* **1987**, *109*, 3559-3568.

(121) Houk, K. N.; Eksterowicz, J. E.; Wu, Y.-D.; Fuglesang, C. D.; Mitchell, D. B. *J. Am. Chem. Soc.* **1993**, *115*, 4170-4177.

(122) Tsuzuki, S.; Uchimaru, T.; Tanabe, K. *Chem. Phys. Lett.* **1995**, *246*, 9-12.

(123) Ohno, K.; Yoshida, H.; Watanabe, H.; Fujita, T.; Matsuura, H. *J. Phys. Chem.* **1994**, *98*, 6924-6930.

(124) Wakisaka, A.; Komaisu, S.; Usui, Y. *J. Mol. Liq.* **2001**, *90*, 175-184.

(125) Wakisaka, A.; Mochizuki, S.; Kobara, H. *J. Sol. Chem.* **2004**, *33*, 721-732.

(126) Dynarowicz, P. *Colloid Surface* **1989**, *42*, 39-48.

(127) Bowren, D. T.; Finney, J. L. *Phys. Rev. Lett.* **2002**, *89*, 215508.

(128) Daiguji, H. *J. Chem. Phys.* **2001**, *115*, 1538-1549.

(129) Demou, E.; Donaldson, D. J. *J. Phys. Chem. A* **2002**, *106*, 982-987.

(130) Clark, D. J.; Williams, G. *J. Chem. Soc.* **1957**, 4218 - 4221.

(131) McKenna, F. E.; Tartar, H. V.; Lingafelter, E. C. *J. Am. Chem. Soc.* **1953**, *75*, 604-607.

(132) Fuoss, R. M. *J. Am. Chem. Soc.* **1943**, *65*, 78-81.

(133) Palmer, K. F.; Williams, D. *Appl. Opt.* **1975**, *14*, 208-219.